AD-A062 374 ROCKWELL INTERNATIONAL COLUMBUS OHIO COLUMBUS AIRCRA--ETC F/G 21/5
COMPUTER-AIDED DESIGN STUDY OF HYPERMIXING NOZZLES.(U)
JUL 78 L A MEFFERD, P M BEVILAQUA N00019-77-C-0527

UNCLASSIFIED NR78H-91 NL

1 OF 1
AD
AD 62374

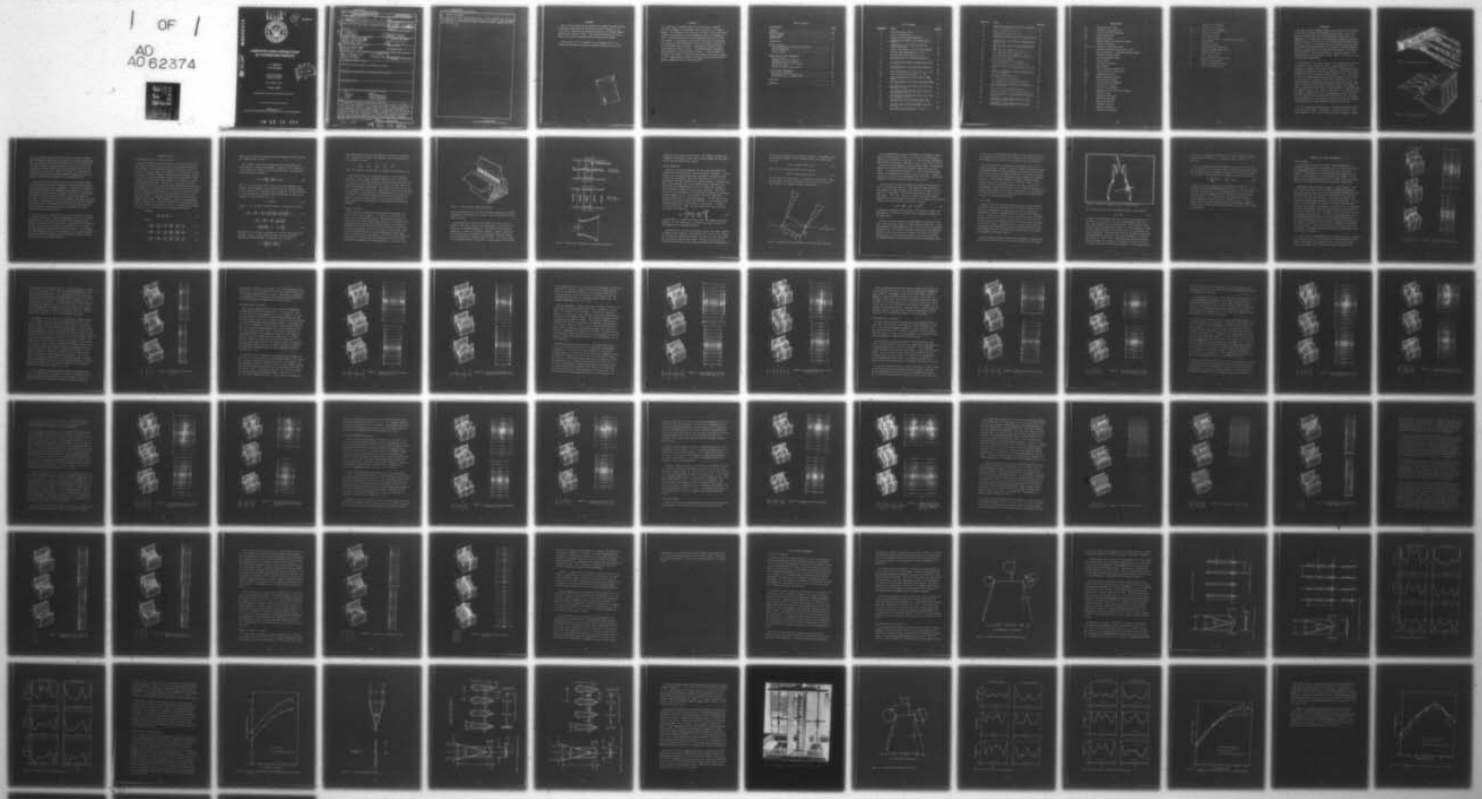

END
DATE FILMED
3-79
DDC

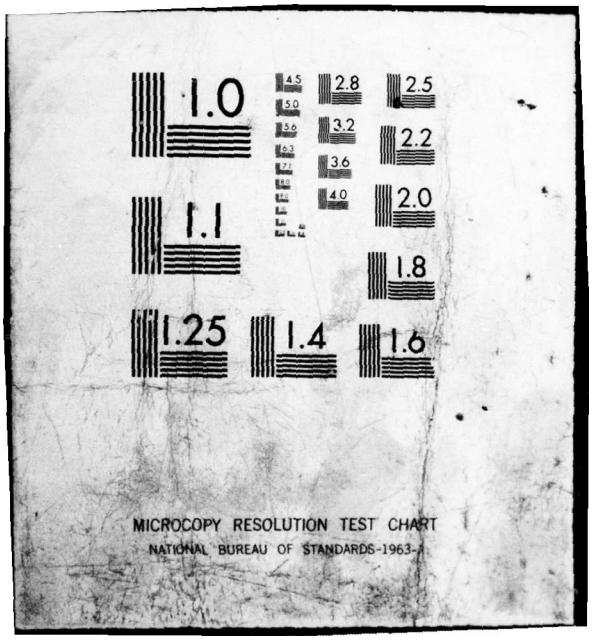
1.0
1.1
1.25
1.4
1.6
1.8
2.0
2.2
2.5
2.8
3.2
3.6
4.0
4.5
5.0
5.6
6.3
7.1
8.0
9.0
MICROCOPY RESOLUTION TEST CHART
NATIONAL BUREAU OF STANDARDS-1963-A

NR78H-91

COMPUTER-AIDED DESIGN STUDY OF HYPERMIXING NOZZLES

L. A. Mefferd

P. M. Bevilaqua

Rockwell International
Columbus Aircraft Division
Columbus, Ohio 43216

Contract N00019-77-C-0527

19 July 1978

FINAL REPORT FOR PERIOD 19 October 1977—19 July 1978

PREPARED FOR THE
NAVAL AIR SYSTEMS COMMAND, DEPARTMENT OF THE NAVY, WASHINGTON, D.C.

UNCLASSIFIED

SECURITY CLASSIFICATION OF THIS PAGE (When Data Entered)

REPORT DOCUMENTATION PAGE	READ INSTRUCTIONS BEFORE COMPLETING FORM
1. REPORT NUMBER (14) NR78H-91	2. GOVT ACCESSION NO.
3. RECIPIENT'S CATALOG NUMBER (9)	
4. TITLE (and Subtitle) (6) Computer-Aided Design Study of Hypermixing Nozzles	5. TYPE OF REPORT & PERIOD COVERED Final Report 19 Oct 1977 - 19 Jul 1978
6. PERFORMING ORG. REPORT NUMBER NR78H-91	
7. AUTHOR(s) (10) L. A. Mefferd, P. M. Bevilaqua	8. CONTRACT OR GRANT NUMBER(s) (15) N00019-77-C-0527
9. PERFORMING ORGANIZATION NAME AND ADDRESS Rockwell International Corp. Columbus Aircraft Division Columbus, Ohio 43216	10. PROGRAM ELEMENT, PROJECT, TASK AREA & WORK UNIT NUMBERS (11) 19 Jul 78
11. CONTROLLING OFFICE NAME AND ADDRESS Naval Air Systems Command Washington, D.C. 20361	12. REPORT DATE
	13. NUMBER OF PAGES
14. MONITORING AGENCY NAME & ADDRESS (if different from Controlling Office) Naval Postgraduate School Dept. of Aeronautics Monterey, CA 93940 (12) 85p.	15. SECURITY CLASS. (of this report) Unclassified
	15a. DECLASSIFICATION/DOWNGRADING SCHEDULE

16. DISTRIBUTION STATEMENT (of this Report)

Approved for Public Release, distribution unlimited

17. DISTRIBUTION STATEMENT (of the abstract entered in Block 20, if different from Report)

18. SUPPLEMENTARY NOTES

19. KEY WORDS (Continue on reverse side if necessary and identify by block number)

jets	ejectors
turbulence	thrust augmentation
vortices	V/STOL aerodynamics
mixing	aircraft propulsion

20. ABSTRACT (Continue on reverse side if necessary and identify by block number)

A combination of computer analysis and scale model testing was utilized to compare the entrainment rates of a variety of jet mixer nozzles. The objective of the study was to develop a nozzle which would increase the performance of thrust augmenting ejectors on V/STOL aircraft. Various multi-lobe and vortex generating nozzles were devised and studied. The spreading of the jet from each nozzle was predicted by calculating a finite-difference solution of Reynolds' equations for the three dimensional flow field. A two-equation turbulence kinetic energy model was used for closure. Limited experimental testing was

DD FORM 1 JAN 73 1473 EDITION OF 1 NOV 65 IS OBSOLETE

UNCLASSIFIED

SECURITY CLASSIFICATION OF THIS PAGE (When Data Entered)

407 390

78 12 14 004

20. ABSTRACT (Continued)

then performed to verify the predicted trends. It was concluded that increasing the length of the nozzle lobes produces the greatest increase in thrust augmentation, and that an alternating slot nozzle yields the greatest augmentation for a given lobe size.

FOREWORD

This report describes work performed at the Columbus Aircraft Division of Rockwell International during the period from 19 October 1977 to 19 July 1978. This work was supported by the Naval Air Systems Command, under Contract N00019-77-C-0527. The technical monitor was Dr. Max F. Platzer of the Naval Postgraduate School, Monterey, California.

We would also like to acknowledge the contributions of Mr. A. D. DeJoode, who developed the computer program and advised us on its use.

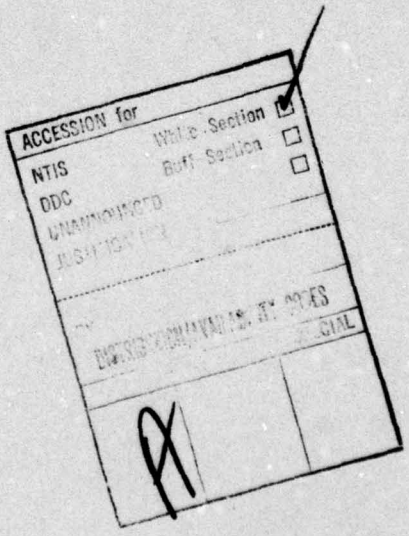

ABSTRACT

A combination of computer analysis and scale model testing was utilized to compare the entrainment rates of a variety of jet mixer nozzles. The objective of the study was to develop a nozzle which would increase the performance of thrust augmenting ejectors on V/STOL aircraft. Various multi-lobe and vortex generating nozzles were devised and studied. The spreading of the jet from each nozzle was predicted by calculating a finite-difference solution of Reynolds' equations for the three dimensional flow field. A two-equation turbulence kinetic energy model was used for closure. Limited experimental testing was then performed to verify the predicted trends. It was concluded that increasing the length of the nozzle lobes produces the greatest increase in thrust augmentation, and that an alternating slot nozzle yields the greatest augmentation for a given lobe size.

TABLE OF CONTENTS

LIST OF FIGURES

NOMENCLATURE

A_o	Total nozzle exit area
A_n	Individual nozzle exit area
A_i	Jet area at initial data plane
A_2	Ejector throat area
A_3	Ejector exit area
c	Spanwise width of computational domain
C_v	Velocity coefficient
c_μ, c_1, c_2	Constants in turbulence model
d	Chordwise distance between ejector walls
G	Rate of generation of turbulence kinetic energy
k	Turbulence kinetic energy
l	Cross slot element elngth
L_e	Ejector length
p'	Perturbation pressure
$\bar{p}$	Mean pressure
P_o	Static pressure at nozzle exit
P_3	Static pressure at ejector exit
P_{atm}	Atmospheric pressure
P_s	Nozzle stagnation pressure
P_R	Pressure ratio, P_s/P_{atm}
ΔP	Pressure drop below ambient
R	Universal gas constant
r	Radius of jet curvature
s	Separation between cross slot elements
t	Nozzle exit gap
T_s	Stagnation temperature
W	Ejector throat width
x	Mainstream direction
y	Chordwise direction
z	Spanwise direction
u	Velocity in x-direction

v	Velocity in y-direction
w	Velocity in z-direction
u_i, v_i, w_i	Initial velocity components
U_o	Nozzle exit velocity
δ	Diffuser half angle
ϵ	Rate of dissipation of turbulence kinetic energy
ρ	Fluid density
μ_t	Turbulent viscosity
σ_k	Turbulent Prandtl number for k
σ_ϵ	Turbulent Prandtl number for ϵ
τ	Turbulent shear stress
T_e	Total ejector thrust
T_j	Wall jet thrust at ejector exit
γ	Ratio of specific heats
θ	Initial jet deflection angle
ϕ	Thrust augmentation ratio

INTRODUCTION

The static thrust of turbojet engines can be significantly increased by diverting the exhaust flow through an ejector pump. Such a thrust augmenting ejector functions like a ducted fan or high bypass ratio compressor. According to the laws of momentum and energy conservation, greatest thrust is obtained from a given energy input by accelerating a large mass of air to a low exhaust velocity. Within an ejector, thrust is increased by transferring the kinetic energy of the engine exhaust stream to a larger mass of air drawn from the atmosphere. The ejector duct experiences a reaction force which is equal but opposite to the momentum change of the accelerated stream. Details of this process have been discussed by Bevilaqua.[1]

The mechanism of this energy transfer is the turbulent mixing of the two streams. Thus, increases in ejector thrust augmentation can be obtained by increasing the turbulent mixing rate. Appreciable increases in mixing and augmentation have been achieved with the so-called hypermixing[2,3] and cross slot nozzles shown in Figures 1 and 2. The alternating exit of the hypermixing nozzle serves to introduce a row of streamwise vortices into a plane jet. The flow on the shorter side of each element expands to atmospheric pressure more rapidly than on the longer side. The resultant local pressure difference deflects each segment of the jet towards the shorter side, as shown in Figure 1. The alternating jet segments function like a series of jet flaps at the trailing edge of the nozzle; streamwise vorticity, corresponding to the tip vortices of each jet flapped section of the nozzle, are shed into the flow between alternating sections. These vortices serve to accelerate the turbulent mixing, and thus to entrain additional fluid into the ejector.

The cross slot nozzle divides the jet into many thin sheets spread across the ejector inlet. In addition, cutting back the exit of the nozzle elements to form a kind of wedge, as shown in Figure 2, produces

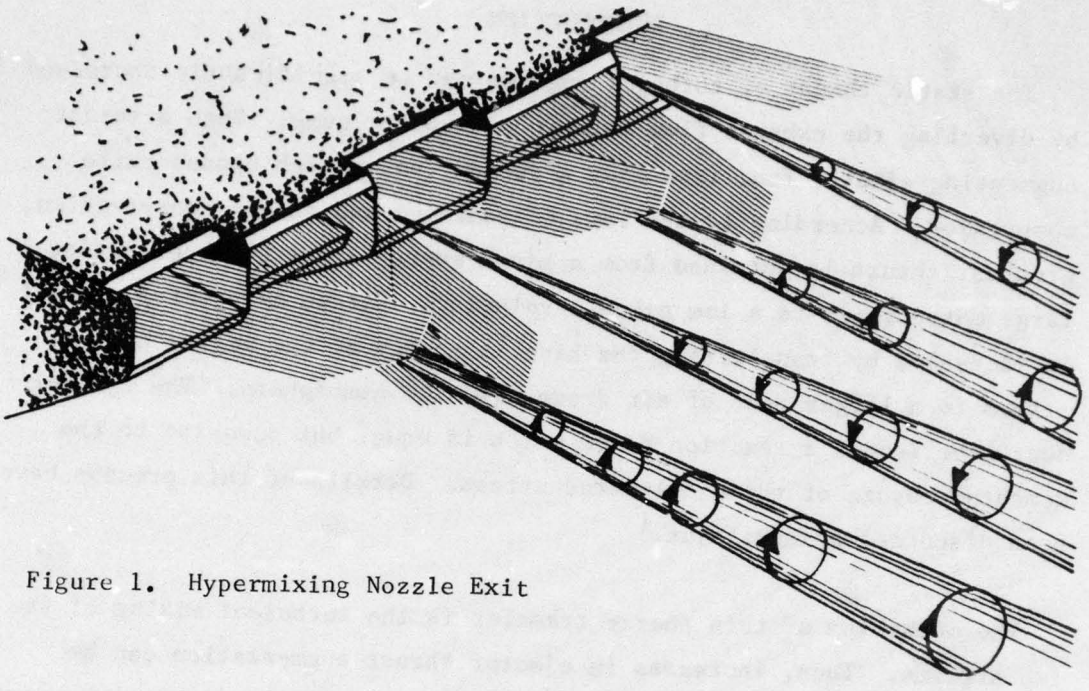

Figure 1. Hypermixing Nozzle Exit

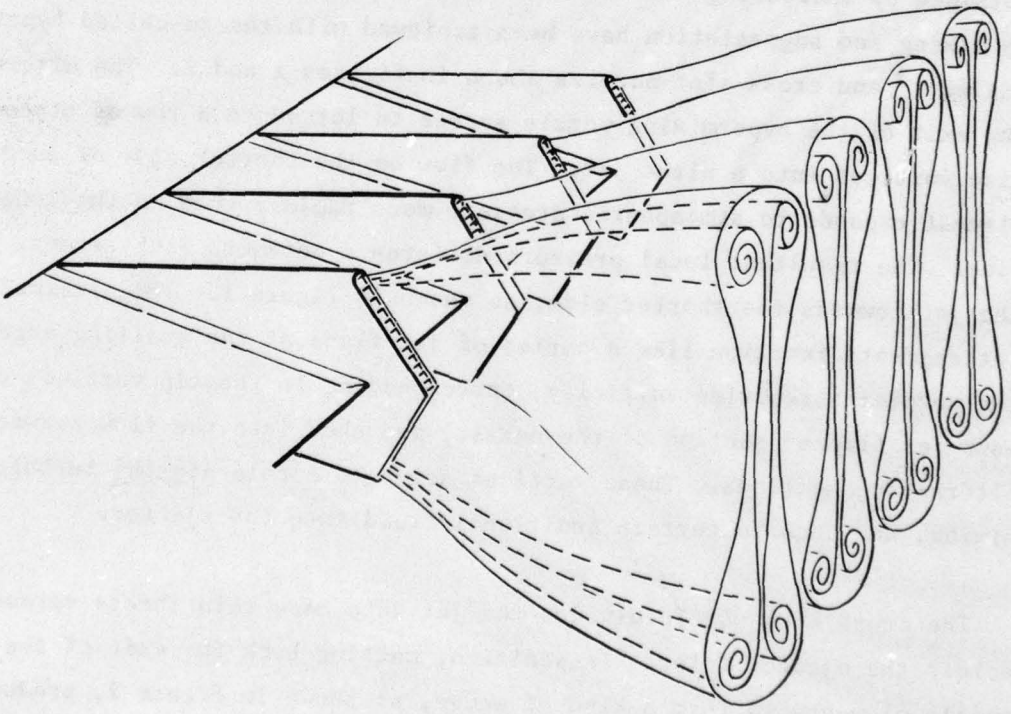

Figure 2. Cross Slot Nozzle Exit

a pair of counter-rotating vortices at the ends of each jet segment. These vortices are generated by an interaction of the secondary stream with the diverging flow in the jets; the roll-up process is similar to that which forms the vortex pair within a jet in a cross flow.[4] The increased entrainment caused by the vortices distorts each jet cross section into a "dog bone" or "dumb bell" shape. This combination of jet furcation and vortex production generates approximately the same increase in mixing and entrainment as the hypermixing nozzle.

The objective of this study was to develop a nozzle which combines the hypermixing and cross slot mechanisms to achieve further increases in jet entrainment and ejector performance. A combination of analytical and experimental methods were employed to investigate this possibility. A previously developed computer program,[5] incorporating a sophisticated two-equation turbulence model, was used to predict and compare the evolution of the jets from various nozzle designs. This made it possible to consider a large number of nozzle concepts without having to fabricate and test each one. Experimental testing was then used to verify predicted trends and to determine the actual performance of a nozzle developed from the analytic results.

In the next section particulars of the analytic method will be given and sample calculations for baseline hypermixing and cross slot nozzles will be shown. Predictions of the analytic study comparing the performance of alternate nozzle concepts will be presented in the following section. The last section includes a description of the test ejector and experimental facility as well as the test results. It is concluded that the hypermixing and cross slot mechanisms are not readily combined, but that performance increments can be achieved with nozzles developed through the use of the analytic method.

METHOD OF ANALYSIS

Governing Equations and Solution Procedure

In order to predict the complex jet flow fields which develop from the nozzles to be studied, it is necessary to determine the solution for a turbulent, three-dimensional velocity and pressure field. This requires a very large number of calculations to be performed. However, considerable savings in computer storage and running time were achieved by utilizing a procedure developed by Patankar and Spalding[6] to reduce solution of the three dimensional problem to the solution of a series of two dimensional problems. Since there is a primary direction of flow (through the ejector) a thin shear layer approximation was applied. The gradients of the normal stress are thus neglected, and the streamwise velocity component is considered to be "driven" by a mean pressure $\bar{p}(x)$, which is decoupled from the perturbation pressures $p'(x,y,z)$ in the transverse planes. An additional assumption that the fluid density ρ is constant was also made. These assumptions reduce the governing fully elliptic equations to a set which is parabolic in the streamwise direction, but elliptic in planes across the flow. In Cartesian coordinates, the equations for the conservation of mass and momentum become

Continuity

$$\frac{\partial u}{\partial x} + \frac{\partial v}{\partial y} + \frac{\partial w}{\partial z} = 0 \tag{1}$$

Momentum

$$\rho u \frac{\partial u}{\partial x} + \rho v \frac{\partial u}{\partial y} + \rho w \frac{\partial u}{\partial z} = \frac{\partial \tau_{yx}}{\partial y} + \frac{\partial \tau_{zx}}{\partial z} - \frac{d\bar{p}}{dx} \tag{2}$$

$$\rho u \frac{\partial v}{\partial x} + \rho v \frac{\partial v}{\partial y} + \rho w \frac{\partial v}{\partial z} = \frac{\partial \tau_{yy}}{\partial y} + \frac{\partial \tau_{zy}}{\partial z} - \frac{\partial p'}{\partial y} \tag{3}$$

$$\rho u \frac{\partial w}{\partial x} + \rho v \frac{\partial w}{\partial y} + \rho w \frac{\partial w}{\partial z} = \frac{\partial \tau_{yz}}{\partial y} + \frac{\partial \tau_{zz}}{\partial z} - \frac{\partial p'}{\partial z} \tag{4}$$

Here, u, v, w are the time averaged velocity components and the τ_{ij} are the turbulent shear stresses.

The turbulent stresses are calculated using the two equation turbulence model of Launder and Spalding.[7] An eddy viscosity assumption is used to relate the stresses to the velocity gradients. The expression in Cartesian tensor notation is:

$$\tau_{ij} = \mu_t \left(\frac{\partial u_i}{\partial x_j} + \frac{\partial u_j}{\partial x_i} \right) - \frac{2}{3} \rho k \delta_{ij} \tag{5}$$

where δ_{ij} is the Kronecker delta, and k is the kinetic energy of turbulence. For the parabolic flow considered here, the velocity gradients in the x direction (i.e., $\partial u_i / \partial x_1$) will be neglected. The eddy viscosity μ_t is calculated from the turbulent kinetic energy and its rate of dissipation, ϵ. The expression for μ_t is

$$\mu_t = c_\mu \rho k^2 / \epsilon \tag{6}$$

in which c_μ is a constant of proportionality. The equations for k and ϵ are

$$\rho u \frac{\partial k}{\partial x} + \rho v \frac{\partial k}{\partial y} + \rho w \frac{\partial k}{\partial z} = \frac{\partial}{\partial y} \left(\frac{\mu_t}{k} \frac{\partial k}{\partial y} \right) + \frac{\partial}{\partial z} \left(\frac{\mu_t}{k} \frac{\partial k}{\partial z} \right) + G - \rho \epsilon \tag{7}$$

$$\rho u \frac{\partial \epsilon}{\partial x} + \rho v \frac{\partial \epsilon}{\partial y} + \rho w \frac{\partial \epsilon}{\partial z} = \frac{\partial}{\partial y} \left(\frac{\mu_t}{\sigma \epsilon} \frac{\partial \epsilon}{\partial y} \right)$$

$$+ \frac{\partial}{\partial z} \left(\frac{\mu_t}{\sigma \epsilon} \frac{\partial \epsilon}{\partial z} \right) + (c_1 G - c_2 \rho \epsilon) \left(\frac{\epsilon}{k} \right) \tag{8}$$

The quantity G is the rate of generation of k by the action of velocity gradients. Since, in the present situation, the only significant gradients are $\partial u/\partial y$ and $\partial u/\partial z$, the expression for G becomes

$$G = \mu_t \left[\left(\frac{\partial u}{\partial y} \right)^2 + \left(\frac{\partial u}{\partial z} \right)^2 \right] \tag{9}$$

The turbulence model involves five empirical constants. According to the recommendation of Launder and Spalding,[7] the following values of the constants are used:

c_μ	c_1	c_2	σ_k	σ_ϵ
0.09	1.44	1.92	1.0	1.3

Thus, the turbulence constants were not adjusted for the present case.

These equations were put in finite difference form by integrating them over a control volume surrounding each grid point in the domain of solution. The resulting non-linear equations are linearized by using upstream values of the flow variables to evaluate the cross stream convection and diffusion coefficients. The equations are solved by the use of a tri-diagonal matrix algorithm. From known conditions at an upstream cross section, x, the flow field at the downstream cross section, $x + \Delta x$, is computed. This streamwise marching process is continued until the domain of interest has been covered. A more complete description of this program and an illustration of its use were given by DeJoode and Patankar.[5]

Boundary Conditions

The nozzles were compared by calculating their performance in the type of ejector shown in Figure 3. In addition to the central jet, there are jets on the diffuser walls. These increase the total jet surface area and provide boundary layer control for the diffuser. This configuration was developed for the XFV-12A ejector wing technology demonstrator aircraft.[8] An inlet area ratio of $A_2/A_0 = 13$ was chosen for these calculations, since it is an average of the wing and canard area ratios on the XFV-12A. The ejector length/throat width ratio, $L_e/W = 2.4$, diffuser area ratio, $A_3/A_2 = 1.77$, and flow split, 50% to the central nozzle, were also chosen as representative of this aircraft. Although the performance of the nozzles depends to some extent on the

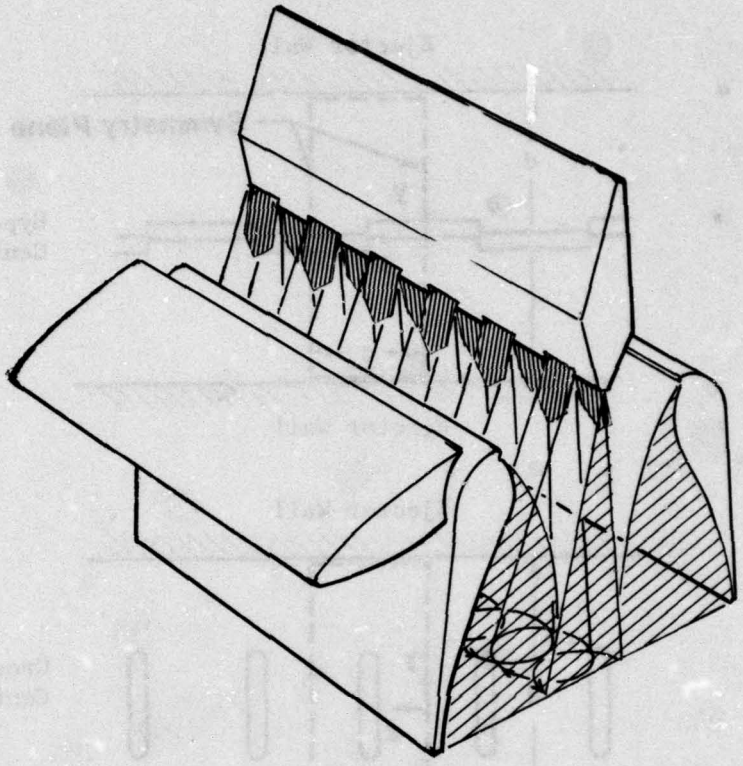

Figure 3. Typical Ejector Wing Configuration

ejector configuration, we felt that conclusions regarding the relative performance of alternate nozzle concepts could be generalized for this type of ejector.

The computational boundaries are outlined with dashed lines in Figure 4. The ejector shroud is two dimensional, so that there is no change in the chordwise dimension, y, with respect to the spanwise dimension, z. There are no physical endwalls. Symmetry planes were used as computational boundaries in the spanwise direction, because most nozzle designs are periodic along the span. The velocity normal to the symmetry planes is zero, and the normal gradients of other flow

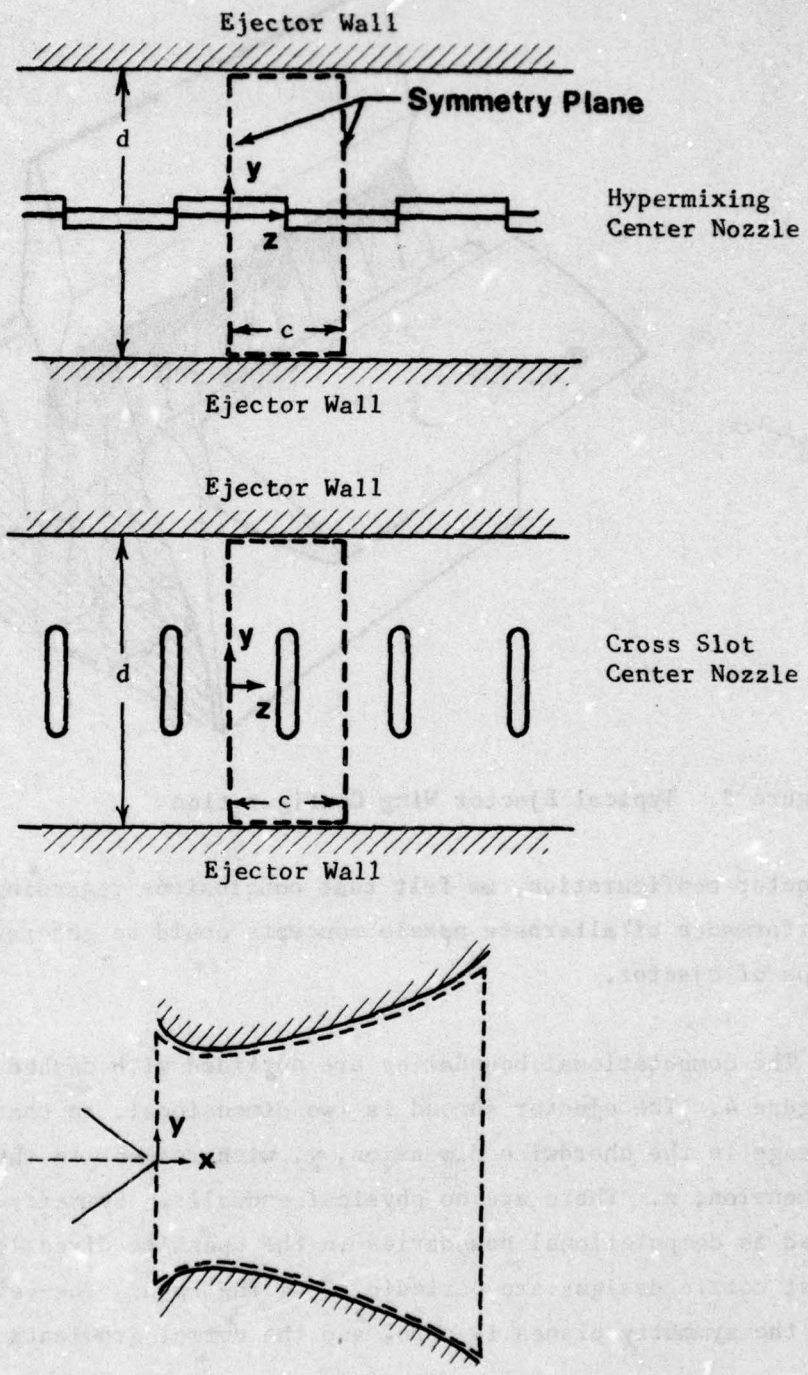

Figure 4. Computational Boundaries for Representative Nozzles

variables are also zero at these planes. This symmetry condition put a constraint on the type of nozzle that could be studied, but only a few nozzles were excluded for this reason.

Initial Conditions

Solution of the ejector equations has thus been transformed to an initial value problem which is solved by streamwise integration. Initial values of all the flow variables must therefore be specified in order to start the calculation. The initial data plane ($x = 0$) is at the beginning of the inlet contraction, as shown in Figure 4. Because there were no data available for the new nozzle concepts, experience with previously tested hypermixing and cross slot nozzles was utilized to make reasonable assumptions for the initial conditions. The initial jet velocity of each nozzle was calculated by multiplying the isentropic velocity computed for the nozzle pressure ratio by an appropriate velocity coefficient, $C_v \equiv V_{actual}/V_{isentropic}$. The same value of this coefficient was used for every nozzle; that is, it was assumed that the internal viscous losses were the same for every nozzle. A value of $C_v = 0.925$ was chosen. Thus, the nozzle exit velocity was calculated according to the relation,

$$U_o = C_v \left[\frac{2\gamma R T_s}{\gamma - 1} \left(1 - \left(\frac{P_o}{P_s} \right)^{\frac{\gamma - 1}{\gamma}} \right) \right]^{1/2} \tag{10}$$

in which values of γ and R for air were used. The stagnation pressure, $P_s/P_{atm} = 2.1$, and temperature, $T_s = 550^\circ R$, were chosen as typical of the primary jets of laboratory ejectors.

Some deflection of the jet is utilized in each of the nozzles studied to promote vortex formation. The associated tilt loss in the jet thrust was calculated by inclining the initial jet velocity vector. The actual exit area was the same for each nozzle. However, since the jets are inclined, the area used in the initial data plane was the intersection of

the jet cross sectional area, as shown in Figure 5. The product of this area and the streamwise velocity component yields the correct nozzle mass flow

$$\rho A_i u_i = \rho(A_n/\cos\theta)(U_o \cos\theta) \tag{11}$$

while the tilt loss in jet thrust is also obtained

$$\rho A_i u_i^2 = \rho(A_n/\cos\theta)(U_o \cos\theta)^2 \tag{12}$$

θ is the angle the thrust vector is tilted off the ejector axis. Thus, the predictions of ejector performance balance the tilt loss in jet thrust against the resulting increase of entrainment.

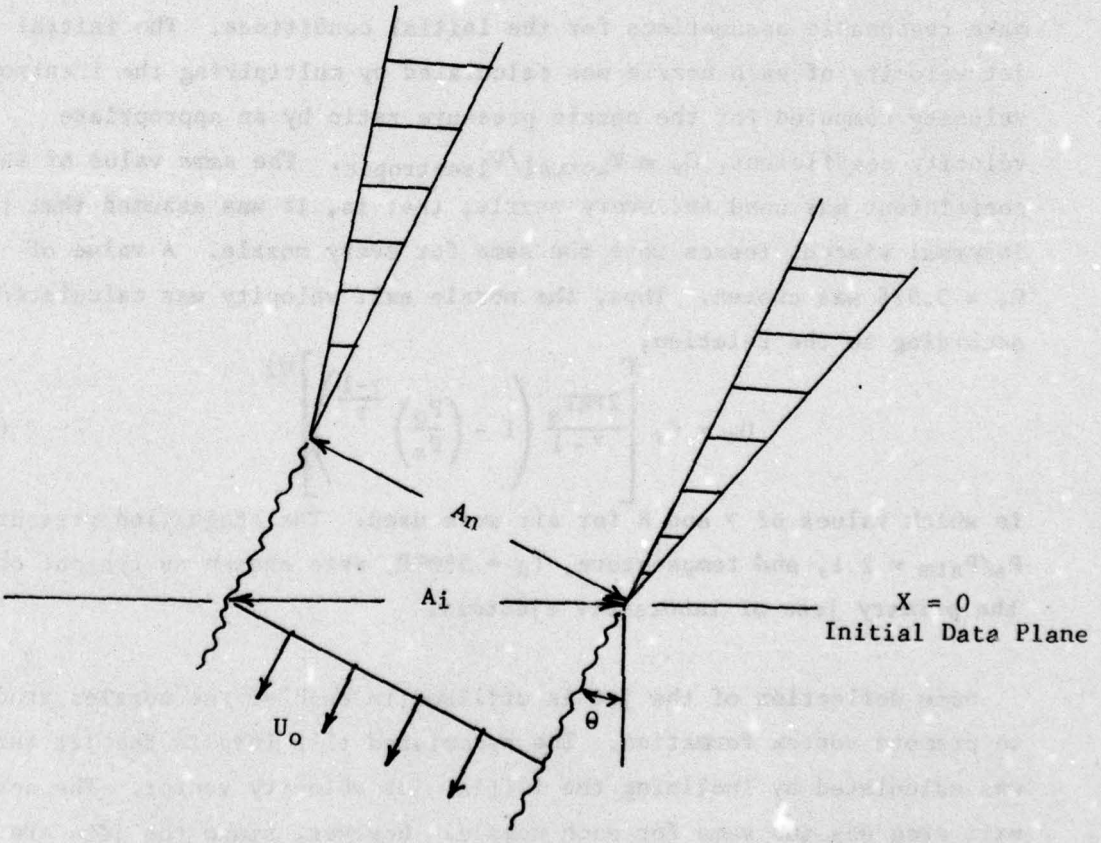

Figure 5. Intersection of an Inclined Jet with the Initial Data Plane

For the hypermixing sections of the nozzle, the streamwise velocity component had the constant value, $u_i = U_o \cos \theta$, and the transverse component was alternately +/- $U_o \sin \theta$. In order to match experimental data, DeJoode and Patankar[5] found that it was also necessary to specify a transverse velocity component in the secondary stream. This component represents the deflection of the secondary stream by the jet flap effect. It was sufficiently accurate to set the secondary flow angle equal to the hypermixing tilt angle, θ, near the jet and to linearly decrease it to zero at the point midway to the inlet wall. The velocity component in the third direction was set equal to zero.

For the cross slot nozzle a somewhat more detailed specification of the jet velocities was necessary. The angularity along both axes of each segment was varied from zero at the point of the wedge to $\pm 15^o$ at both ends of the segment. This value represented the effect of a 35^o wedge angle. Thus, $v_i(y) = w_i(y) = U_o \sin \theta(y)$. Both these velocity components are directed away from the axes. The streamwise axial velocity component was then calculated from the total velocity,

$$u_i(y) = \left[U_o^2 - v_i(y)^2 - w_i(y)^2\right]^{1/2} \tag{13}$$

No transverse components were specified in the secondary stream. This distribution of velocities was found to best represent the effect of the wedge angle.

The wall jets were specified as being tangent to the surface of the inlet contraction, which made a 30^o angle with the ejector axis. Thus, the streamwise velocity component was $u_i = U_o \cos 30^o$ and the tangential component was $v_i = U_o \sin 30^o$. The area in the initial data plane was increased to give the correct mass flow, as in the case of the hypermixing nozzles. No corrections were made to the turbulence model or the momentum equations to account for the effect of centrifugal forces

on these jets. The entrainment and thrust of the wall jets were therefore underpredicted, but since this treatment was the same in every case, the comparison of the central nozzles should not have been affected.

The initial turbulence intensity was not measured in any of the previous experiments. However, sensitivity studies performed by DeJoode and Patankar[5] showed that the development of the velocity profiles was relatively insensitive to probable variations in the initial turbulence level. This is because the hypermixing vortices dominate the turbulent processes. For the present analysis the initial turbulence kinetic energy in the jet was specified to be 6% of the jet energy. In the secondary stream the turbulence energy was set equal to 0.01% of the stream energy. Similarly, the initial level of turbulence dissipation did not have a significant effect on the jet development. An initial value of $\epsilon = 0.13\ U_o^3/t$, where t is the initial nozzle gap, was chosen as being typical of the jets previously tested.

Closure Scheme

Although the elliptic boundary value problem has been transformed to a parabolic initial value problem, the basic elliptic character of the flowfield is unchanged. This means that the initial conditions are determined by feedback from downstream of the ejector exit. Therefore, closure is obtained by iterating on the inlet pressure until the exhaust pressure matches the pressure at the ejector exit. This exit pressure is determined by the curvature of the jet sheet leaving the trailing edge of the ejector shroud. Centrifugal forces in the curved jet support a low pressure region behind the ejector, as sketched in Figure 6. Morel and Lissaman[9] noted the similarity to the jet flap effect, and called the phenomenon a "jet flap diffuser."

The exit pressure boundary condition was determined by requiring that the pressure difference across the jet sheet be balanced by centrifugal

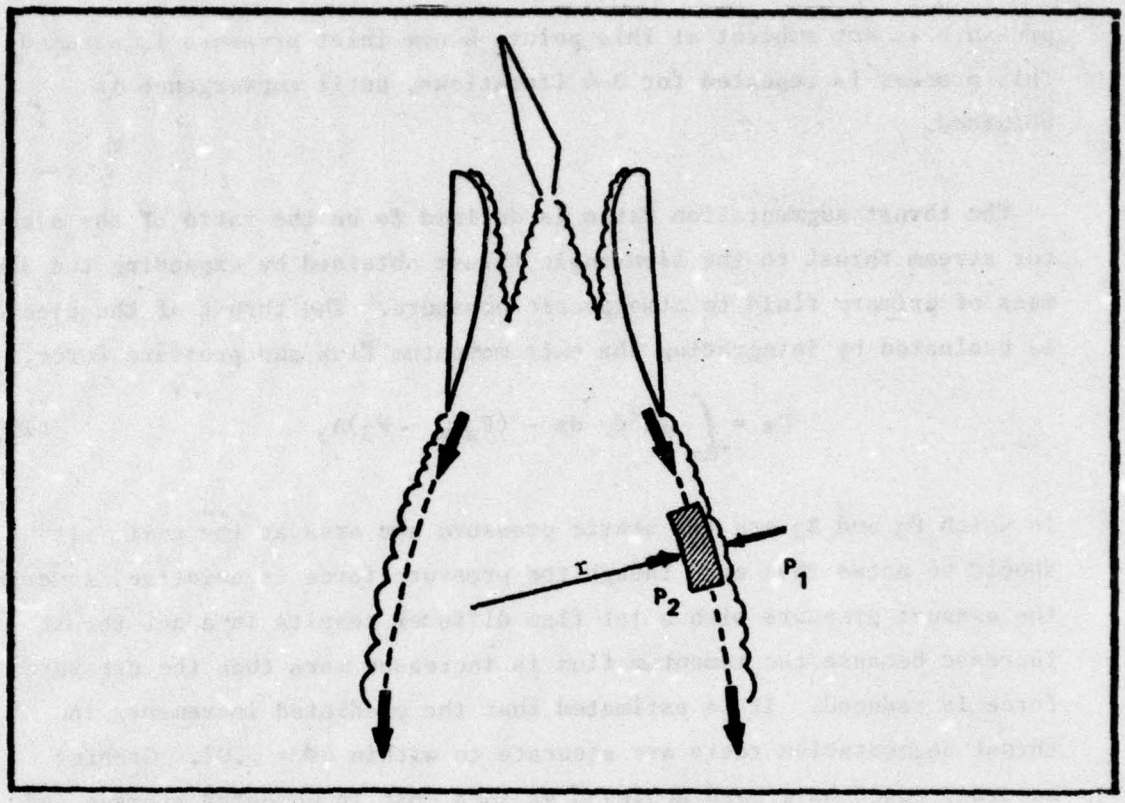

Figure 6. Radial Force Balance in the Jet Flap Diffuser

forces within the jet. This equilibrium condition is expressed as

$$\Delta P = T_j/r \tag{14}$$

in which T_j is the thrust of the wall jet at the ejector exit and r is the radius of jet curvature. To a first approximation, both the jet thrust and curvature can be assumed constant. This relation is used to iterate on the inlet pressure as follows: an initial assumption is made for the secondary pressure at the ejector inlet. This determines the initial velocities. The exit pressure and wall jet thrust calculated by marching through the ejector are then used in equation (14) to define the curvature of the jet sheet. Considering this sheet to represent a physical boundary, the calculation is continued to the point at which the opposite sides of the sheet become parallel. If the computed static

pressure is not ambient at this point, a new inlet pressure is assumed. This process is repeated for 3-4 iterations, until convergence is obtained.

The thrust augmentation ratio is defined to be the ratio of the ejector stream thrust to the isentropic thrust obtained by expanding the same mass of primary fluid to atmospheric pressure. The thrust of the ejector is evaluated by integrating the exit momentum flux and pressure force,

$$T_e = \int_{A_3} \rho u^2 dy\, dz - (P_{atm} - P_3)A_3 \qquad (15)$$

in which P_3 and A_3 are the static pressure and area at the exit. It should be noted that even though the pressure force is negative, lowering the exhaust pressure with a jet flap diffuser results in a net thrust increase because the momentum flux is increased more than the pressure force is reduced. It is estimated that the predicted increments in thrust augmentation ratio are accurate to within $\Delta\phi = \pm.02$. Greater accuracy could have been achieved at some cost in computer storage and running time, but differences of this magnitude were not felt to represent an improvement.

PREDICTIONS OF NOZZLE PERFORMANCE

Baseline Nozzles

To illustrate the predictions of the computer program and to establish a baseline level of performance, the jets from a representative hypermixing nozzle and a comparable cross slot nozzle were examined. The performance of the hypermixing nozzle depends upon the aspect ratio and deflection of the alternating jet segments. On the basis of earlier hypermixing nozzle tests, an aspect ratio 5.3:1 nozzle with a 15° tilt angle was selected as the baseline configuration.

Development of the jet from this nozzle is shown in Figure 7. The axial velocity profiles at three streamwise stations corresponding to the ejector throat ($X/L_e = 0.1$), a point approximately midway through the diffuser ($X/L_e = 0.4$), and the ejector exit ($X/L_e = 1.0$), are shown on the left. The convection velocities in the transverse planes at the throat and midway through the diffuser are shown on the right. The exit plane is not shown because the transverse velocities have virtually decayed by that station. The spanwise axis runs from left to right along the base of each profile, while the chordwise axis runs from bottom to top along the side. Note that the spanwise scale on the axial plots has been elongated to show detail. The location of the grid points is the same for the axial and transverse velocity profiles at each station. In the transverse planes, each velocity vector is centered on a grid point; the surface of the axial velocity profiles is defined by lines passing over these points. A sketch of the nozzle exit is shown at the bottom of the page. To simplify making comparisons, these same profiles will be shown for every nozzle.

In the figures, the hypermixing jet runs along the span on the centerline. There is a wall jet on each side of the hypermixing jet, and the relative magnitude of the secondary velocity is seen in the region between the primary jets. At the throat station in Figure 7, the

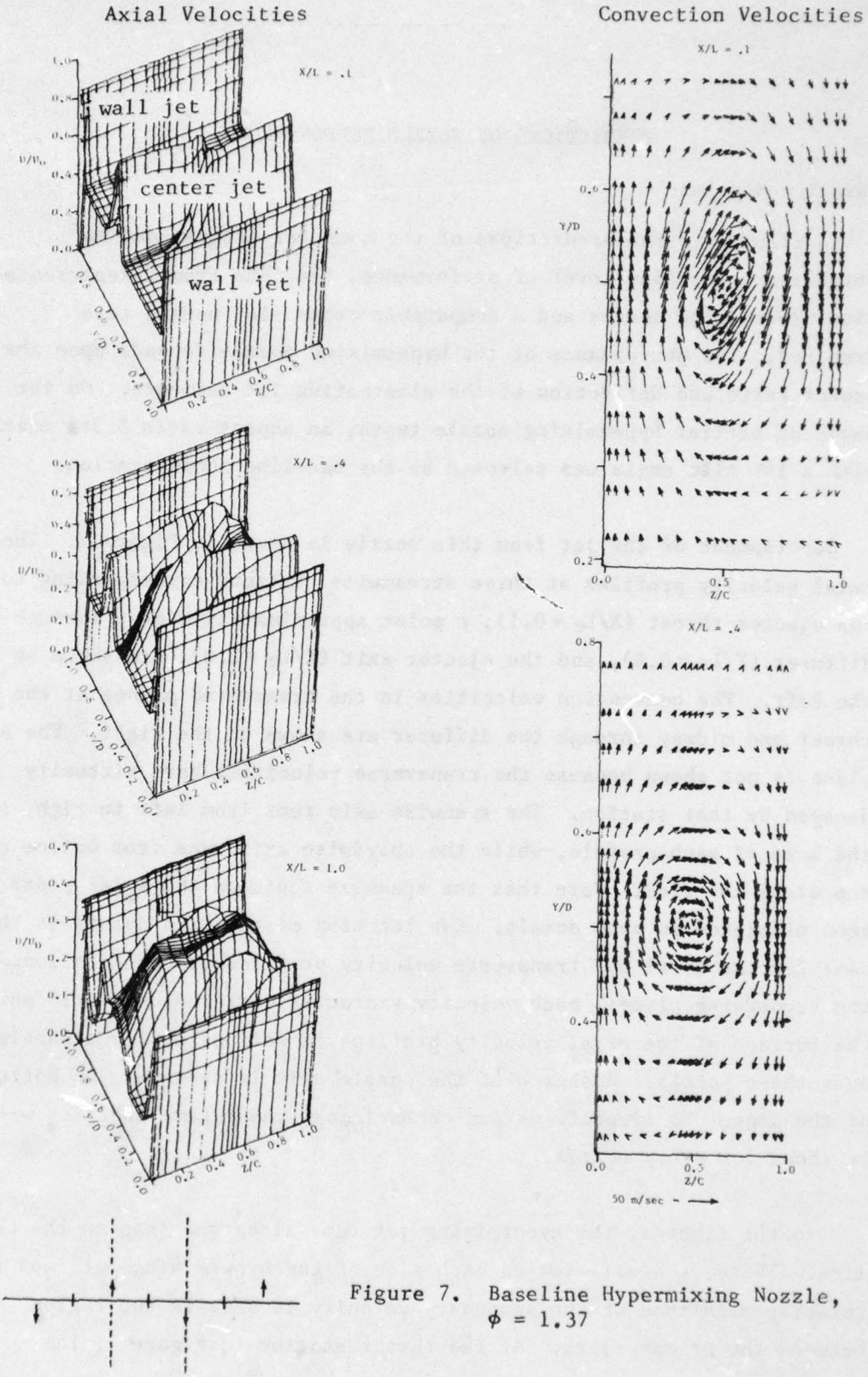

Figure 7. Baseline Hypermixing Nozzle, $\phi = 1.37$

displacement of the adjoining segments of the hypermixing jet is apparant in the axial velocity profiles, while the streamwise vortex can be seen in the transverse plane. The vortex rotation convects each jet segment around and behind the adjoining segment, as seen at the second axial station. This produces the characteristic double peak in the chordwise velocity profiles. Continued mixing acts to merge these peaks and broaden the profiles, as seen at the exit station. This action of the hypermixing vortices augments the turbulent transport of momentum and therefore increases the rate of entrainment by the jet. A thrust augmentation ratio of $\phi = 1.37$ was predicted for this nozzle.

Development of the jet from the cross slot nozzle is shown in Figure 8. The length of the cross slot was limited to 0.266 of the ejector throat so that it could be folded into a thin wing, as on the XFV-12A. An aspect ratio of 4.7:1 was selected for this nozzle to provide a nozzle gap comparable to that of the hypermixing nozzle. In the figure the left-hand symmetry plane runs through the center of the segment so that only half of the jet is seen. One side of the vortex pair which develops at the ends of each segment are visible in the transverse planes. The mixing action of the vortices increases the entrainment in this region, which causes the jet to develop the "dog bone" shaped cross section seen in the figure. Since the spanwise dimension is elongated, the profiles shown are distorted. The low velocity region at the center of the jet is due to the initial wedge angle which directs the jet away from the ejector centerline. A thrust augmentation ratio of $\phi = 1.34$ was predicted for this nozzle configuration. Because these baseline configurations were selected on the basis of previous test experience, no attempt was made to optimize them. As a point of reference, the augmentation predicted for a plane slot nozzle is $\phi = 1.20$.

In the following sections nozzles which combine the hypermixing and cross slot mechanisms will be analytically studied to identify one which provides improved thrust augmentation. The basic nozzle consists of alternating cross slot and span slot segments. Nozzles in which the

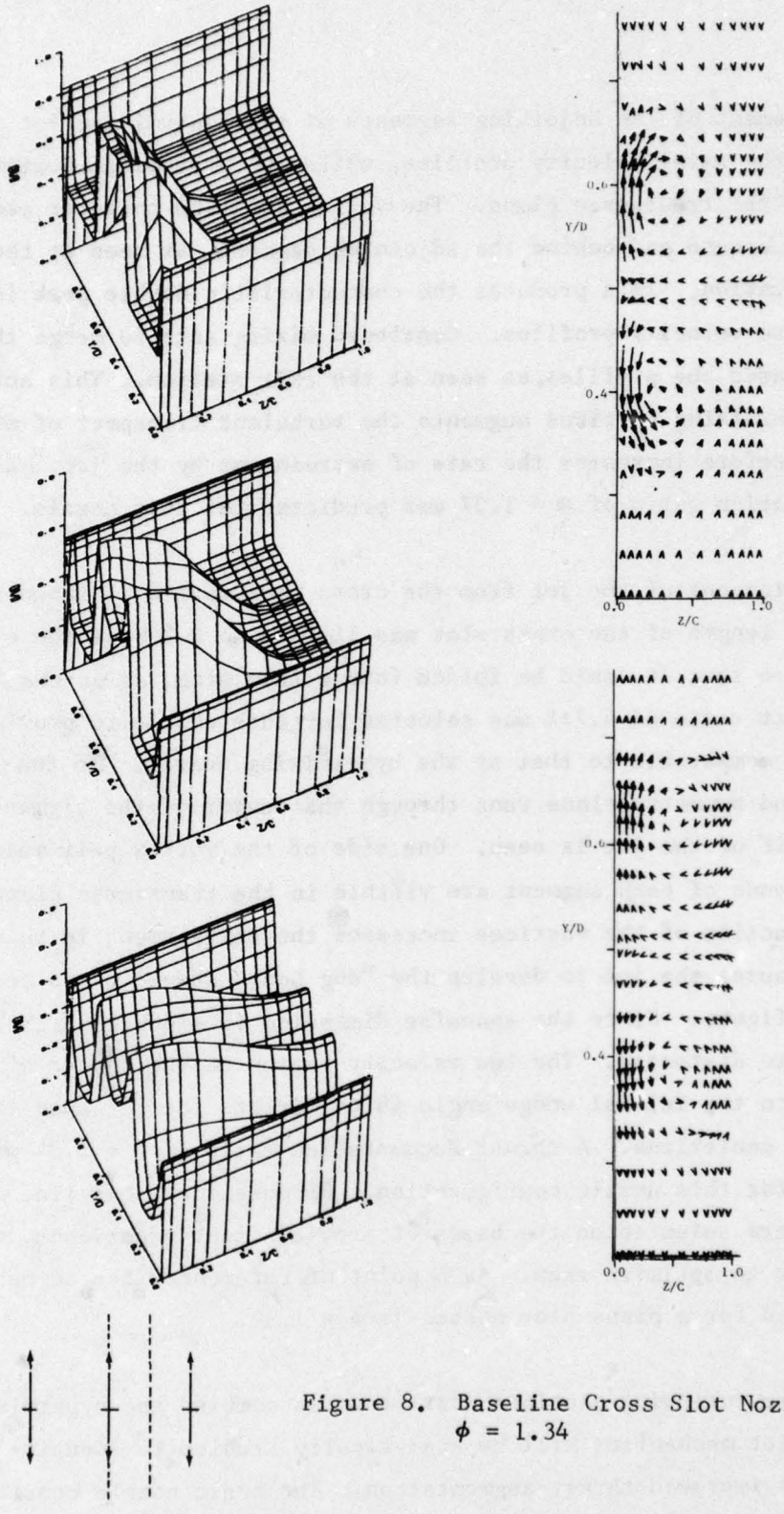

Figure 8. Baseline Cross Slot Nozzle, $\phi = 1.34$

hypermixing is confined to the spanwise slot will be considered in the next section. In the following section nozzles in which only the cross slot is made hypermixing will be examined. Then nozzles in which both are hypermixing will be analyzed. Some nozzles which do not fall into these classifications are considered in the last section.

Hypermixing Span Slot Nozzles

This class of nozzles consists of those in which the hypermixing vortices originate from the spanwise slot. Unless otherwise noted, the deflection of the hypermixing and cross slot segments is the same as on the baseline nozzles; the nozzle exit area is always the same. The first nozzle of this class is shown in Figure 9. Cross slot segments are located midway between the hypermixing vortices. As a result, an array of five streamwise vortices develops in every section of the nozzle. In the figure the hypermixing vortex is at the center and the vortex pair eddies are on the sides. The velocities induced by the vortex pairs reinforce the hypermixing velocities on the diagonal running from lower left to upper right, but oppose them on the other diagonal. Comparison of the exit velocity profile with those of the baseline nozzles reveals that this interaction reduces the spreading of the hypermixing segment. However, the addition of the pair vortices increases the net entrainment and the thrust augmentation ratio is increased to $\phi = 1.41$.

On the nozzle shown in Figure 10, the entire cross slot segment was deflected in the same direction as the hypermixing segment. This reduces the interference between the hypermixing and cross slot segments, but also eliminates one pair of vortices. As seen in the transverse planes, the vortex pair eddies which do develop are considerably weaker than in the previous nozzle. Consequently, the cross slot jets do not spread into the region behind the adjoining segment. The net effect is to reduce the thrust augmentation ratio. In the interest of economy, the

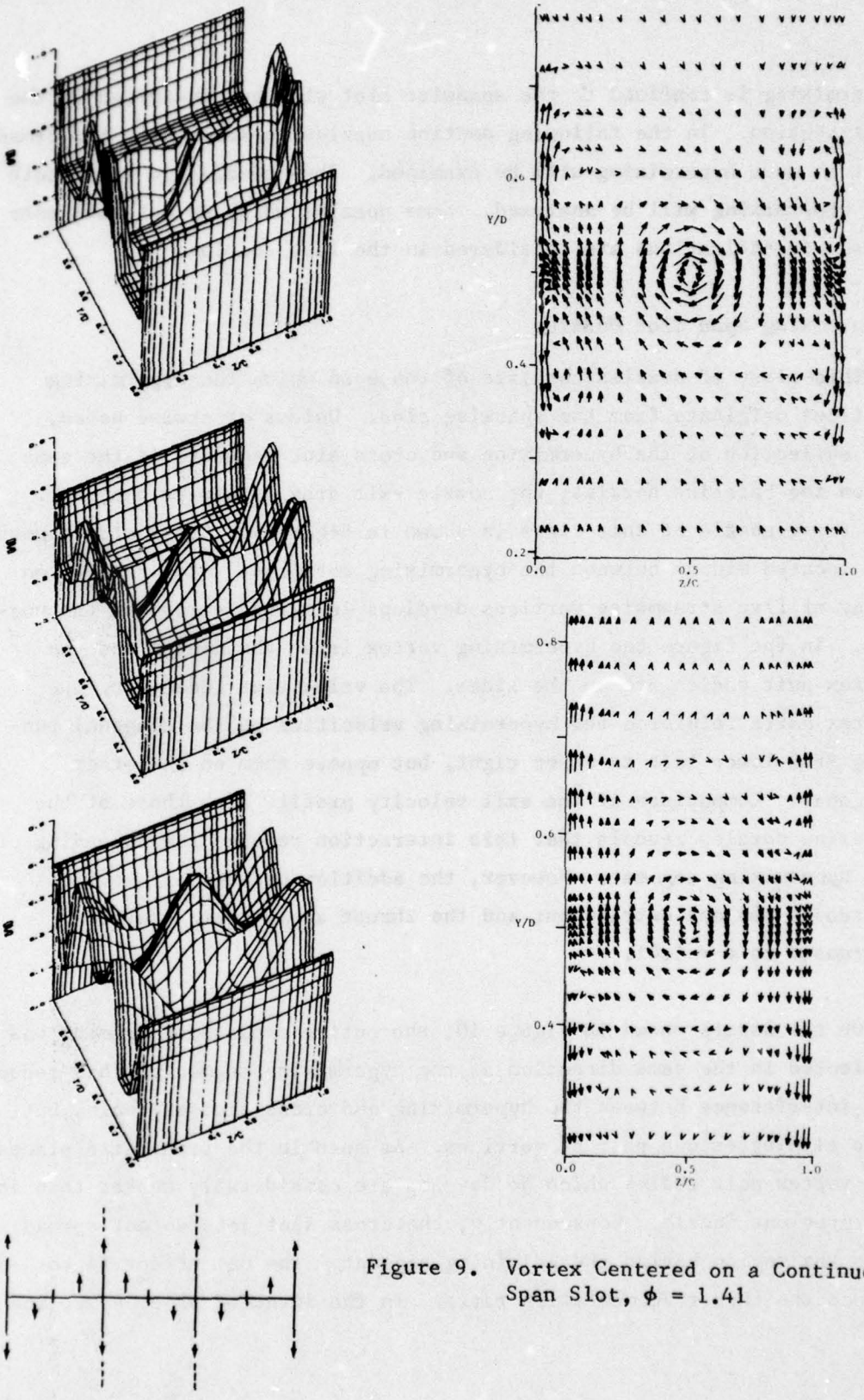

Figure 9. Vortex Centered on a Continuous Span Slot, ϕ = 1.41

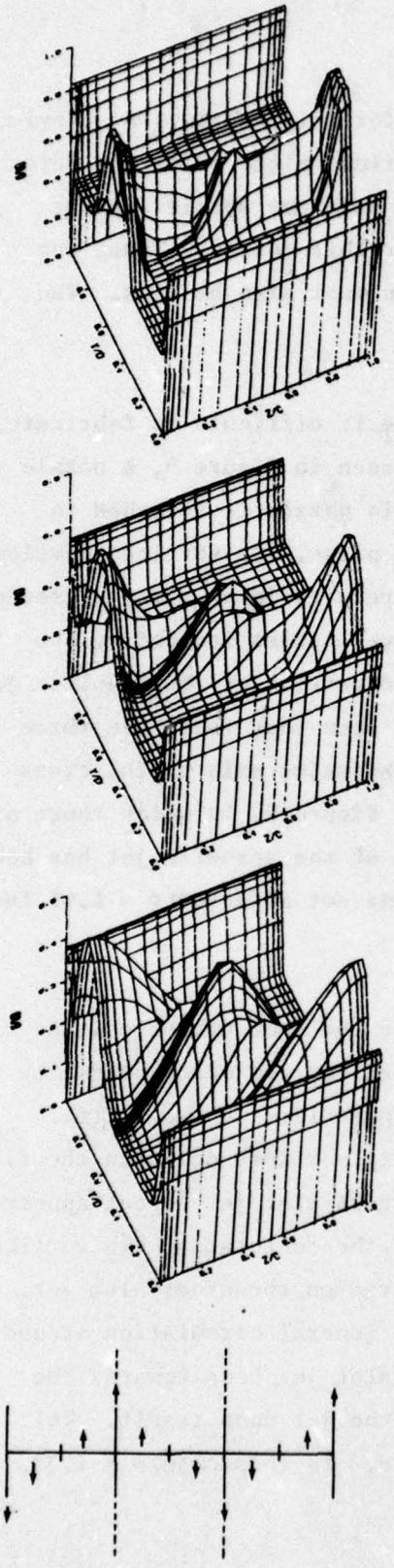

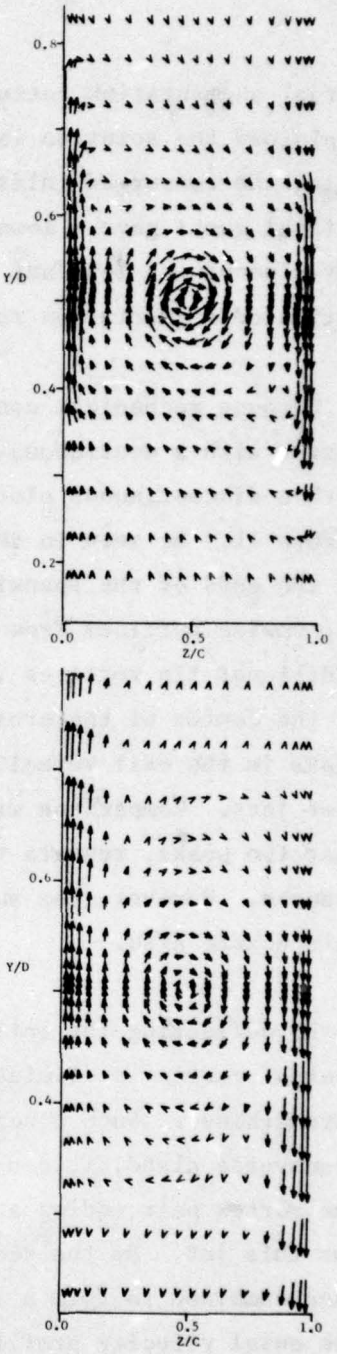

Figure 10. Vortex Centered Between Co-blowing Cross Slots, $\phi \sim 1.36$

actual augmentation ratio was not computed for this nozzle. As previously explained the solution is obtained by iterating on the inlet pressure. Using the converged inlet pressure from the previous nozzle for the initial guess gave a lower exit pressure for this nozzle. Thus, the entrainment was less and so the augmentation must also be less. The estimated augmentation ratio is $\phi \sim 1.36$.

Because mechanical constraints would make it difficult to fabricate a nozzle with a continuous spanwise slot, as seen in Figure 9, a nozzle with a discontinuous slot was examined. This nozzle is sketched in Figure 11. As seen in the first transverse plane, tip vortices develop at the ends of the spanwise segment. This results in an array of seven streamwise vortices from this nozzle. The velocities induced by the additional tip vortices is opposite to the direction of the spanwise jet at the center of the cross slot. It can be seen that there are three peaks in the exit velocity profiles along the major axis of the cross slot jets. Comparison with the profiles of Figure 9, in which there are just two peaks, reveals that the deflection of the spanwise jet has been reduced. However, the augmentation ratio was not affected; $\phi = 1.41$ for this nozzle also.

By deflecting the entire spanwise slot in the same direction, the central vortex is eliminated and the tip vortices are correspondingly strengthened. Such a nozzle is shown in Figure 12. In the initial transverse plane, it can be seen that the tip vortices dominate the flow. The vortex pair eddies at the ends of the cross slot jet do not appear for this jet. By the second station shown, the co-rotating tip vortices have combined to form a single vortex centered on the cross slot jet. The axial velocity profiles reveal that the general circulation around the pair of tip vortices rotates the cross slot jet back towards the centerline of the ejector, thus collapsing the jet upon itself. This causes a reduction in the augmentation ratio. In this case $\phi = 1.33$.

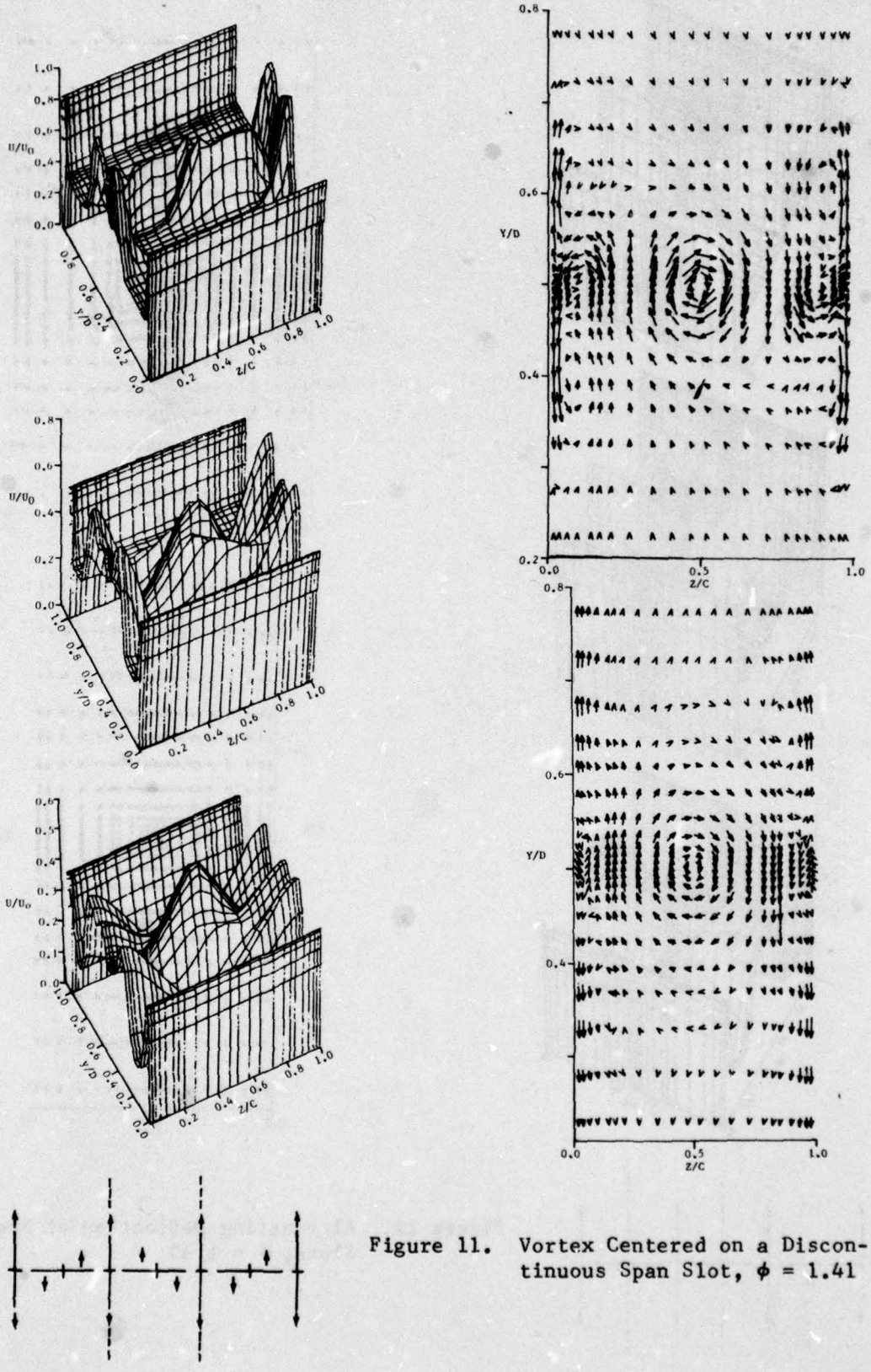

Figure 11. Vortex Centered on a Discontinuous Span Slot, ϕ = 1.41

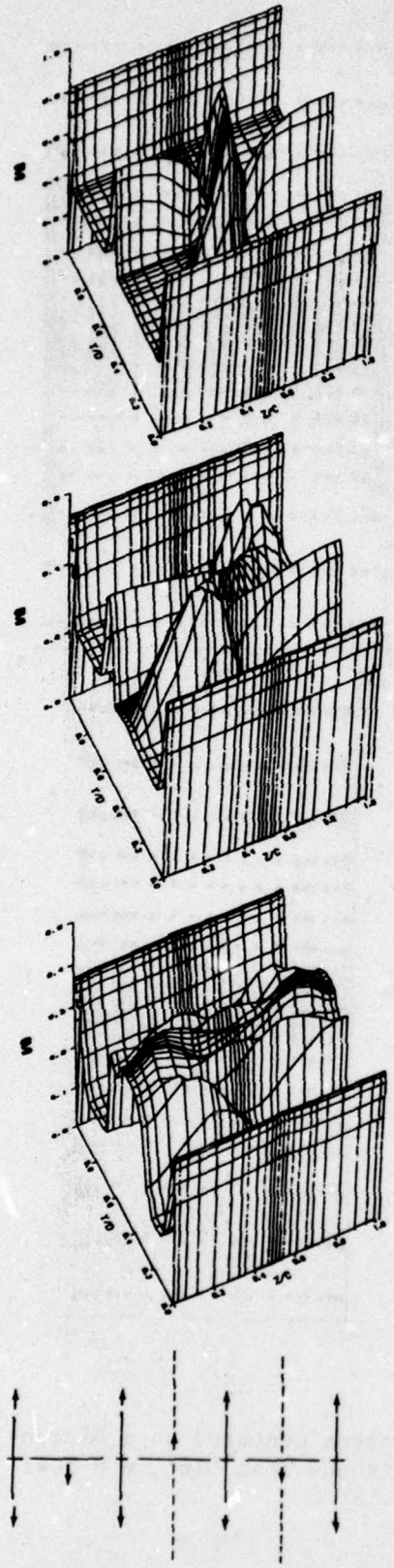

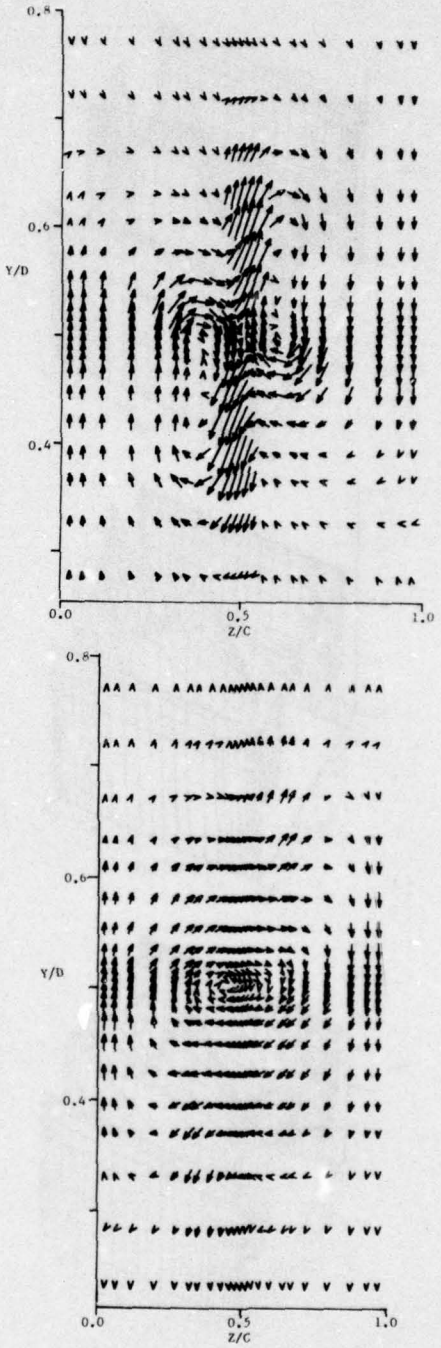

Figure 12. Alternating Deflection of Span Slots, ϕ = 1.33

Since the hypermixing vortex may actually interfere with the development of the cross slot jet, a nozzle without any hypermixing vortex was also considered. Development of the jet from this nozzle is shown in Figure 13. Only the vortex pair eddies at the ends of the cross slot jet appear in this case. They induce a flow which convects the spanwise jet away from its center and into the low velocity region at the center of the cross slot jet. By the exit of the ejector, the segments of the spanwise jet have merged to form a continuous sheet. The development of the cross slot jet is actually about the same as previously. The augmentation ratio is surprisingly large, $\phi = 1.42$ in this case.

Hypermixing Cross Slot Nozzles

In this group of nozzles the hypermixing vortex originates from the cross slot. The influence of the wedge was treated differently in this case. As before, the chordwise component of the jet velocity, $v_i(y)$, was varied from zero to 15°. However, the spanwise velocity component, $w_i(y)$ was either +/- U_o sin 15°, corresponding to the deflection of the jet for hypermixing. Exceptions will be pointed out.

No wedge angle at all was specified for the first nozzle in this group. Alternate sides of each cross slot segment were simply deflected in opposite directions, as sketched in Figure 14. Three streamwise vortices develop in each section of the nozzle, as seen in the transverse planes. The vortex at the center of the cross slot must be twice as strong as either tip vortex, since it is formed by the combination of the two complementary root vortices. The vortex pair eddies do not appear in this case because there is no chordwise deflection of the jet.

In the axial velocity profiles, it can be seen that the central vortex causes some deflection of the spanwise jets away from the centerline, but the displacement of the cross slot jets is significantly greater. This motion may be enhanced by the mutual attraction of each tip vortex

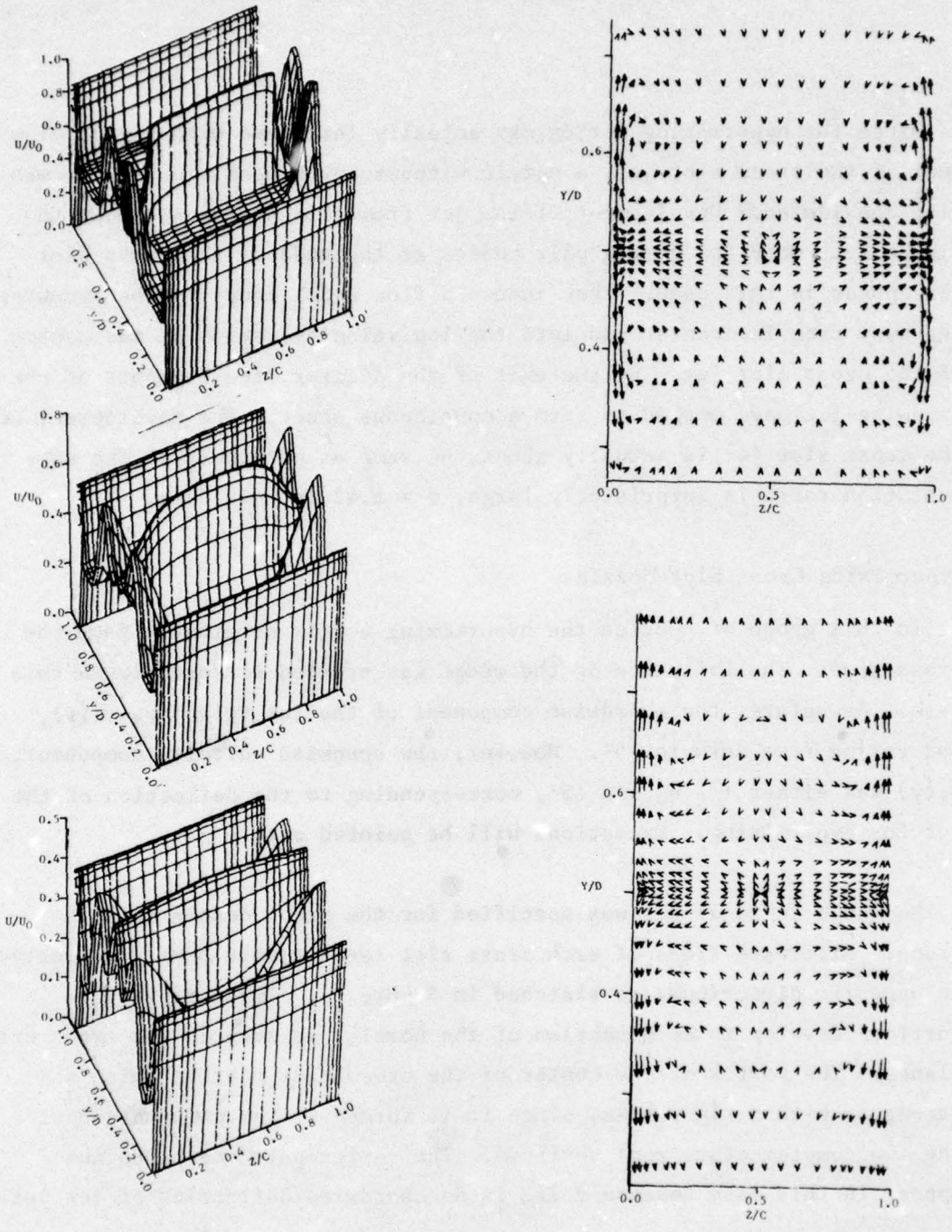

Figure 13. Plane Alternating Slot Nozzle, ϕ = 1.42

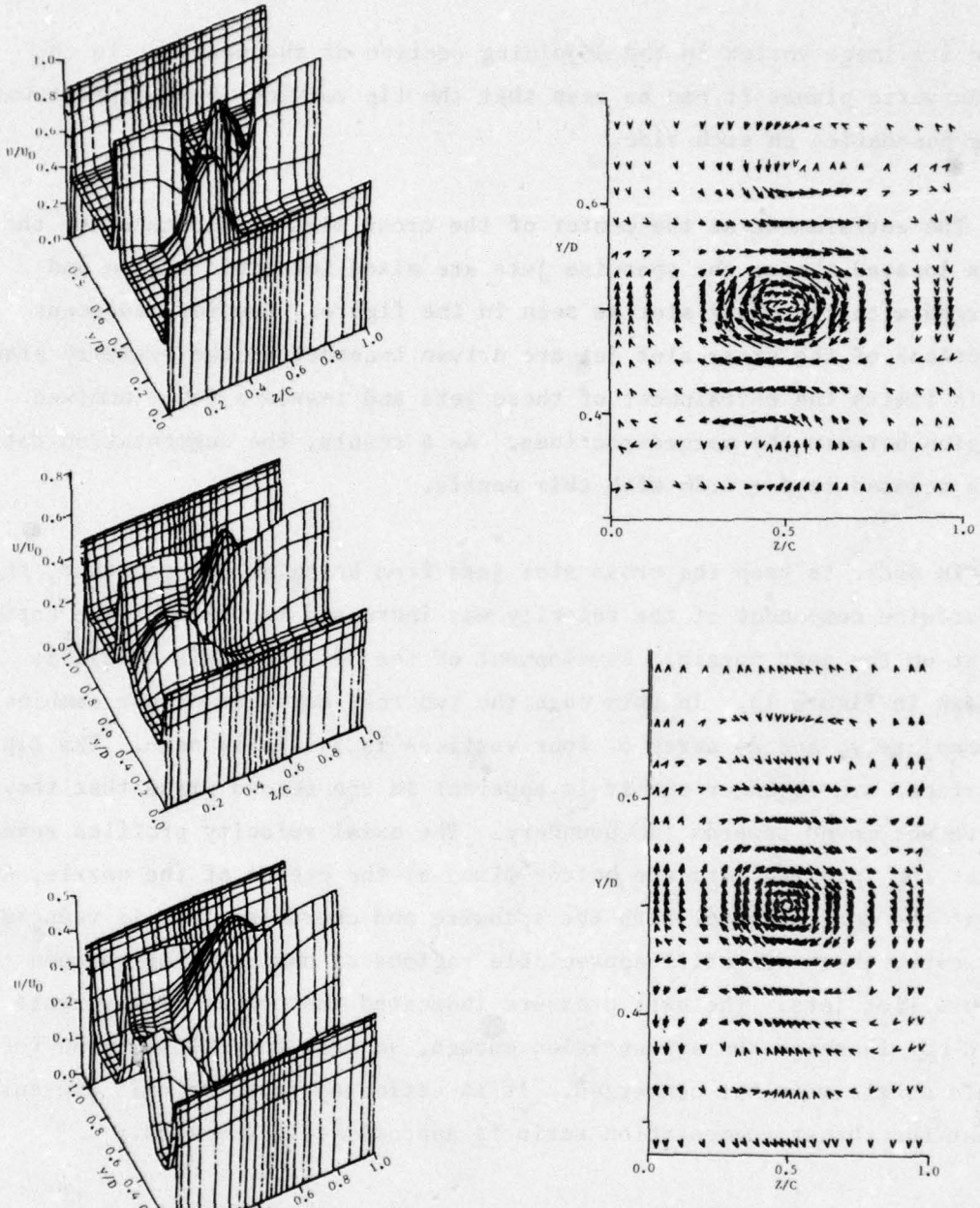

Figure 14. Vortex Centered on Cross Slots with No Wedge Angle, ϕ = 1.26

and its image vortex in the adjoining section of the nozzle. In the transverse planes it can be seen that the tip vortices have moved toward the boundaries on each side.

The entrainment at the center of the cross slot is increased by the vortex located there; the spanwise jets are mixed into this region and merged with the cross slot as seen in the figure. However, adjacent sections of the cross slot jet are driven together at the symmetry plane. This limits the entrainment of these jets and leaves a large unmixed region between the merged sections. As a result, the augmentation ratio was reduced to $\phi = 1.26$ with this nozzle.

In order to keep the cross slot jets from being driven together, the chordwise component of the velocity was increased to 15° over the entire slot on the next nozzle. Development of the jet from this nozzle is shown in Figure 15. In this case the two root vortices do not combine immediately, and an array of four vortices is initially seen. The tip vortices are stronger and it is apparent in the second plane that they have not moved towards the boundary. The axial velocity profiles reveal that the spanwise jets are better mixed at the center of the nozzle, and that the deflection of both the spanwise and chordwise jets is reduced. However, there are still appreciable regions of unmixed flow between the cross slot jets. The exit pressure indicated that these improvements did not increase the augmentation enough, so that the calculations for this nozzle were not converged. It is estimated from the exit pressure that the thrust augmentation ratio is approximately $\phi \sim 1.33$.

Because the entrainment of the cross slot jet was insufficient in both of the previous cases, a nozzle having a strong vortex centered on each side of the cross slot was analyzed. This pair of vortices was formed by deflecting the cross slot as shown in Figure 16. A strong vortex is generated at the junction of the alternating segments and a weaker tip

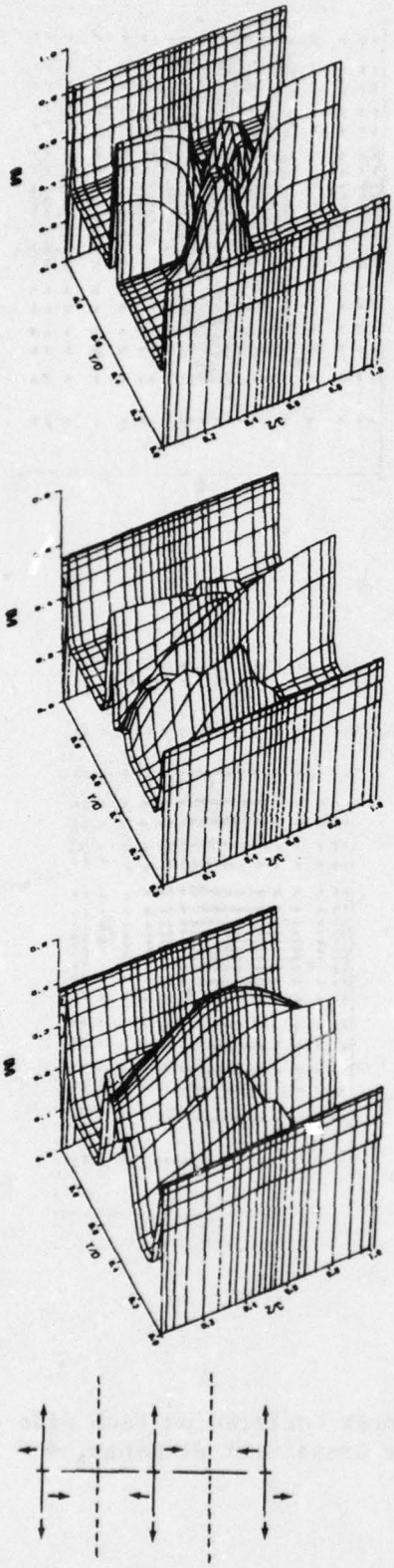

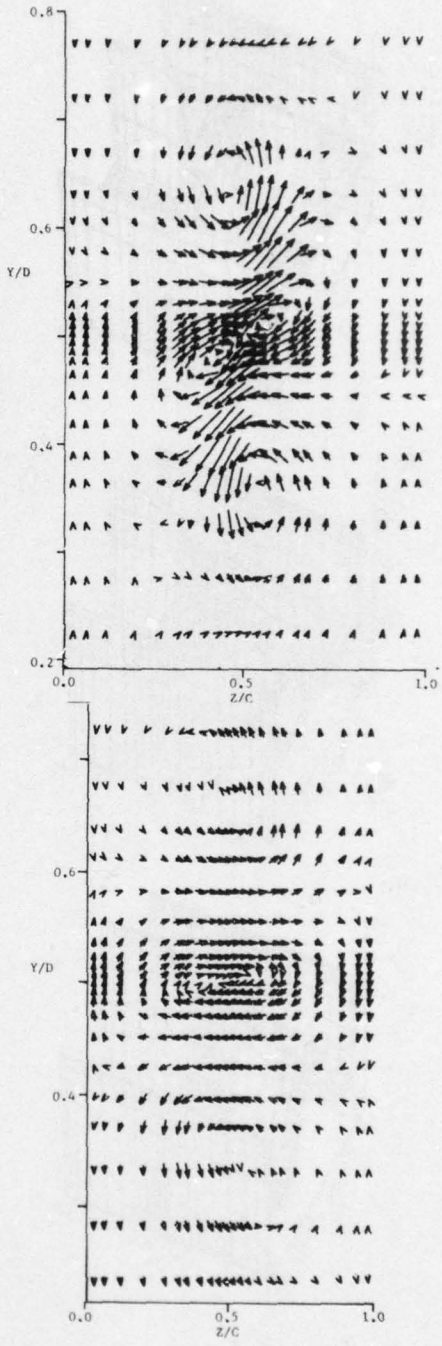

Figure 15. Vortex Centered on Cross Slots with Wedge Angle, $\phi \sim 1.33$

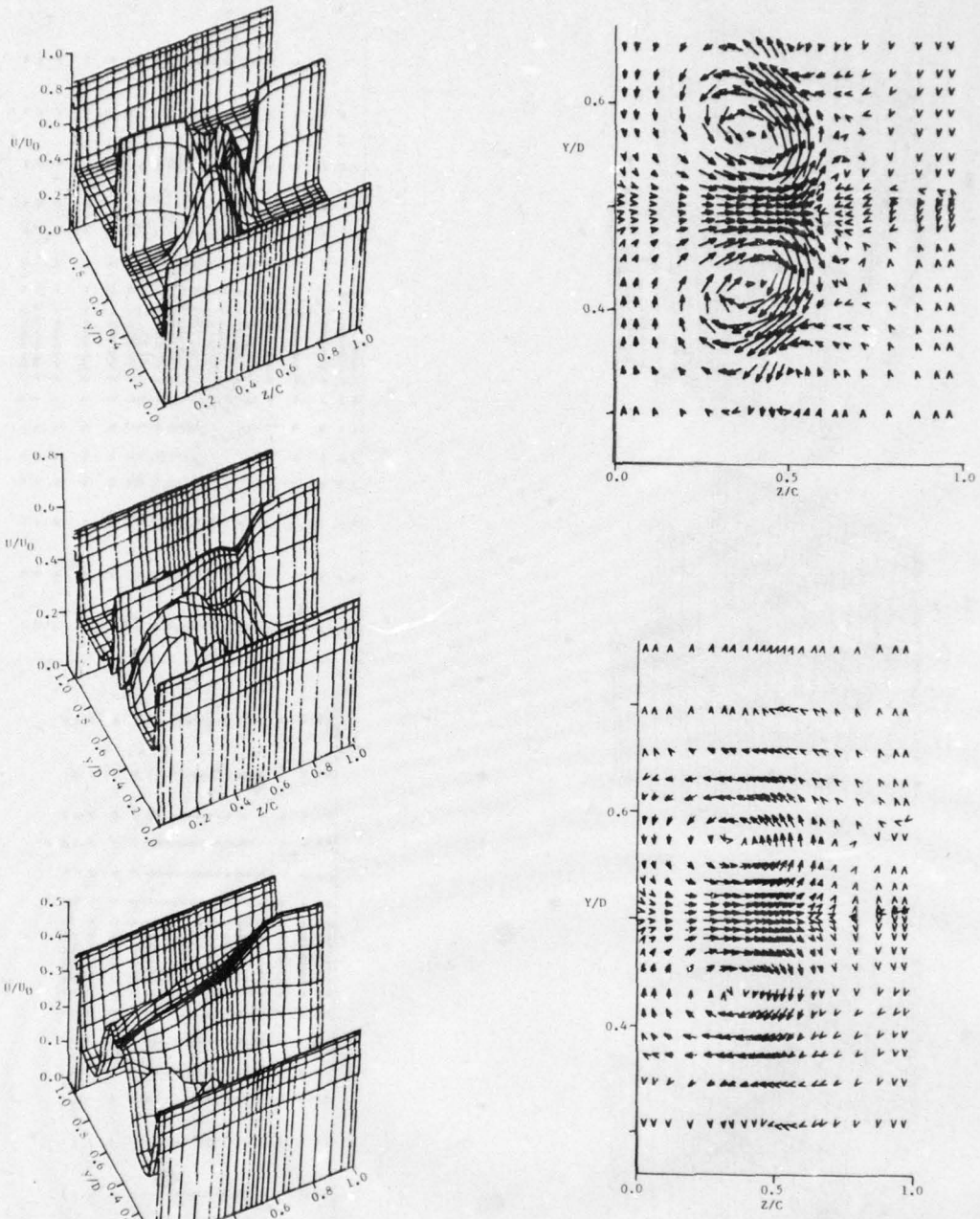

Figure 16. Vortex Centered on Each Side of the Cross Slot Elements, $\phi = 1.26$

vortex appears at the ends of each segment. The inner vortices are stronger because they include the root vortex of each tip section. The tip vortices are dissipated by the second station.

In the figure it can be seen that the dominant vortex pair induces a strong spanwise flow in the region at the center of the cross slot jet. The effect of this flow is to convect one jet spanwise across the gap and into the other, so that alternate spanwise sections of the jet are stretched out or compressed. The entrainment of the stretched sections is increased, while the entrainment of the compressed sections is reduced. Initially, the entrainment of the cross slot jets is increased by the vortices. However, the mutual attraction of the two strong vortices inhibits the chordwise spreading of these jet segments. By the exit of the ejector, the cross slot jets have virtually collapsed onto the centerline. The predicted augmentation ratio was only $\phi = 1.26$ for this nozzle. Another version of this nozzle having increased chordwise angularity was also examined, but virtually the same results were obtained so that the velocity profiles are not shown.

Because the mutual attraction of the counter-rotating vortices near the center of the previous nozzle reduced the chordwise spreading of the jet, a nozzle having a pair of co-rotating vortices was examined to see if they would repel each other and increase the jet spreading. The co-rotating vortices were formed by deflecting the ends of each cross slot segment in opposite directions, as shown in Figure 17. This produced four vortices of equal strength. In the transverse planes it can be seen that the co-rotating vortices were far enough apart that they did not merge together. The chordwise spreading of the jet was enhanced in this case and the spanwise mixing was more uniform. The augmentation ratio was increased to $\phi = 1.36$ by this nozzle.

The last nozzle in this group is shown in Figure 18. An array of six vortices was formed by deflecting the cross slot segments as shown.

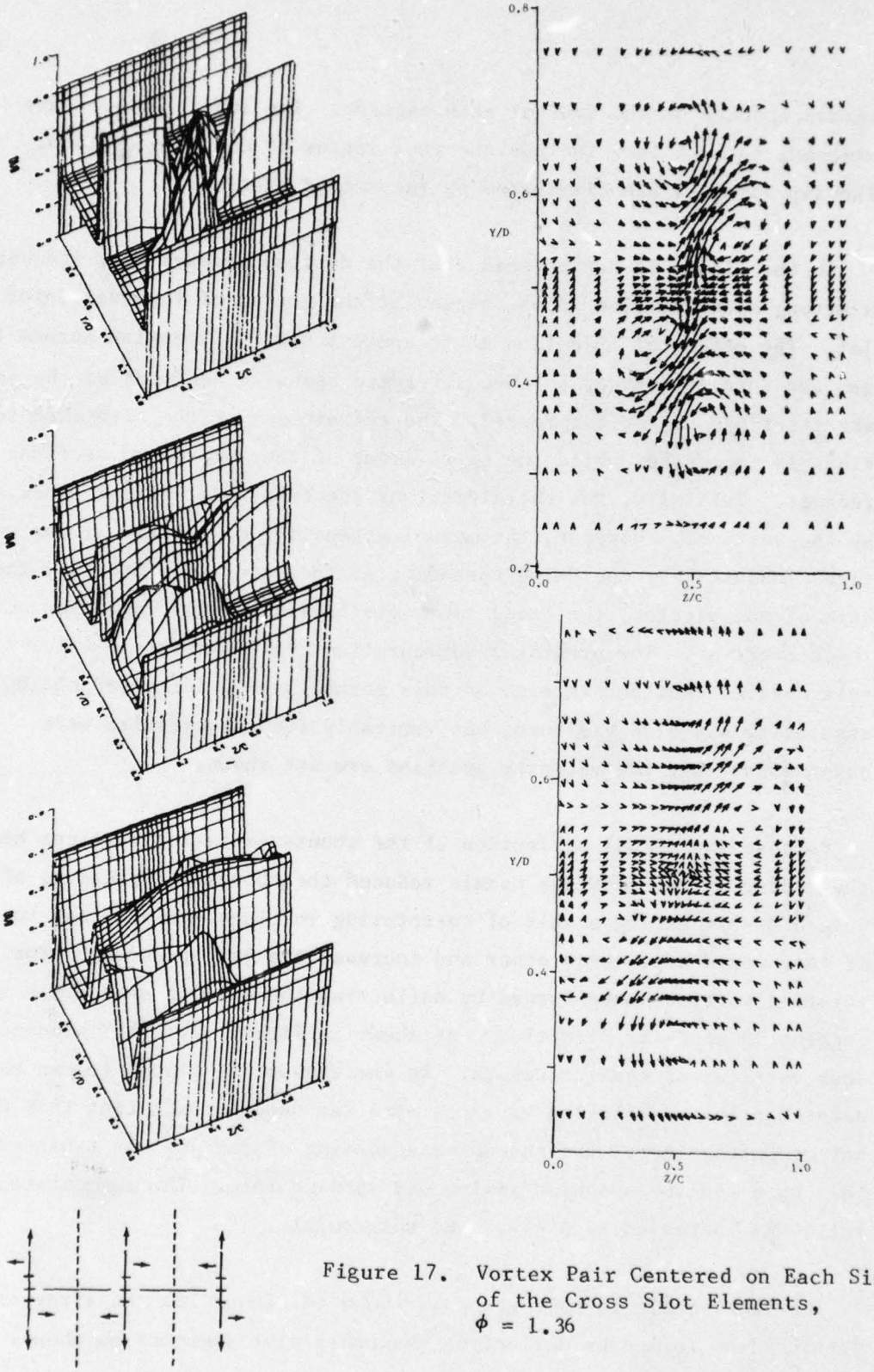

Figure 17. Vortex Pair Centered on Each Side of the Cross Slot Elements, $\phi = 1.36$

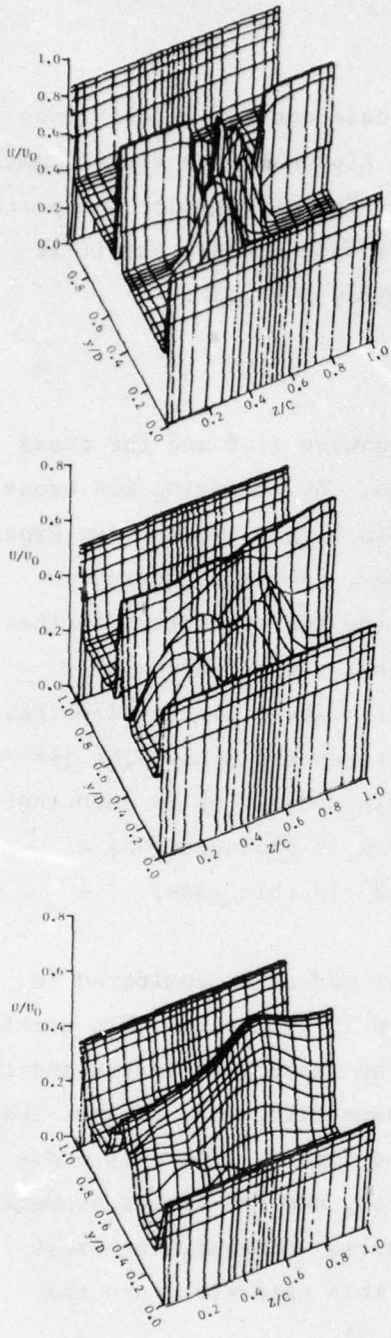

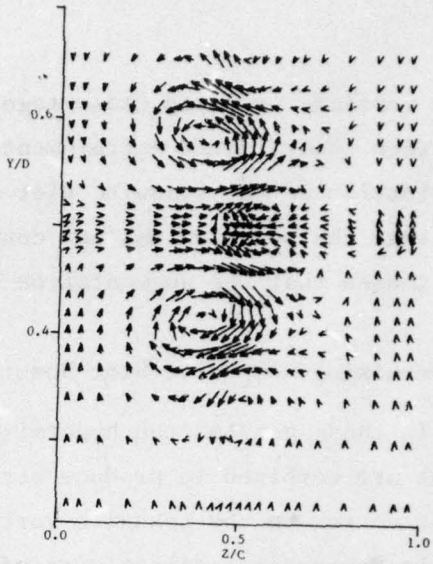

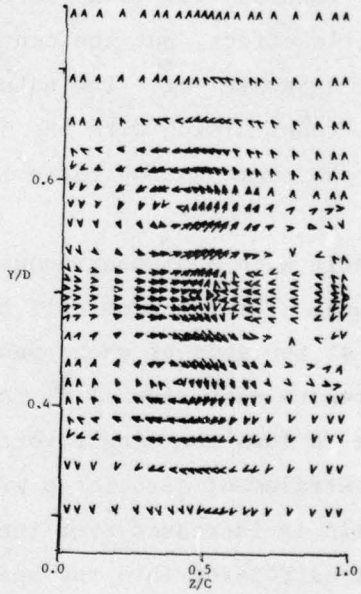

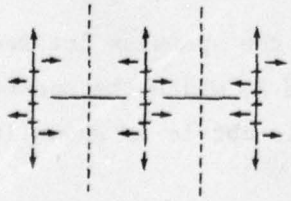

Figure 18. Vortex Array Centered on Each Side of the Cross Slot Elements, $\phi \sim 1.26$

The vortices were too close together in this case and the interference between them limited entrainment by the cross slot although significant distortion of the spanwise slot was produced. The performance was poor, so that the solution was not converged in this case either, but it is estimated that the augmentation was approximately $\phi \sim 1.26$.

Hypermixing Composite Slot Nozzles

In these nozzles the hypermixing in the spanwise slot and the cross slot are combined to produce stronger vortices. By centering the cross slot vortex on the spanwise vortex, as shown in Figure 19, the two hypermixing mechanisms directly reinforce each other. A single vortex is seen in the throat plane, at the junction of the two segments. Further downstream, a pair of weak tip vortices are just visible along the diagonal running from lower left to upper right. These tip vortices have very little effect, but the central vortex rotates the cross slot jet into the spanwise jet. The nature of this bulk convection is such that no significant mixing with the secondary stream is produced. As a result, the augmentation ratio is low--$\phi = 1.27$ in this case.

A nozzle with a discontinuous spanwise slot was also considered in this group. The jet from this nozzle is shown in Figure 20. Tip vortices develop at the ends of each spanwise slot. The cross slot vortex and the tip vortex on each side of it rotate in the same direction, so that they coalesce to form the single vortex seen in the figure. There is additional entrainment associated with this process, and the thrust augmentation ratio is increased over the previous nozzle. However, the cross slot jet is rotated into the spanwise jet in this case also, and the augmentation ratio is only increased to $\phi = 1.31$.

Because the rotation of the cross slot jet into the spanwise jet seems to limit the entrainment of these nozzles, a nozzle in which the spanwise slot rotates with the cross slot was examined. This nozzle is shown in

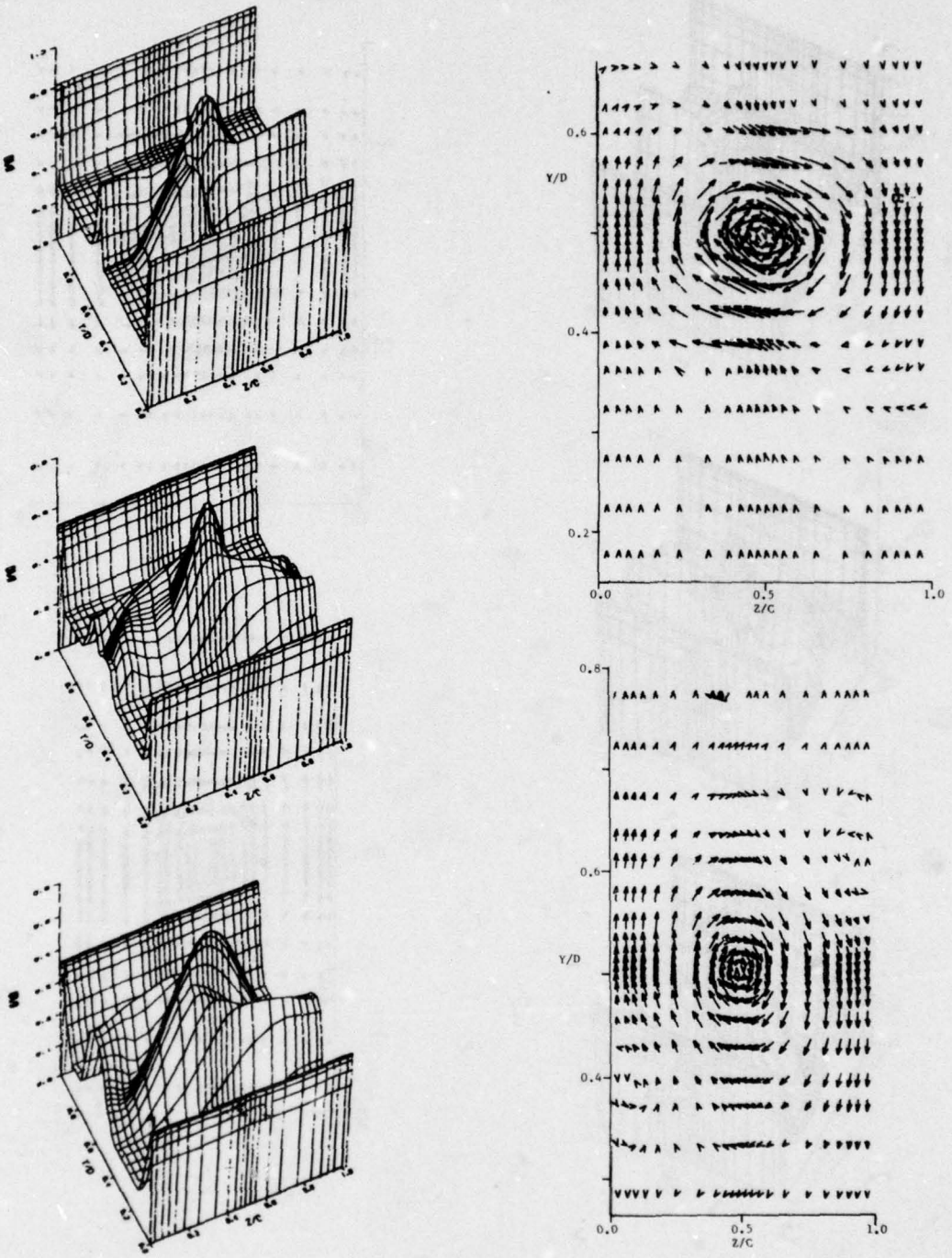

Figure 19. Composite Nozzle with Continuous Span Slot, ϕ = 1.27

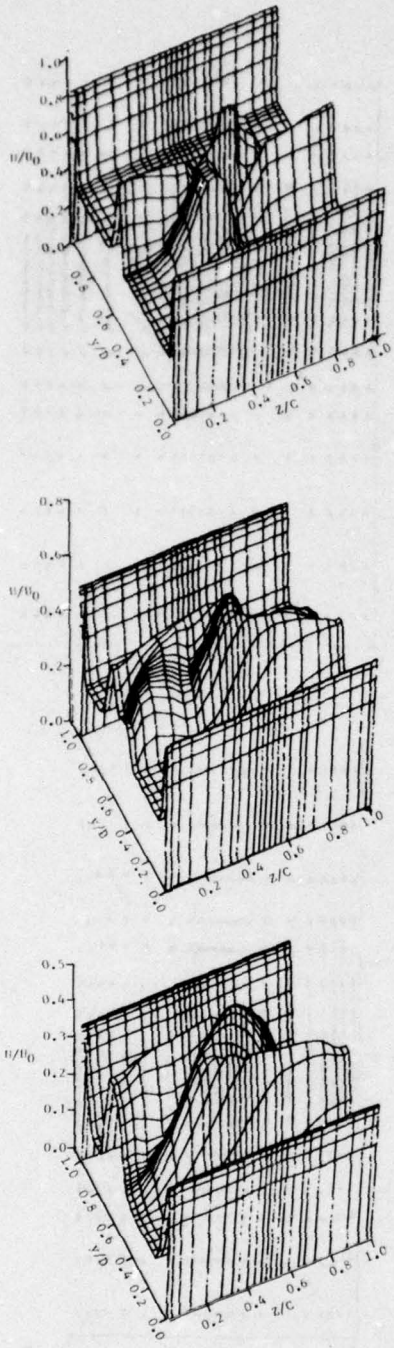

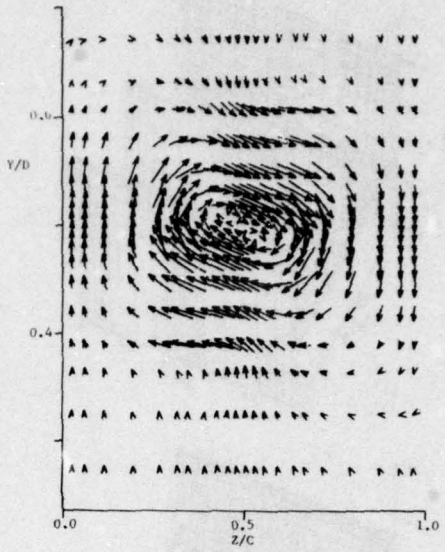

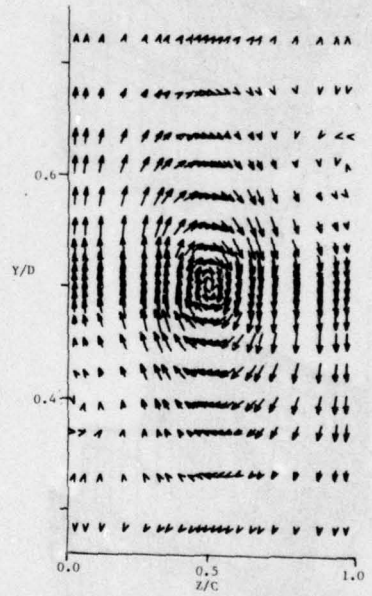

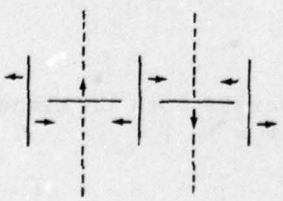

Figure 20. Composite Nozzle with Discontinuous Span Slot, ϕ = 1.31

Figure 21. The "arms" of the cross are initially deflected so that they all rotate in the same direction. A large vortex is generated at the center of the cross, and a weaker tip vortex appears at the end of each arm. At the throat plane only the three vortices on the centerline of the ejector can be seen, but all five vortices are visible in the second transverse plane. The tip vortices are located at the ends of the diagonals in this plane, which indicates that the arms have rotated at the same rate.

However, the entrainment of the jet is reduced by this motion. The augmentation ratio is only $\phi = 1.23$. As previously noted, the effect of centrifugal forces on the turbulence is not included in the model. In an actual jet these forces may be expected to increase the entrainment over what is predicted here, but probably not enough to make the performance of this nozzle competitive.

In order to reduce the rotation of the cross slot jet and thus prevent its collapse, a section at the center of the cross slot was left undeflected, as shown in Figure 22. This nozzle is similar to that in Figure 17, except that hypermixing is added to the spanwise slot. Such a nozzle has no symmetry plane, so that it was necessary to leave out every other hypermixing vortex to create a boundary for the calculations. This artifice causes some asymmetry in the development of the jets, but it can be seen that the hypermixing vortex is relatively weak, anyway. The predicted augmentation ratio, $\phi = 1.36$, is the highest of any nozzle in this group; however, it does not outperform the baseline hypermixing nozzle.

Other Nozzle Types

Some of the nozzles investigated did not fall into any of the previous classifications. These nozzles will be discussed in this section.

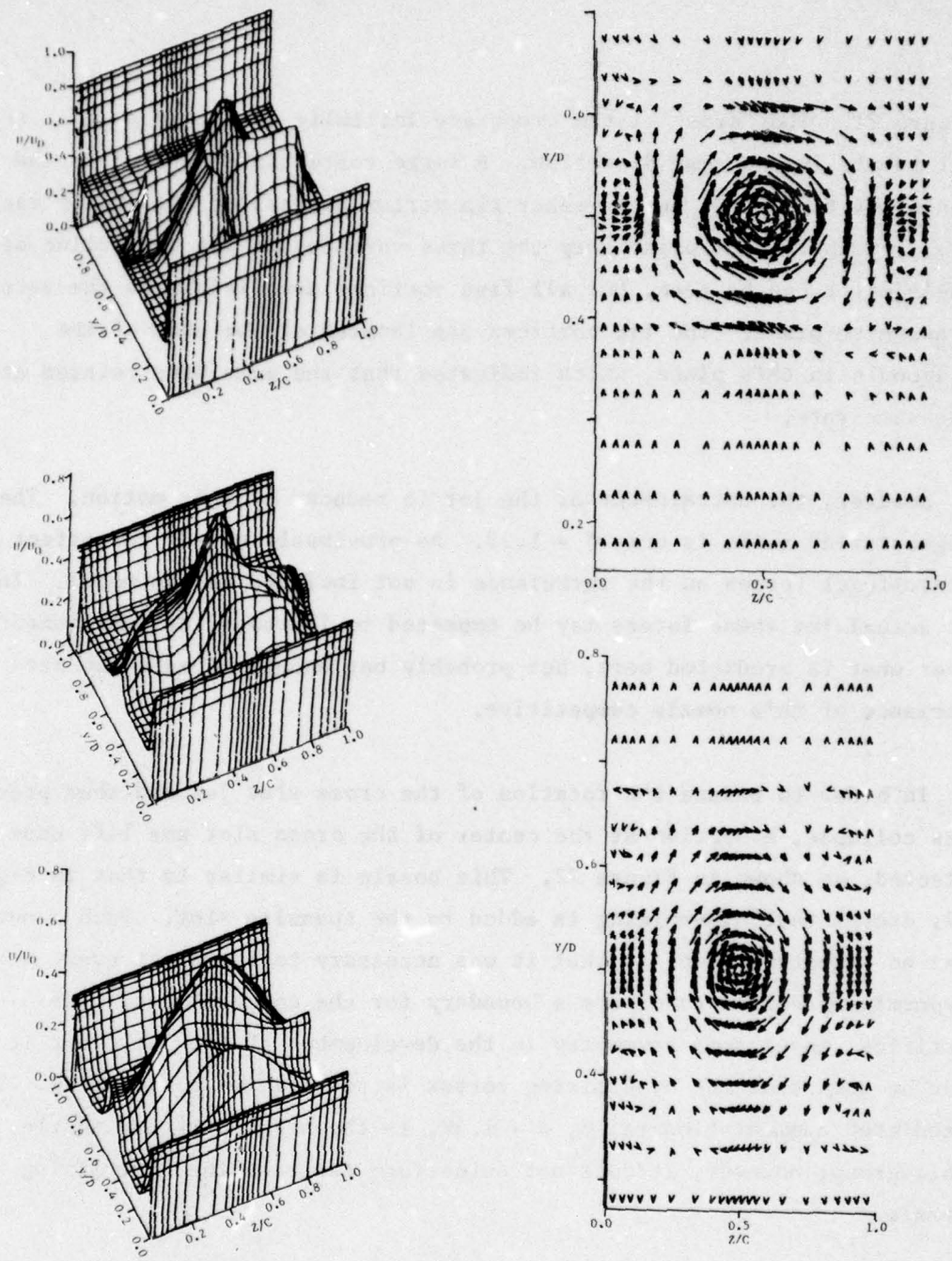

Figure 21. Hypermixing Cruciform Nozzle, ϕ = 1.23

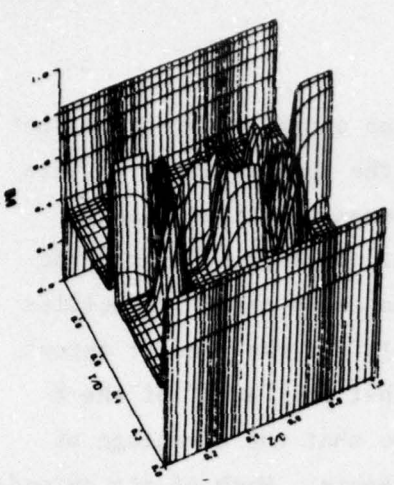

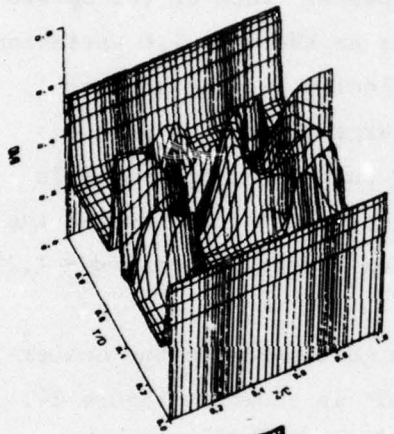

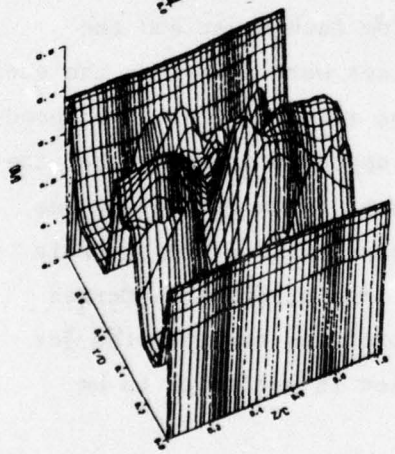

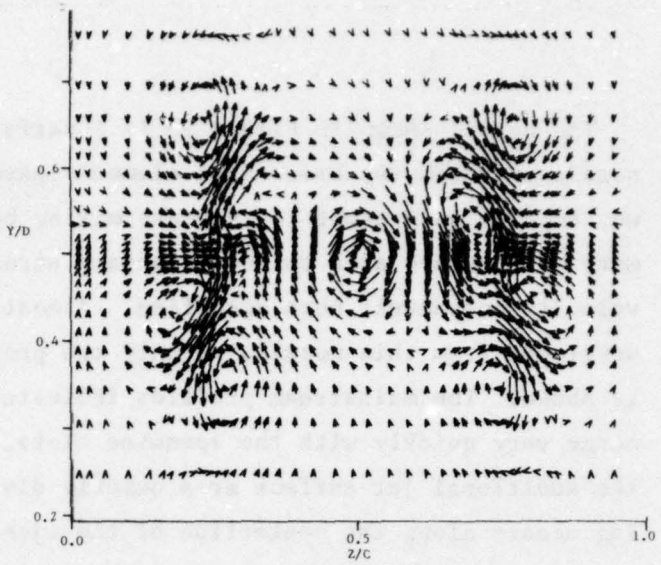

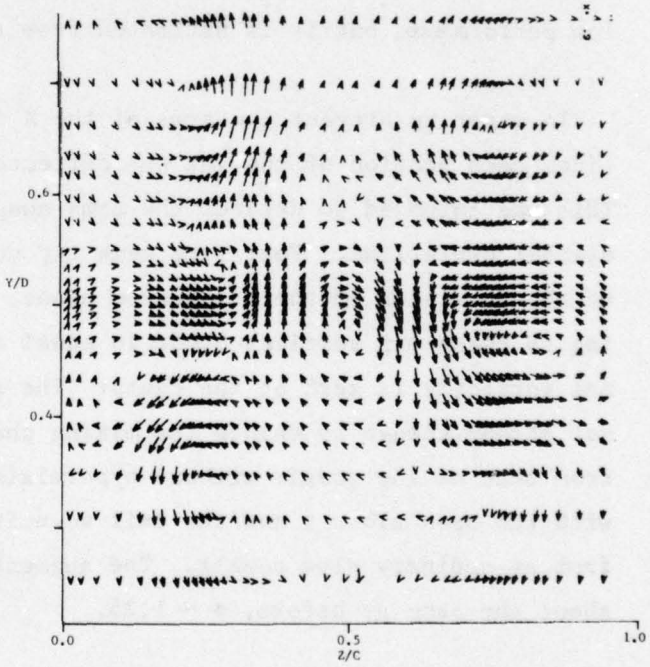

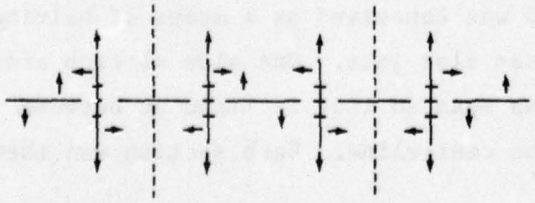

Figure 22. Composite Nozzle with Vortex Centered Between Cross Slot Elements, $\phi = 1.36$

The nozzle shown in Figure 23 is a variation on the alternating slot nozzle in which the cross slot elements have the form of an "X." This was done in an attempt to increase mixing by exposing significantly more jet surface area to the secondary stream. No initial transverse velocity components were specified. Almost no cross stream velocities developed from this nozzle, so only the profile for the ejector throat is shown. The mainstream profiles indicate that the "arms" of the X merge very quickly with the spanwise slots, so that the advantage of the additional jet surface area quickly disappears. Much of the spreading occurs along the centerline of the ejector as the spanwise variations are leveled out. By the ejector exit, the velocity profile appears similar to that from a slot jet. There are large regions of unmixed secondary flow as a result of the poor mixing characteristics of this nozzle. The ejector solution was not converged in this case due to the low performance, but it is estimated from the exit pressure that $\phi \sim 1.25$.

In order to prevent the arms of the X from collapsing on the centerline, each section of the jet was deflected 15° as shown in Figure 24. This was intended to deflect the arms away from each other and the ejector centerline. Four very weak tip vortices were formed on the ends of the X as seen in the transverse plane. The root vortices corresponding to these tip vortices occur in equal and opposite pairs so that the net vorticity is zero at the center The effect of the deflection was not strong enough to change the mixing characteristics of this nozzle from that of the nozzle without hypermixing. Again, the arms merged with the span slots , and the exit velocity profiles resemble the jet from an ordinary slot nozzle. The augmentation is estimated to be about the same as before, $\phi \sim 1.25$.

The nozzle sketched in Figure 25 was conceived as a means of halving the effective separation of the cross slot jets. One side of each cross slot section was displaced along the span so that it lined up between sections on the opposite side of the centerline. Each section was then

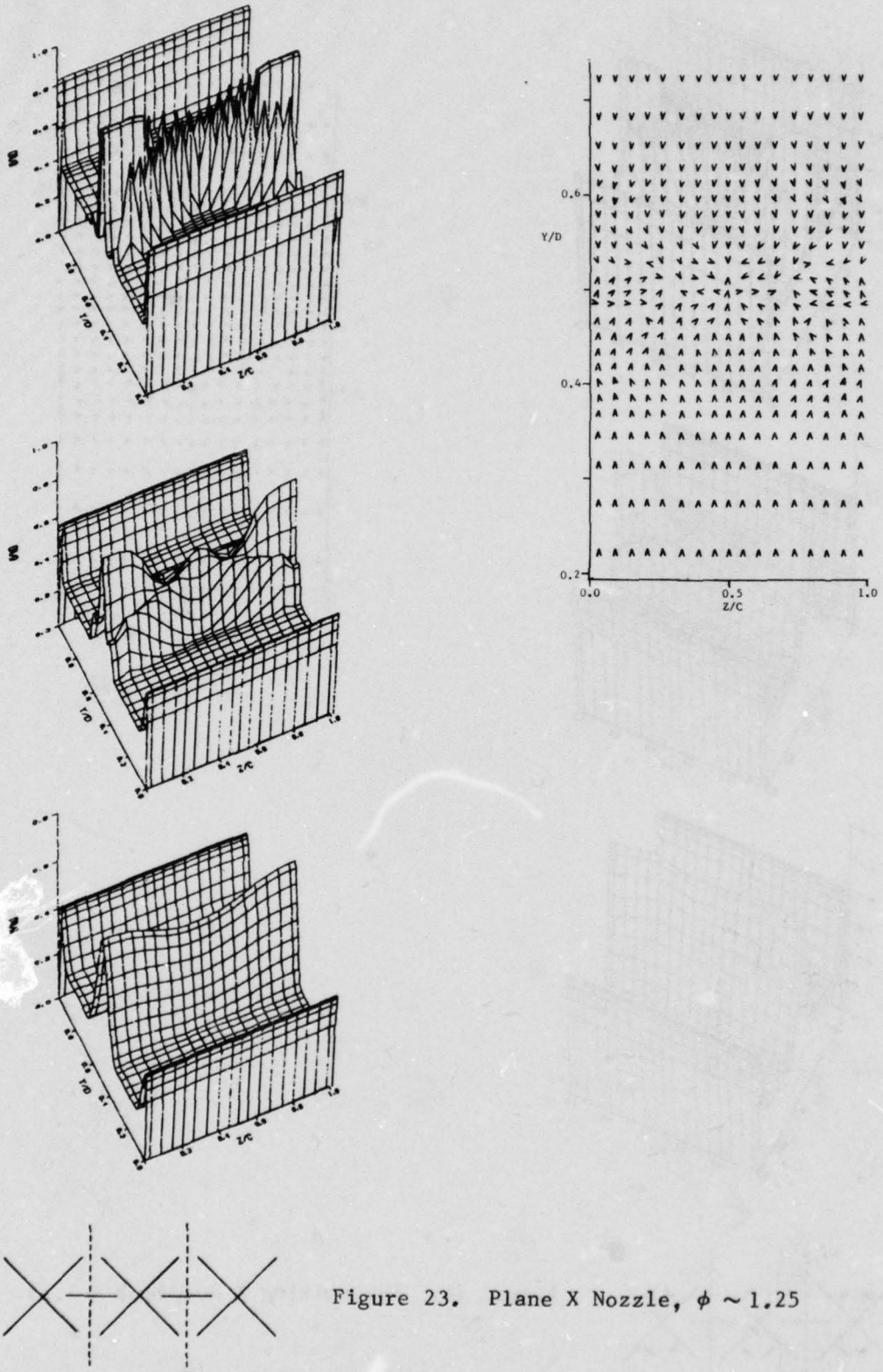

Figure 23. Plane X Nozzle, $\phi \sim 1.25$

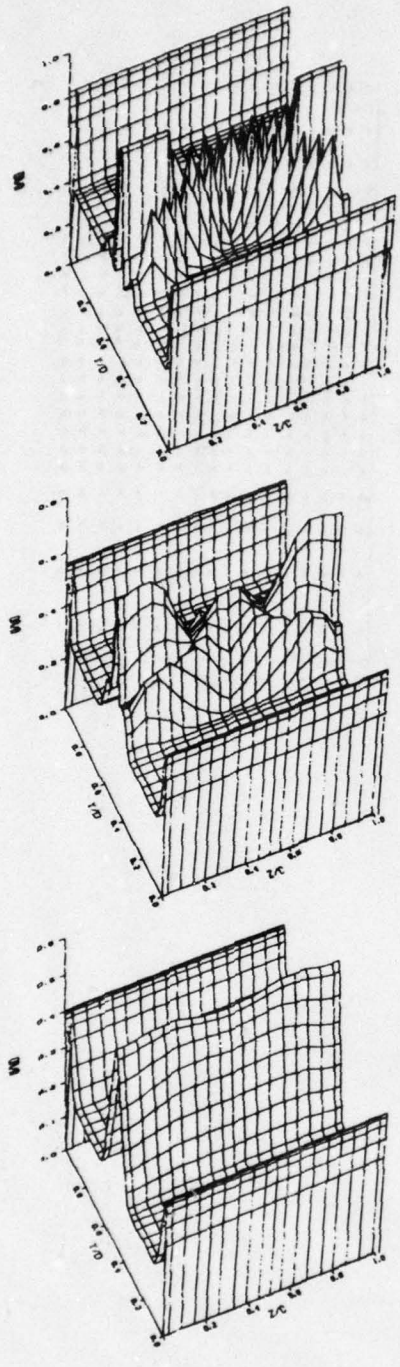

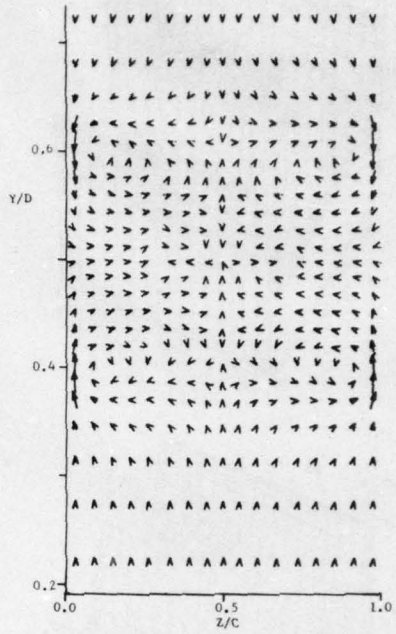

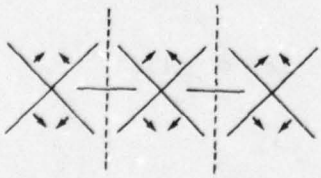

Figure 24. Hypermixing X Nozzle $\phi \sim 1.25$

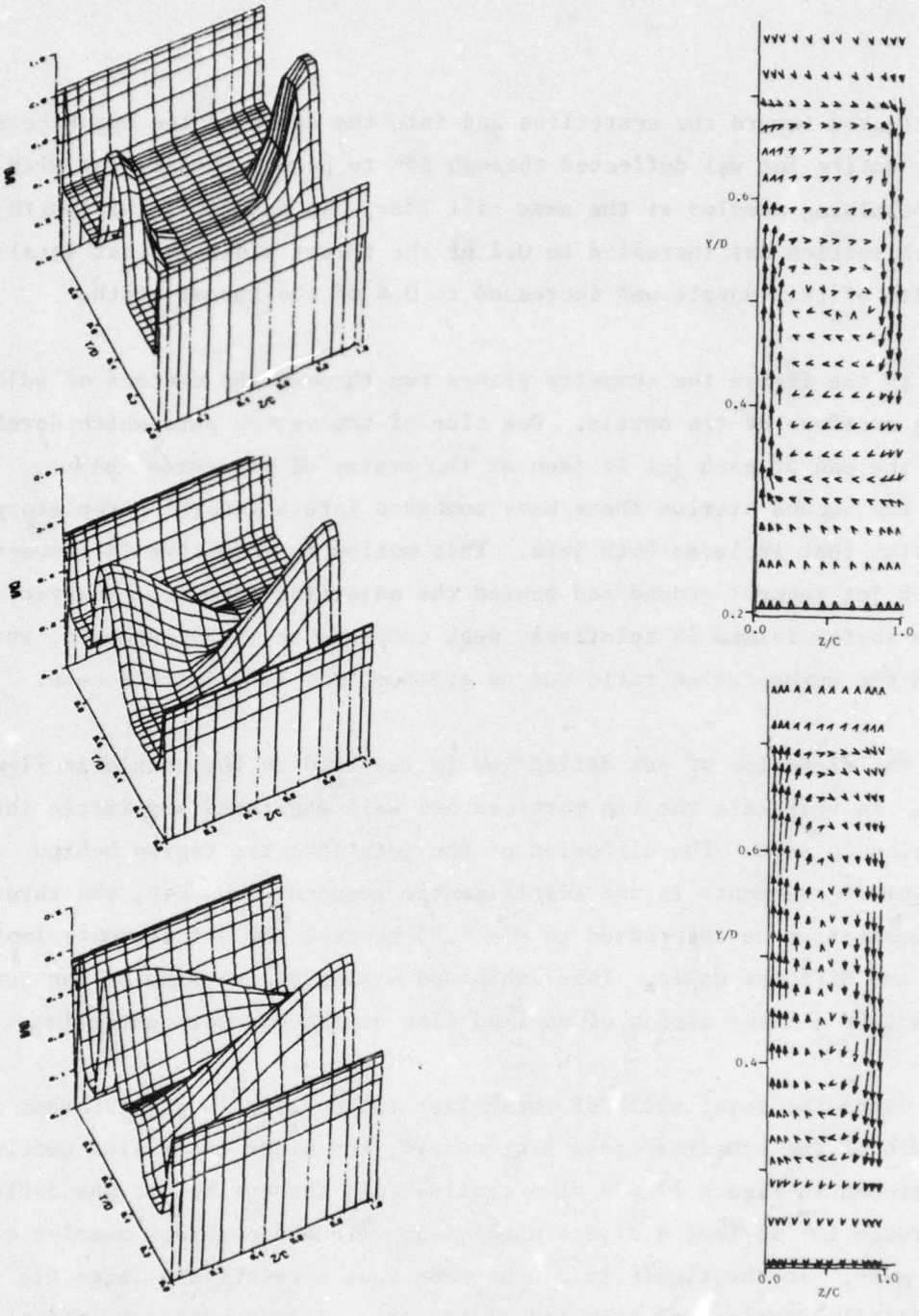

Figure 25. Staggered Cross Slot Nozzle with Inward Blowing, ϕ = 1.37

deflected toward the centerline and into the space on the opposite side. The entire jet was deflected through 15° to permit comparisons with the hypermixing nozzles at the same tiit loss. In addition, the length of each section was increased to 0.2 of the throat width so that total width of this nozzle was increased to 0.4 of the throat width.

In the figure the symmetry planes run through the centers of adjoining sections of the nozzle. One side of the vortex pair which develops at the end of each jet is seen at the center of the throat plane. By the second station these have combined into a general circulatory motion that includes both jets. This motion is effective in convecting each jet segment around and behind the adjoining segment. However, the vortex formed is relatively weak compared to the hypermixing vortex, and the augmentation ratio was no greater, $\phi = 1.37$ in this case.

The direction of jet deflection is reversed on the nozzle in Figure 26. In this case the tip vortices are well separated and little interaction is seen. The diffusion of the jets into the region behind adjoining segments is not significantly reduced. However, the thrust augmentation was decreased to $\phi = 1.33$ because the jet elements impinged on the diffuser walls. This inhibited mixing on one side of the jets and left a large region of unmixed flow on the ejector centerline.

Since the total width of these last two nozzles is greater than the width of the baseline cross slot nozzle, the wider cross slot nozzle sketched in Figure 27 was also considered. The entire jet was deflected through 15° so that a direct comparison with the previous nozzles could be made. In the figure it can be seen that a relatively large tip vortex initially develops at each end of the jet. This produces significant spreading of the jet, at first. However, the jet impinges on the wall in this case also so that the vortices are dissipated and the entrainment is consequently reduced. About the same level of augmentation was obtained with this nozzle as with the staggered versions, $\phi = 1.37$.

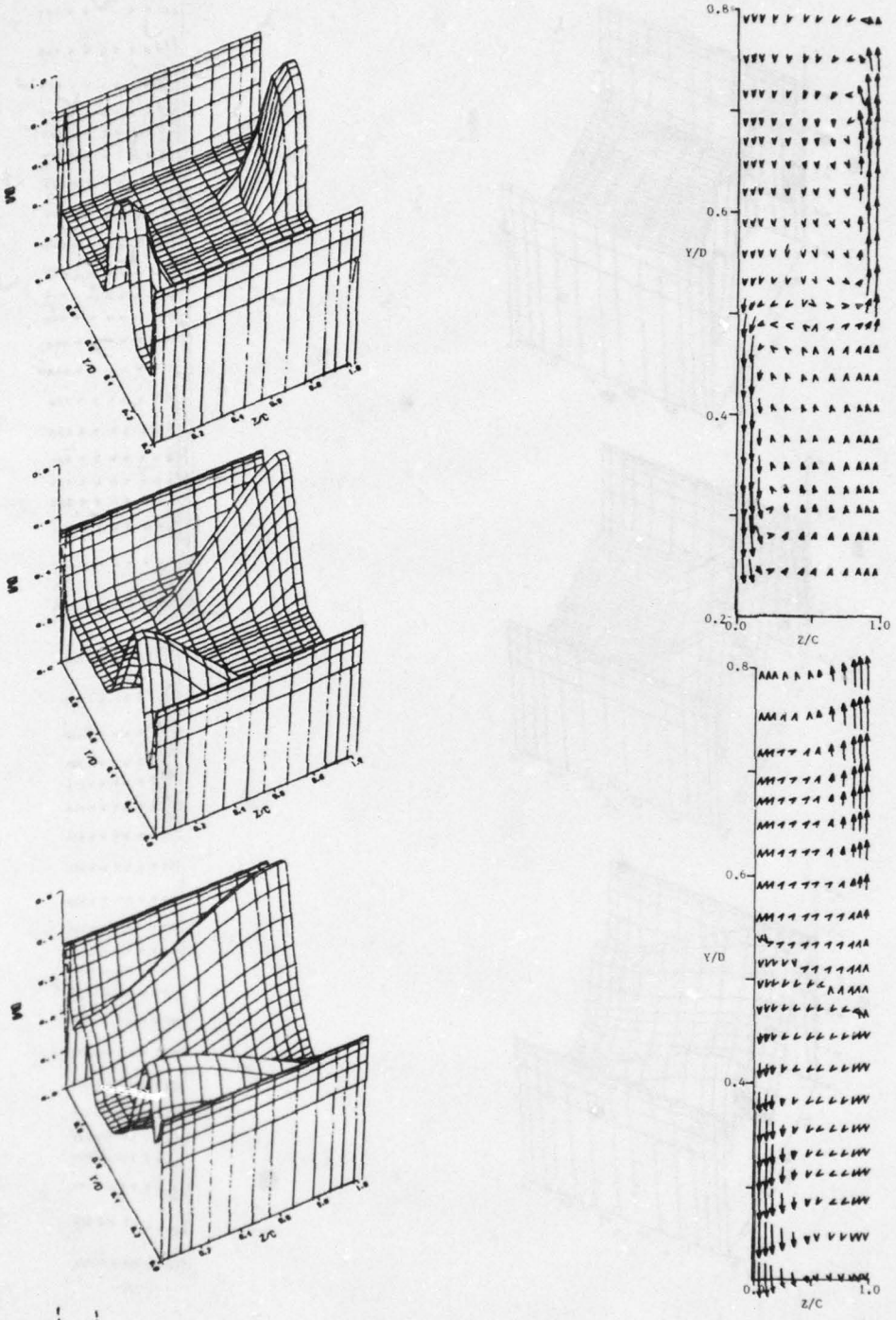

Figure 26. Staggered Cross Slot Nozzle with Outward Blowing, ϕ = 1.33

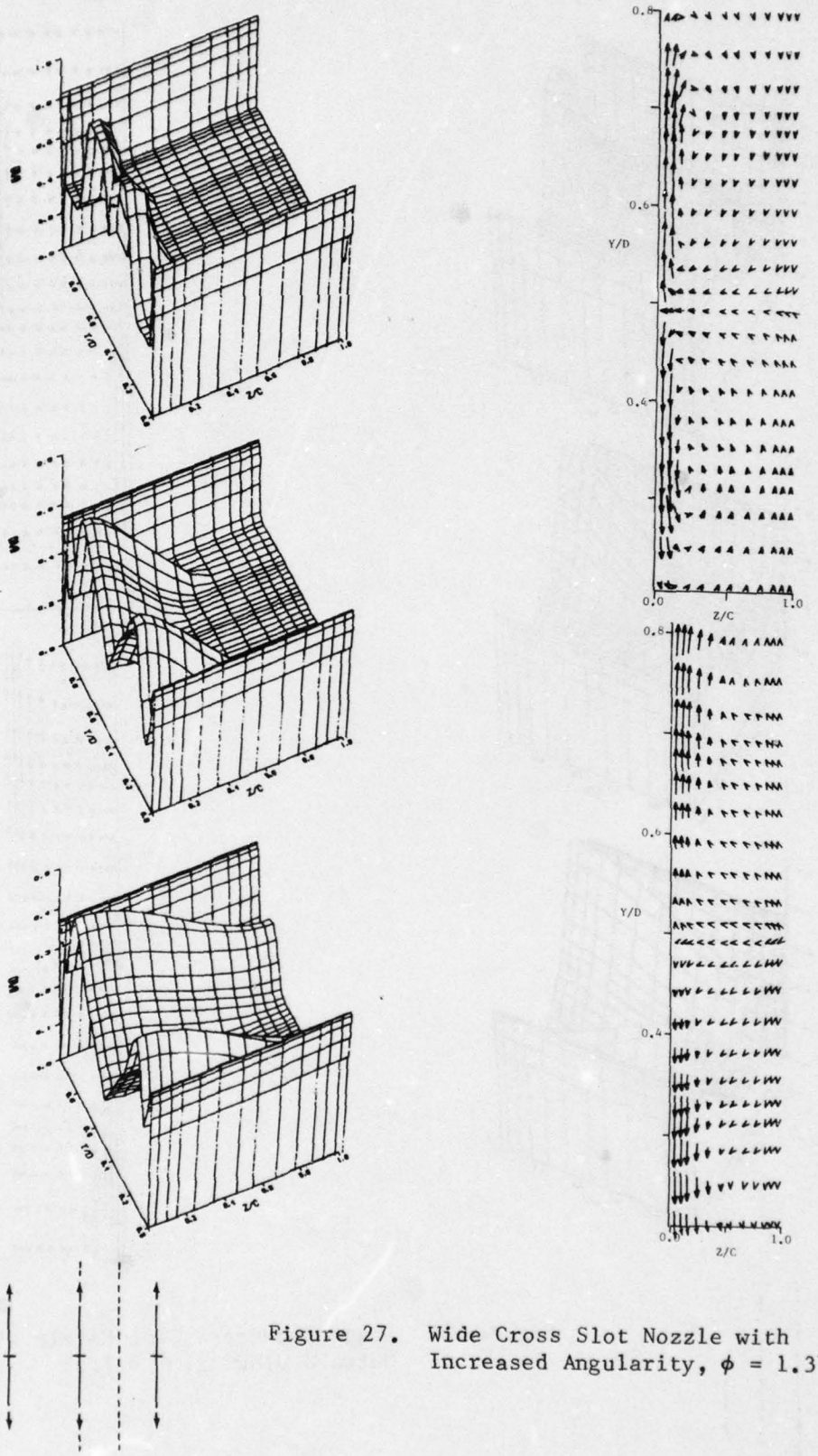

Figure 27. Wide Cross Slot Nozzle with Increased Angularity, ϕ = 1.37

Since the initial deflection of the jet was too large in these nozzles, a version of this nozzle with reduced deflection was examined. As on the narrower baseline nozzle, both transverse velocity components were varied from zero at the center of the nozzle to 15° at the ends. The development of the jet from this nozzle is seen in Figure 28. The tip vortices that developed in this case are about the same strength as on the previous nozzle. However, because this jet does not impinge on the wall, the entrainment is increased and the cross section of the jet develops the "dog bone" shape previously seen in the baseline cross slot nozzle. The greater initial length of the slots on this nozzle resulted in greater spreading of the jet. Comparison with the baseline nozzle in Figure 8 shows the increased spreading achieved by the exit of the ejector. The augmentation was increased to $\phi = 1.45$ with this nozzle.

In the last nozzle to be considered, the length of the cross slot is equal to the ejector throat width. No initial transverse velocity components were specified in this case, since little chordwise spreading was required. Thus, there is no tilt loss associated with the nozzle. The development of the axial velocity profiles for one of the jets is shown in Figure 29. In this orientation the spreading of each jet is greater than if it were aligned with the ejector span, because the jet vorticity is stretched as it passes through the diffuser. Vortex stretching is the primary mechanism of turbulent energy dissipation[10] and entrainment is associated with this dissipation. It can be seen that adjacent jets have just merged with each other by the ejector exit. The augmentation ratio was increased to $\phi = 1.61$ with this configuration.

Summary of Computation Results

For the nozzles considered, the thrust augmentation ratio varied over a range from $\phi = 1.23$ to $\phi = 1.61$. Although the variety of nozzle configurations was by no means exhaustive, certain trends were clearly

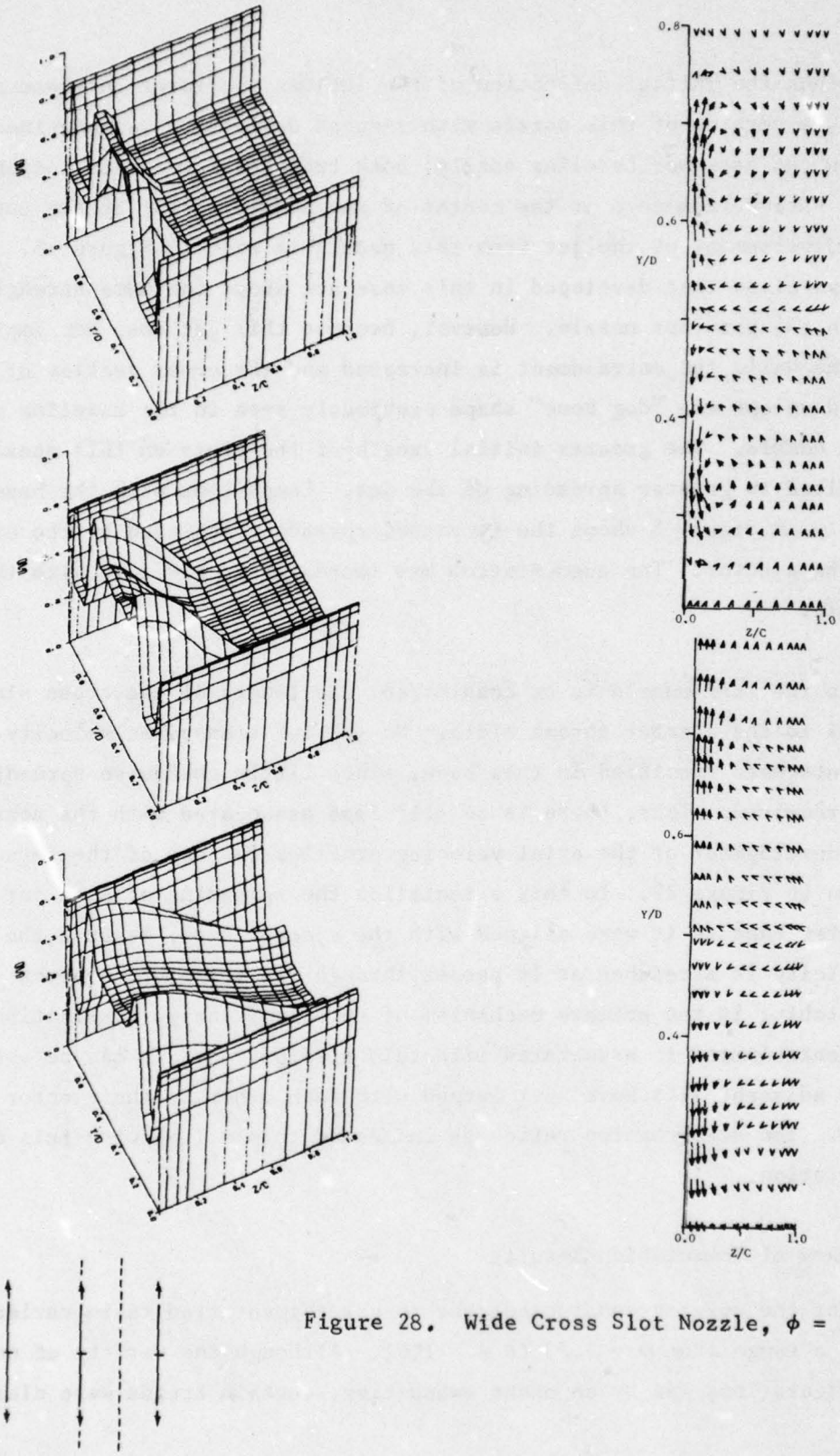

Figure 28. Wide Cross Slot Nozzle, ϕ = 1.45

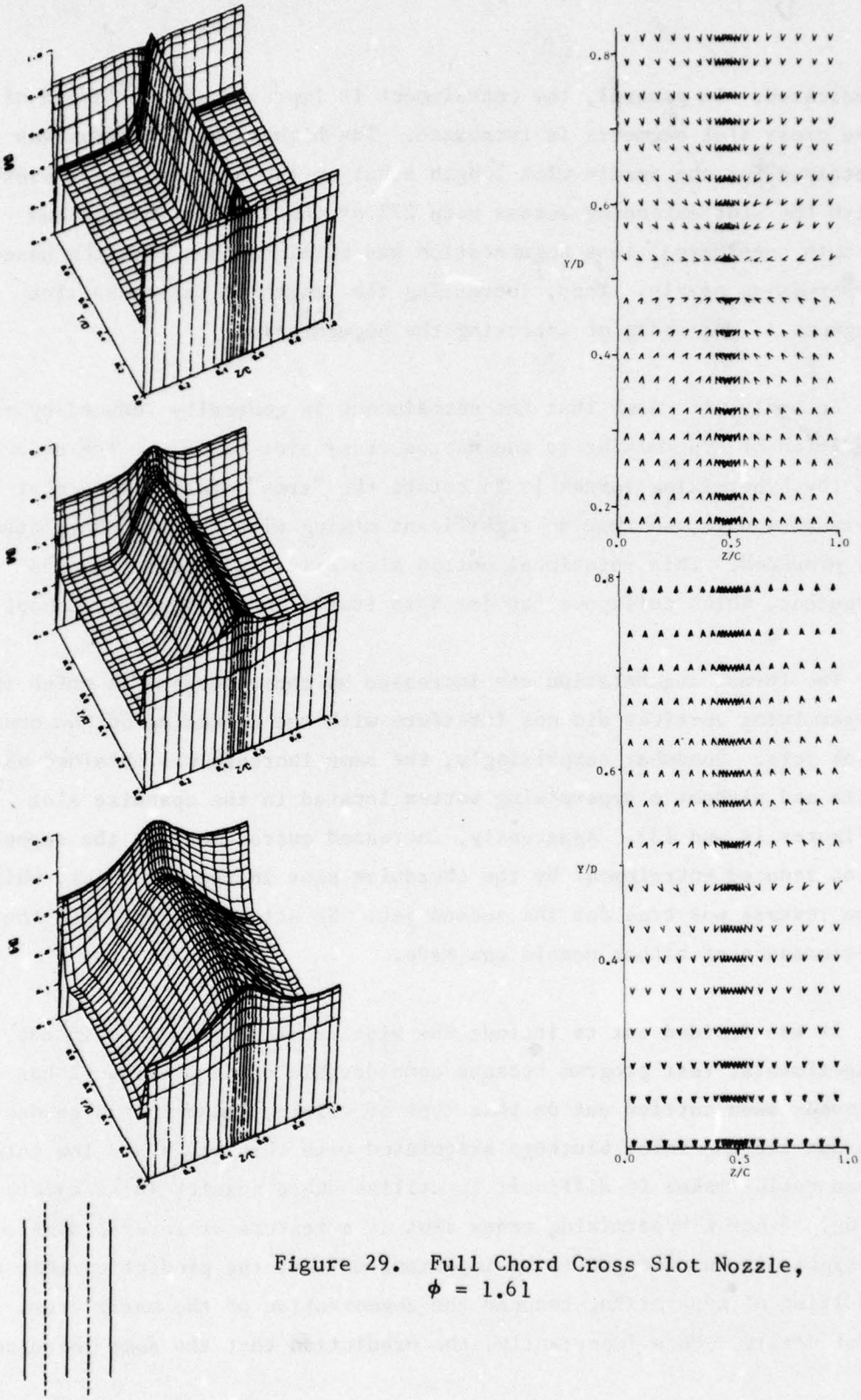

Figure 29. Full Chord Cross Slot Nozzle, ϕ = 1.61

indicated. In general, the entrainment is improved as the length of the cross slot segments is increased. The highest augmentation was obtained for the nozzle with length equal to the ejector throat width. With the slot extending across only 27% of the throat, the minimum length considered, less augmentation was obtained than with the baseline hypermixing nozzle. Thus, increasing the length of the cross slot segment is one means of improving the augmentation.

Secondly, it seems that the entrainment is generally reduced by the addition of hypermixing to the narrow cross slot nozzles. The effect of the hypermixing vortex is to rotate the "arms" of the cross slot jets as a unit, so that no significant mixing with the secondary stream is produced. This rotational motion also drives adjacent segments together, which collapses the jet into itself and limits entrainment.

The thrust augmentation was increased by those nozzles in which the hypermixing vortices did not interfere with the spreading of the cross slot jets. Somewhat surprisingly, the same increase was obtained both with and without a hypermixing vortex located in the spanwise slot (Figures 11 and 13). Apparently, increased entrainment by the spanwise slot reduced entrainment by the chordwise slot in the first jet, while the reverse was true for the second jet. No attempt to optimize the performance of either nozzle was made.

It was decided not to include the wide cross slot nozzles in the experimental test program because considerable development work has already been carried out on this type of nozzle,[11] and the large duct losses and the inlet blockage associated with thin wings and low inlet area ratios makes it difficult to utilize these nozzles in an ejector wing. Since a hypermixing cross slot is a feature of several nozzle designs, it was thought to be important to test the prediction that the addition of hypermixing reduced the augmentation of the basic cross slot nozzle. More importantly, the prediction that the same increase

in augmentation was obtained both with and without a hypermixing vortex in the section between the cross slot jets was also tested. Thus, the test program was planned to verify both trends predicted in the analytic study.

TESTS OF NOZZLE PERFORMANCE

Experimental Apparatus

The test program was actually carried out in two separate phases. Because the prediction of reduced augmentation for the hypermixing cross slot nozzles was fundamental to this study, preliminary testing was performed approximately midway through the analytical program in order to verify this result. In the interest of economy, these tests were performed by modifying the cross slot nozzle in an existing ejector. Analysis of the remaining nozzles was then completed and the hypermixing span slot nozzle was identified as having the greatest entrainment. The test program was completed by fabricating this nozzle and comparing its performance to that of the alternating slot nozzle and a hypermixing nozzle with equal area.

Although the analytic comparison of the nozzles was performed at one diffuser area ratio, testing was conducted over a range of diffuser area ratios in order to be sure of comparing the highest augmentation for each nozzle. Different ejectors were used in each phase of the testing, but both were of the type shown in Figure 3. The exit of the Coanda nozzles was fixed relative to the diffuser flaps, so that the location of this nozzle changed as the flaps were rotated to vary the diffuser angle. The augmentation ratio does have some sensitivity to the location of this nozzle, but the effect of nozzle position was the same for each test. In addition to the primary nozzles, both ejectors also had an array of boundary layer control nozzles on the endwalls to direct high pressure air into the corners of the diffuser. The thrust of these nozzles was included in calculating the thrust augmentation ratio.

The flow to each of the ejector components was measured with a separate venturi, and nozzle pressures were recorded with a total pressure probe in the nozzle exit. Internal screens were used on each of

the nozzles to smooth out spanwise total pressure variations. A static pressure probe was positioned in the ejector throat to record the pressure in the secondary stream. Venturi, nozzle and secondary pressures were read out manually on vertical water or mercury manometers, as appropriate.

The ejector models were mounted on a horizontal cradle suspended by four tie rods attached to a rigid frame. The thrust was measured with two 500-pound load cells installed on connecting arms between the lower endwall and the outer frame. The tares of the primary air supply hoses were recorded as a function of the supply pressure. This calibration was used to correct the force measured by the load cell. The thrust augmentation was calculated as the ratio of the thrust measured with the load cells to the isentropic thrust calculated for an expansion of the measured mass of primary fluid to atmospheric pressure.

During the preliminary tests of the cross slot nozzle, velocity survey data was obtained with a Model 1264 miniature conical hot film probe manufactured by Thermo Systems, Inc. A TSI Model 1050-20 constant temperature anemometer was used with this probe. In the second phase of testing, a pitot static probe was used to obtain the survey data. The probe was connected to a pair of pressure transducers which send an analog signal to an IBM 1800 computer. The total and static pressure profiles are then digitized and the velocity profiles derived from this data.

Hypermixing Cross Slot Nozzle Tests

An existing ejector model was used for testing the effect of hypermixing on a cross slot nozzle. The nozzle and ejector geometry were different from those used in the analysis, but by utilizing an existing model, the tests were performed quickly and at low cost. The test ejector is shown in Figure 30. The inlet area ratio was $A_2/A_0 = 22$ and

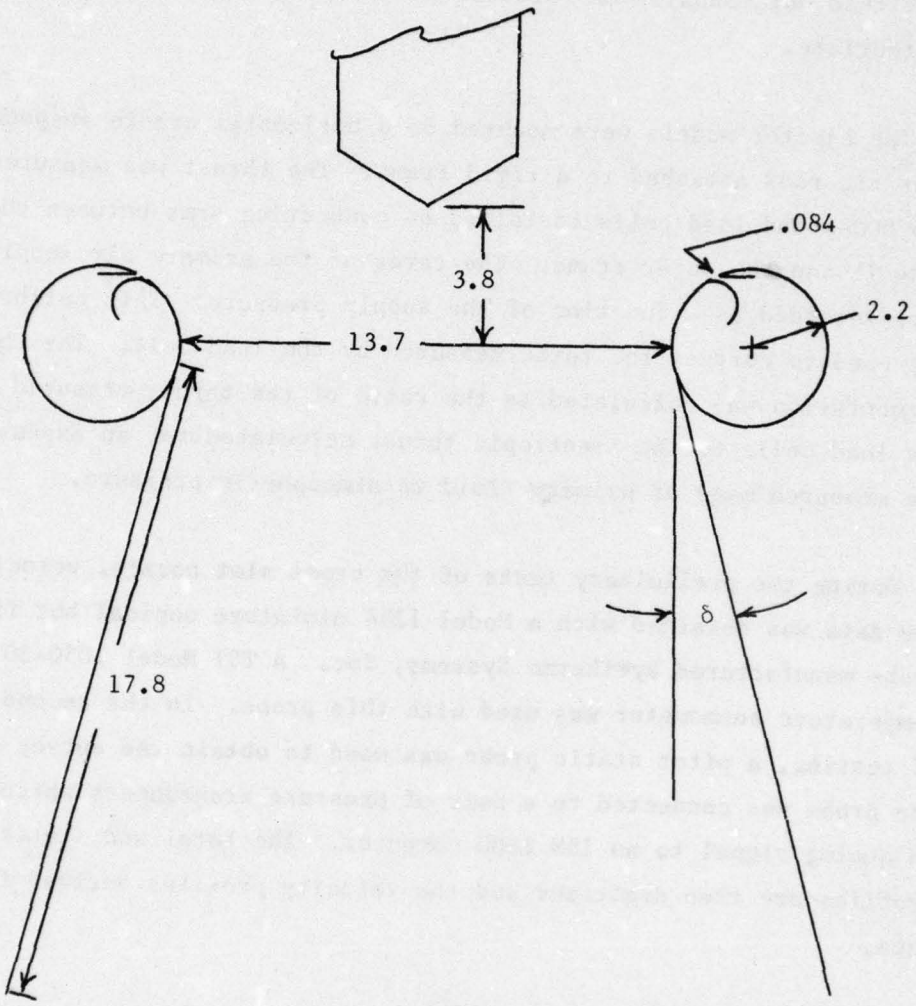

Flow Split:	Coanda	Center Nozzle	Coanda	BLC
	.15	.68	.15	.02

(All dimensions in centimeters)

Figure 30. Sectional View of Preliminary Test Ejector

the ratio of length to width was $L_e/W = 1.5$. These differences in geometry were not expected to affect the outcome of the nozzle comparison.

A sketch of the cross slot nozzle is shown in Figure 31. Each segment has an aspect ratio of 15:1 and has a length equal to 0.32 of the throat. To provide a direct comparison, the hypermixing cross slot nozzle was constructed by modifying this nozzle. Opposite sides of each element of the nozzle were cut back a distance equal to the nozzle gap; the exit of the nozzle was then closed down to restore the same exit area as prior to the modification. The modified nozzle is shown in Figure 32.

Each of the nozzles was checked to insure that the spanwise total pressure distribution was uniform, and the isolated thrust of the nozzle was measured to determine the velocity coefficient, C_V. The nozzles were then installed in the ejector, and the thrust augmentation ratio was measured over a range of diffuser area ratios. These measurements were made for nozzle exit pressure ratios of 1.5, 2.0 and 2.5. For both of the nozzles, the hot film anemometer was used to obtain midspan velocity surveys at a diffuser area ratio of 1.79, which was close to the value for peak performance. The surveys were obtained by making chordwise sweeps at the throat, midway to the augmenter exit, and at the exit. These profiles were used to compare the mixing characteristics and development of the jets through the ejector. They are shown in Figures 33 and 34. The development of the jets is as predicted by the numerical results.

A comparison of the thrust coefficient of the cross slot nozzles, with and without hypermixing, reveals a slight drop from $C_V = .91$ to $C_V = .90$ at a nozzle exit pressure ratio of 2.0. This drop is attributed to the tilt loss associated with the deflection of the jet. Thus, the entrainment of the hypermixing cross slot nozzle must be increased just to compensate for this tilt loss. However, the measured performance

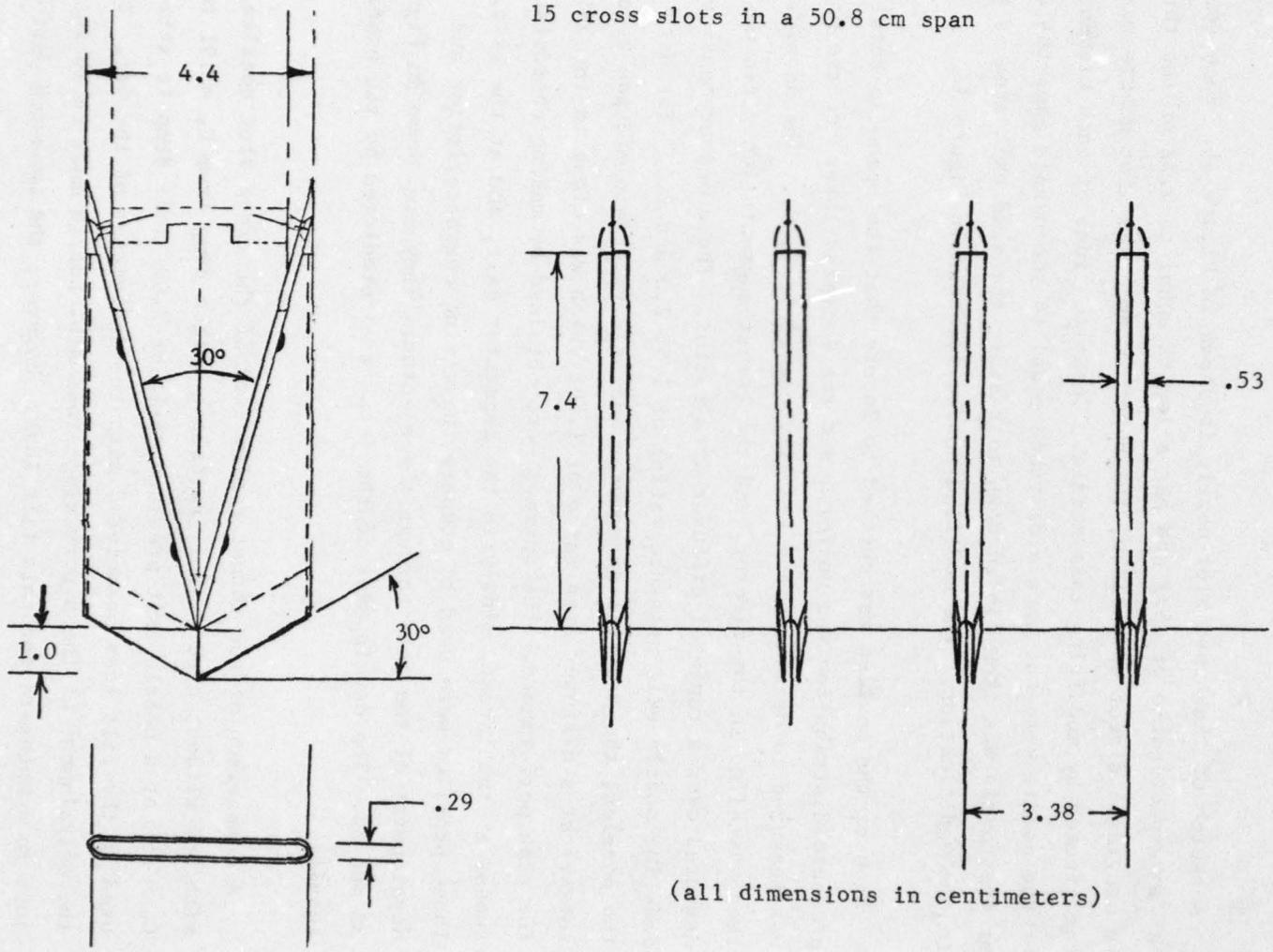

Figure 31. Test Cross Slot Nozzle

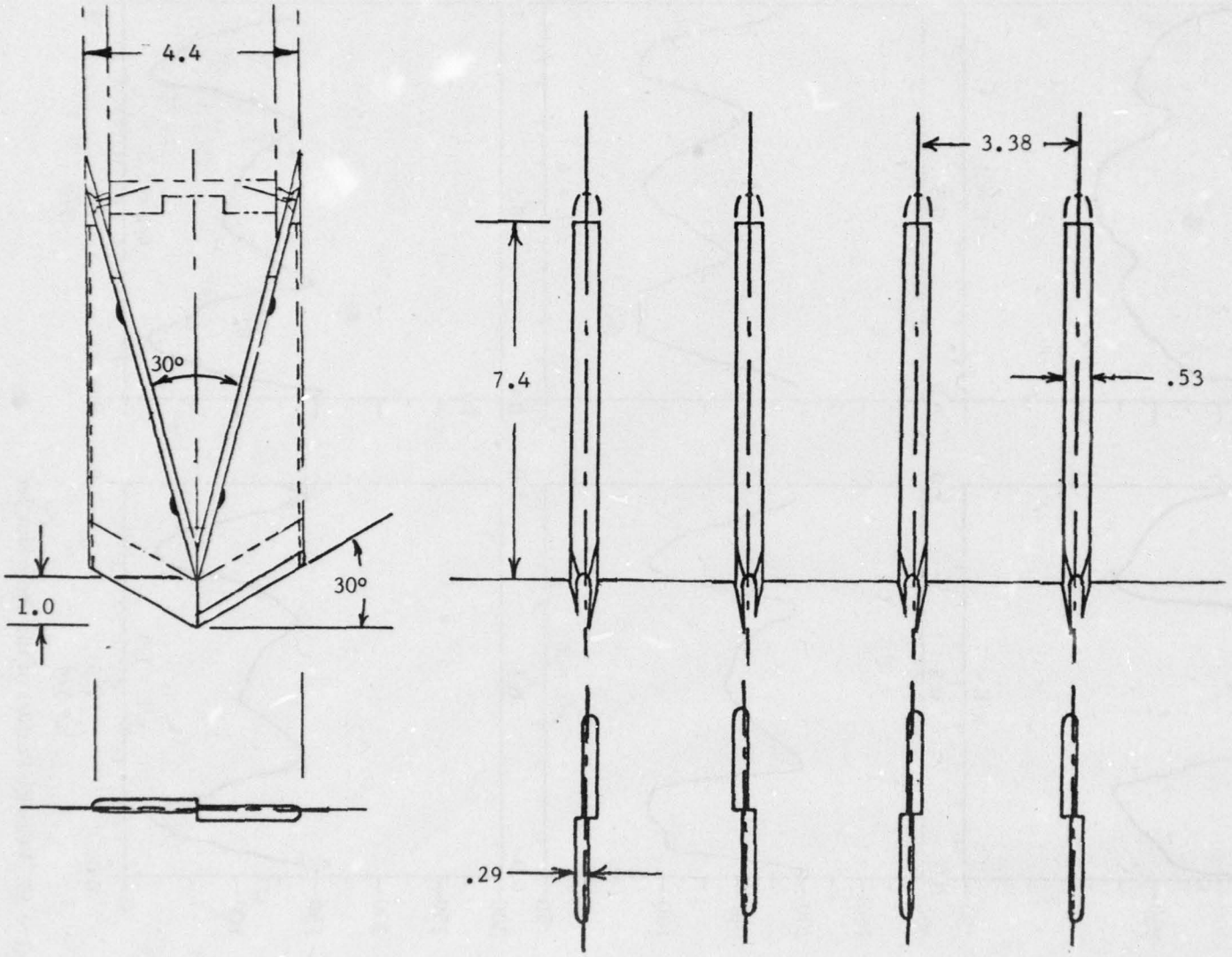

Figure 32. Test Hypermixing Cross Slot Nozzle

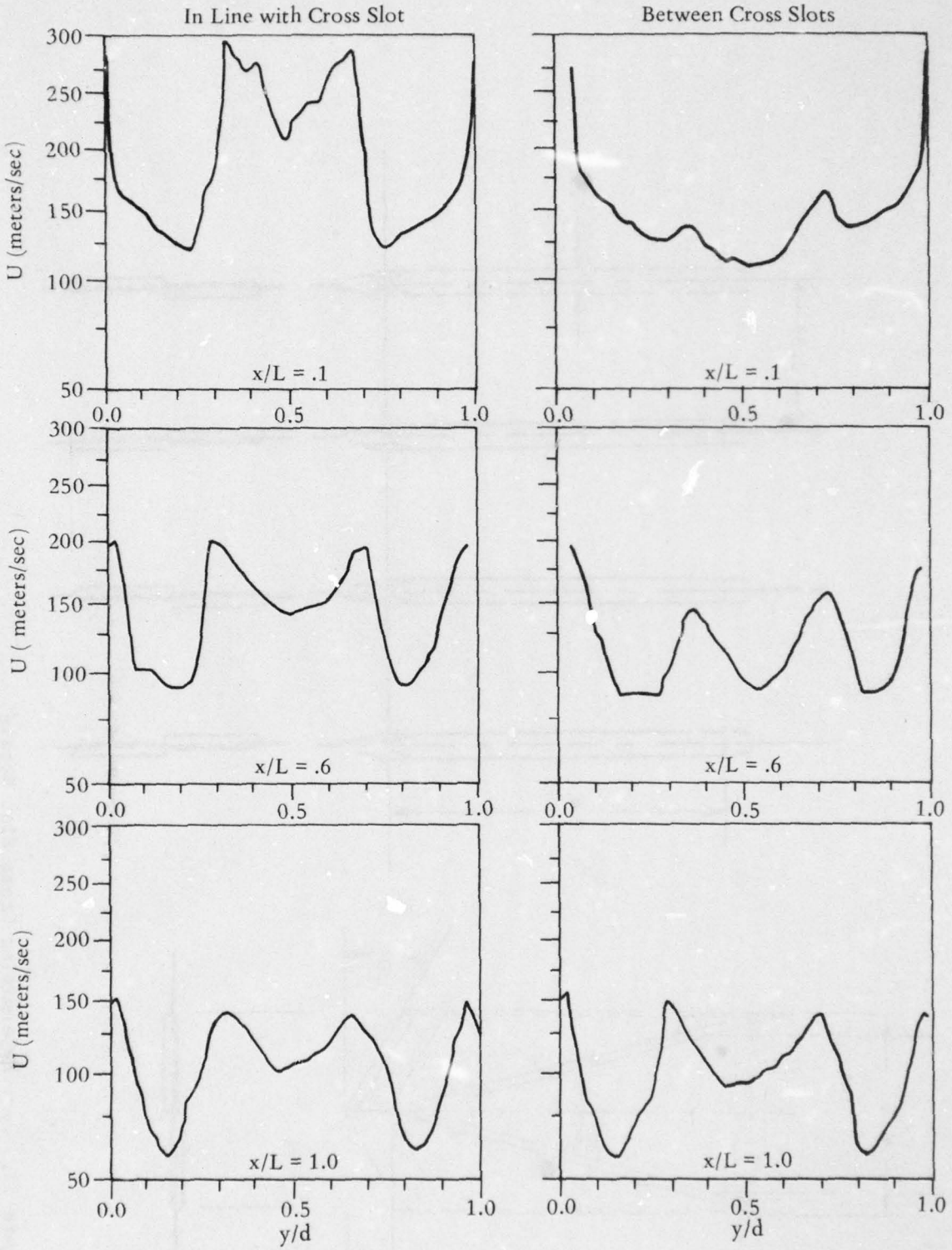

Figure 33. Velocity Profiles of the Cross Slot Jet

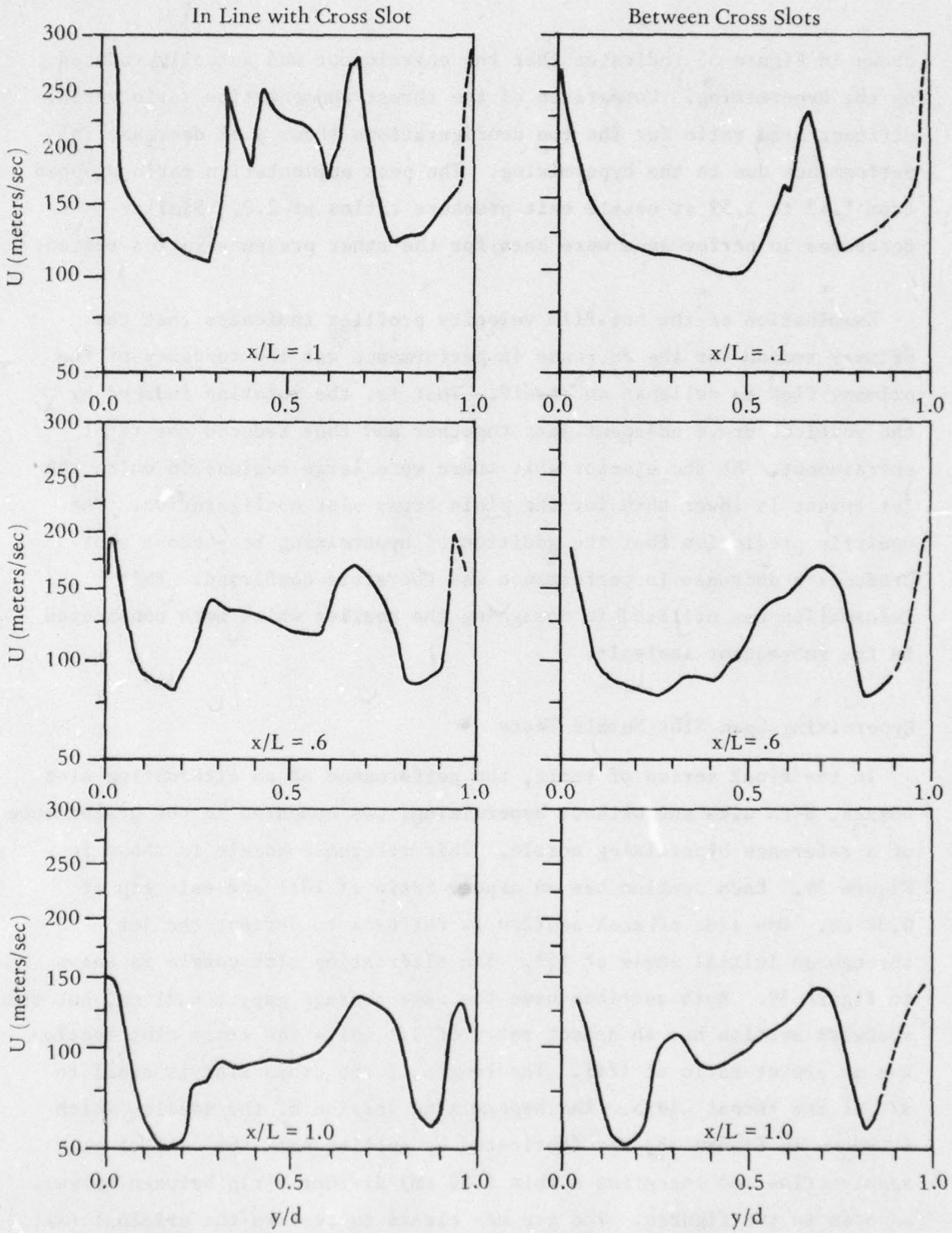

Figure 34. Velocity Profiles of the Hypermixing Cross Slot Jet

shown in Figure 35 indicates that the entrainment was actually reduced by the hypermixing. Comparison of the thrust augmentation ratio versus diffuser area ratio for the two configurations shows a 6% decrease in performance due to the hypermixing. The peak augmentation ratio dropped from 1.62 to 1.52 at nozzle exit pressure ratios of 2.0. Similar decreases in performance were seen for the other pressure ratios tested.

Examination of the hot film velocity profiles indicates that the primary reason for the decrease in performance was the tendency of the primary flow to collapse on itself. That is, the rotation induced by the vortices drove adjacent jets together and thus reduced the total entrainment. At the ejector exit there were large regions in which the jet thrust is lower than for the plain cross slot configuration. The analytic prediction that the addition of hypermixing to a cross slot produces a decrease in performance was therefore confirmed. This information was utilized in designing the nozzles which were considered in the subsequent analysis.

Hypermixing Span Slot Nozzle Tests

In the final series of tests, the performance of an alternating slot nozzle, both with and without hypermixing, was compared to the performance of a reference hypermixing nozzle. This reference nozzle is shown in Figure 36. Each section has an aspect ratio of 10:1 and exit gap of 0.30 cm. One side of each section is cut back to deflect the jet through an initial angle of 15°. The alternating slot nozzle is shown in Figure 37. Both sections have the same average gap, t = .21 cm, but the spanwise section has an aspect ratio of 9:1 while the cross slot section has an aspect ratio of 12:1. The length of the cross slot is equal to 37% of the throat width. The hypermixing version of the nozzle, which is shown in Figure 38, was fabricated by cutting back the exit of each span section and inserting a thin (.05 cm) divider strip between halves, as seen in the figures. The gap was closed to restore the original exit area. These dimensions were chosen so that all three nozzles had about the same exit area.

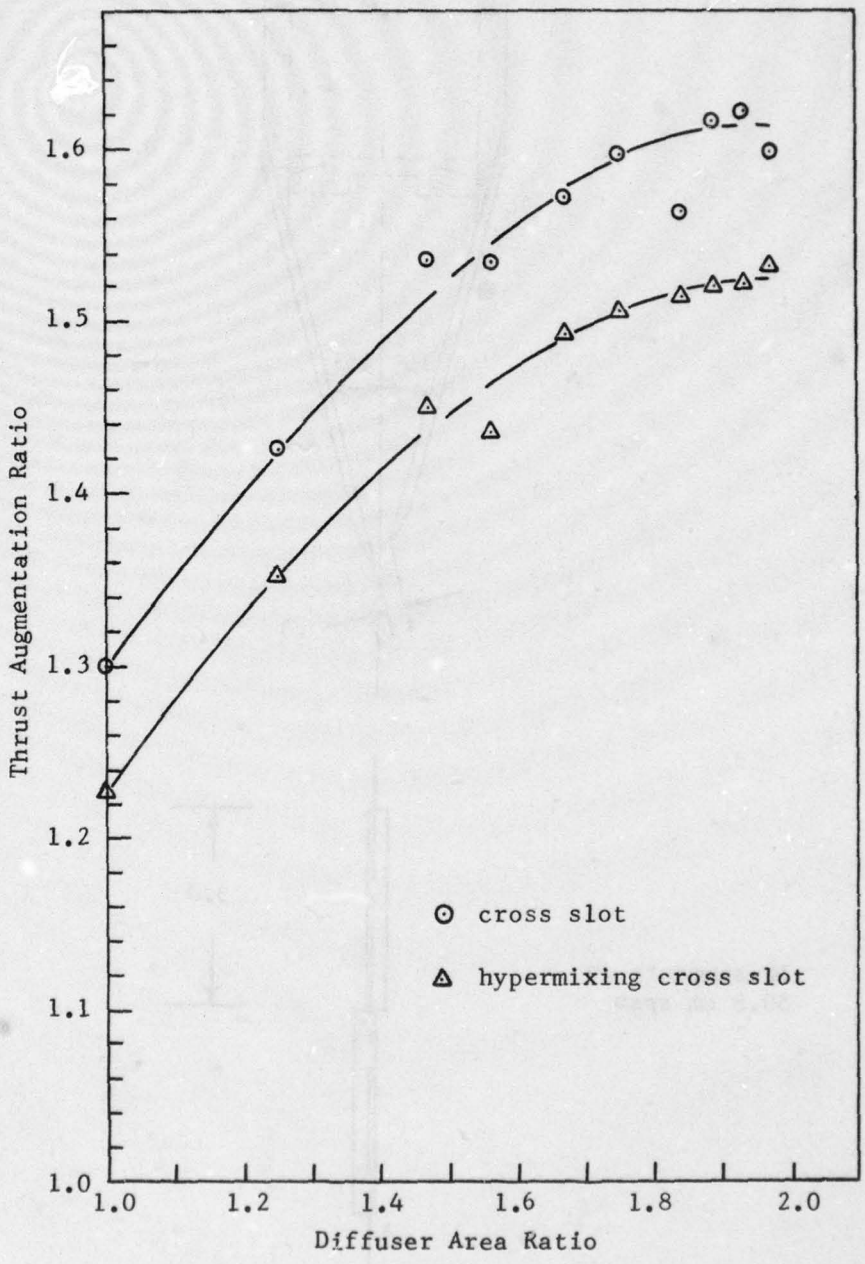

Figure 35. Effect of Hypermixing on Thrust Augmentation of Cross Slot Nozzles

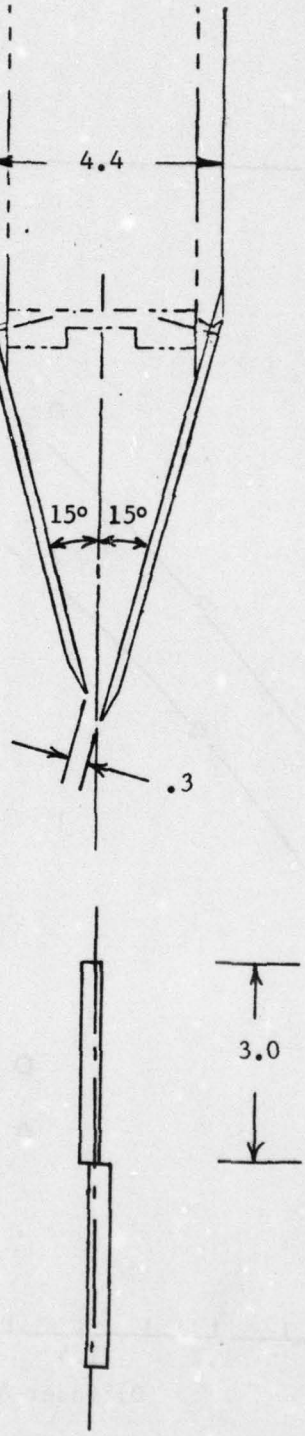

Figure 36. Reference Hypermixing Nozzle

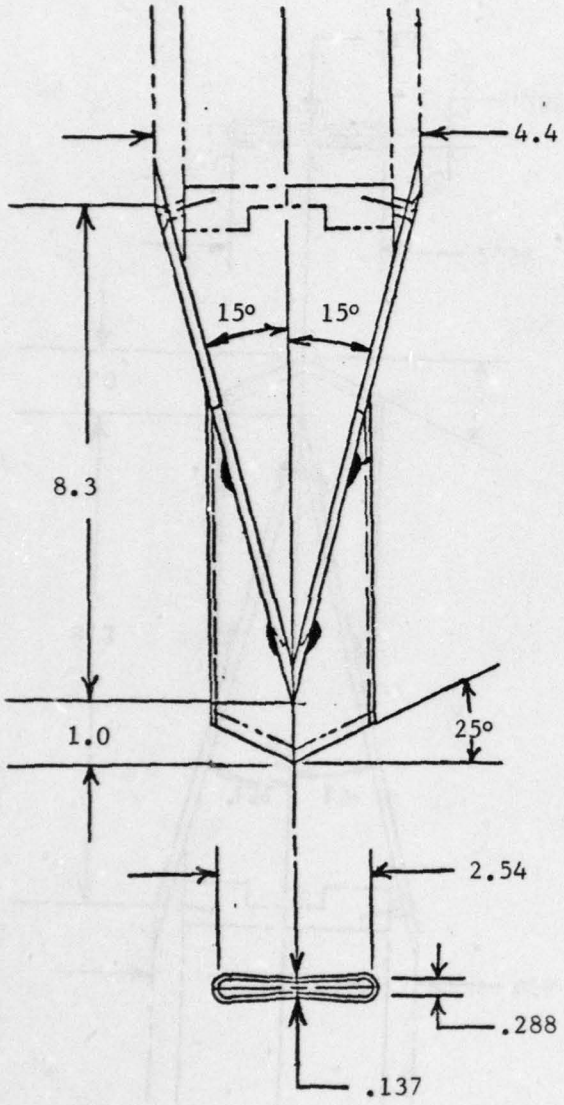

15 cross slot and 14 span slot elements in a 50.8 cm span

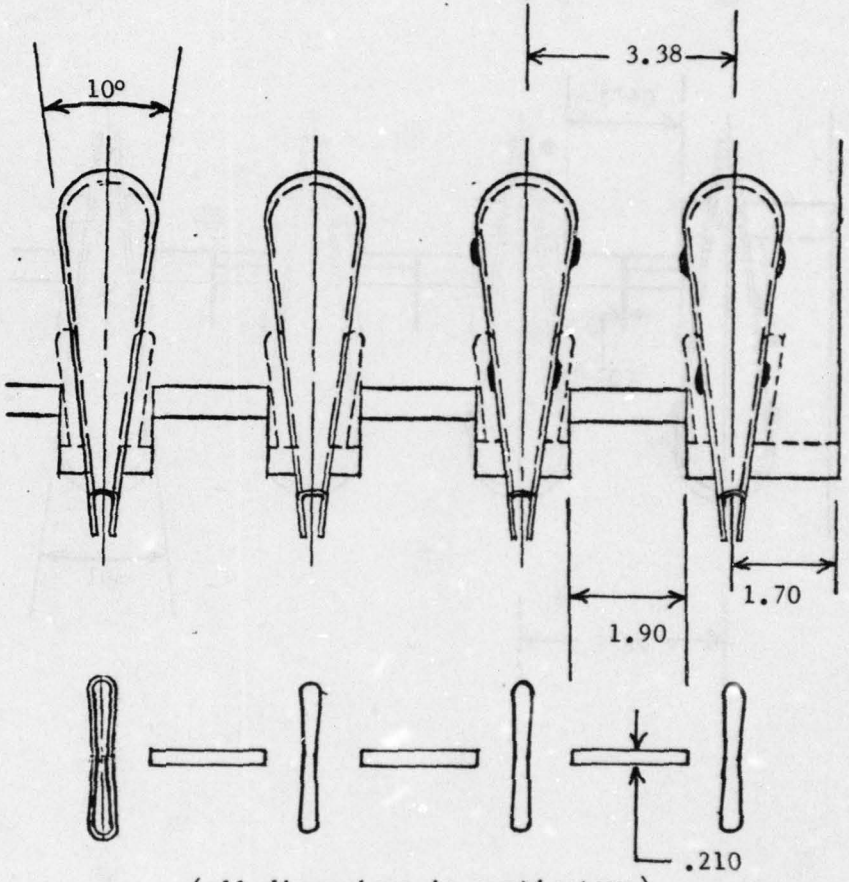

(all dimensions in centimeters)

Figure 37. Test Alternating Slot Nozzle

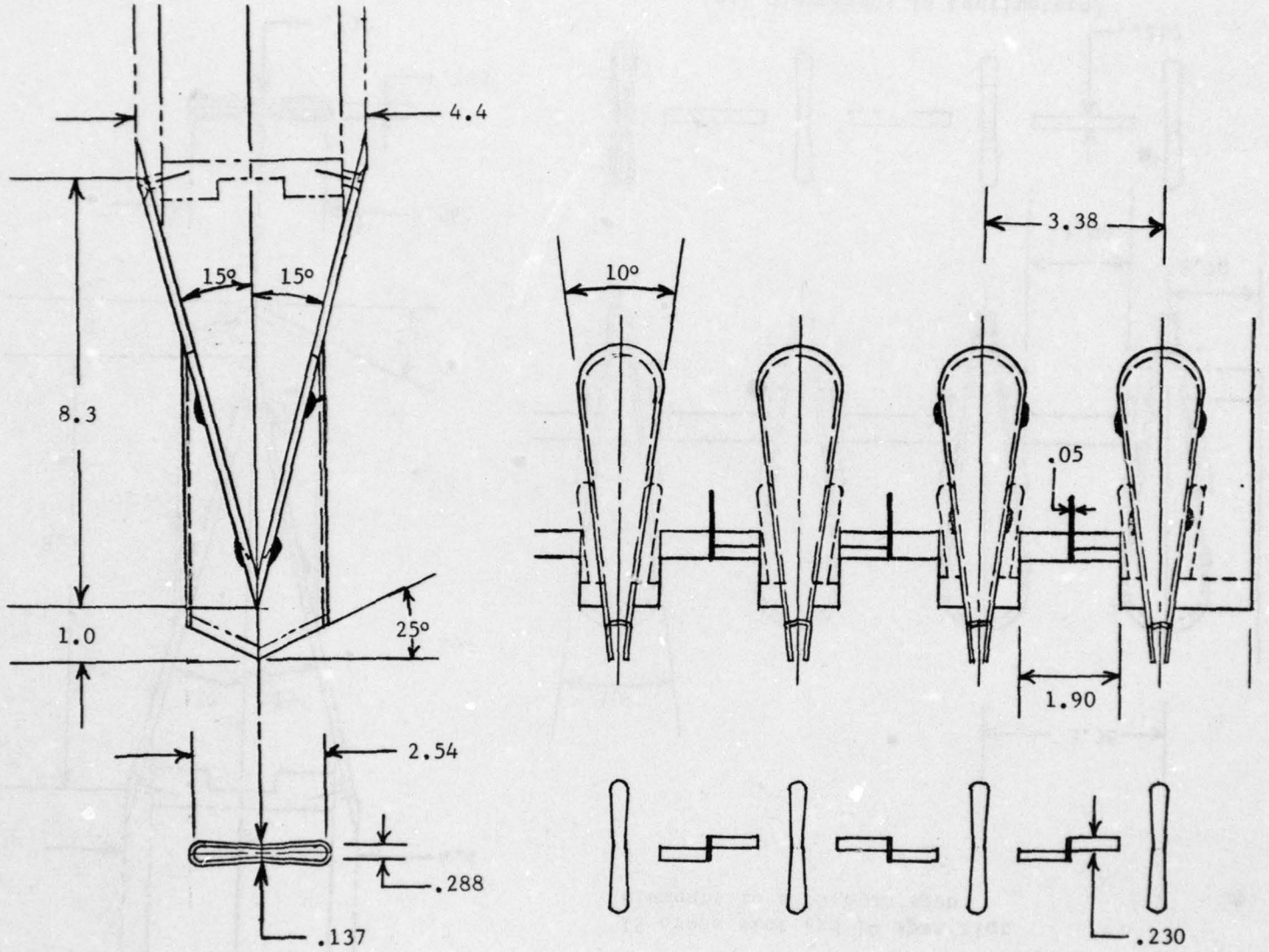

(all dimensions in centimeters)

Figure 38. Test Hypermixed Alternating Slot Nozzle

A view of the ejector model with the hypermixing slot nozzle installed is shown in Figure 39. It has a span of 50 cm and the width at the throat is 7 cm. Three boundary layer control nozzles are visible on each endwall; these can be rotated to optimize the distribution of air. The slotted control arms at the center of the ejector are used to adjust the angle of the diffuser walls. Figure 40 is a cross section of this ejector. The ratio of ejector length to throat width is $L_e/W = 2.1$, and the inlet area ratio is 13.

The pressure distribution of each nozzle was examined to establish its uniformity, and the jet from each section of the hypermixing nozzle was surveyed to verify that it was hypermixing. Necessary adjustments were made and the velocity coefficient was measured prior to installing each nozzle in the ejector. Testing was conducted at three nozzle exit pressure ratios equal to 1.5, 2.1 and 2.5 over a range of diffuser area ratios. Thrust augmentation ratios were computed from venturi measured mass flows and load cell thrust measurements. Midspan pitot static surveys were taken by making chordwise sweeps beginning at the ejector throat and proceeding streamwise in 2.54 cm (one inch) increments to the ejector exit. These surveys were taken at a diffuser area ratio of 2.0, which represented the peak performance for each of the configurations at nozzle exit pressure ratio of 2.1. These may be found in Figures 41 & 42. The development of the profiles is the same as the numerical predictions.

The variation of thrust augmentation ratio as a function of diffuser area ratio for the three configurations tested is shown in Figure 43. The maximum augmentation of $\phi = 1.57$ for the alternating slot case, and $\phi = 1.54$ for the hypermixed alternating slot case, represents substantial increases above the 1.49 attained with the hypermixing reference nozzle. Thus, the analytic prediction that both of these nozzles would produce increases over the baseline was verified.

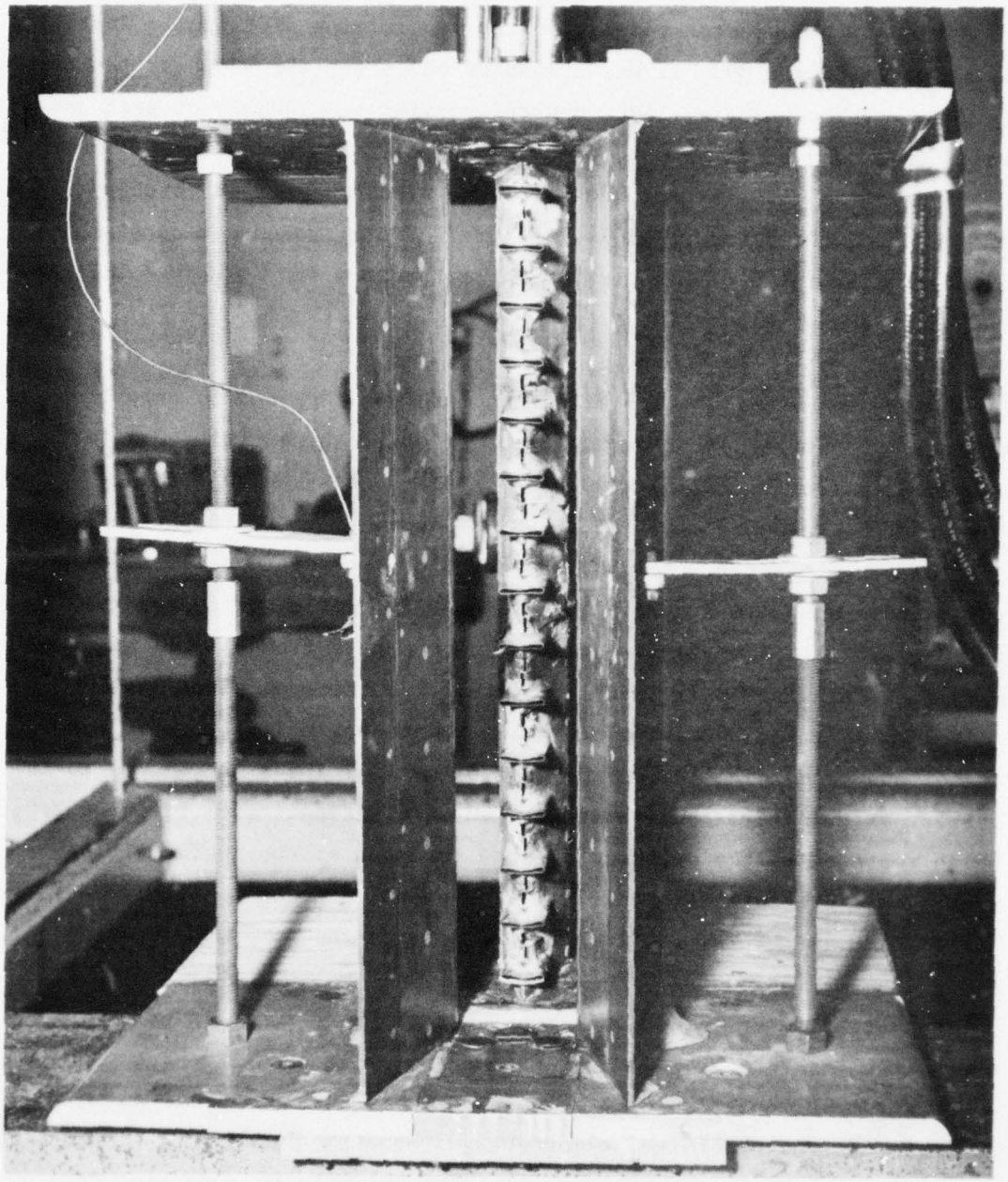

Figure 39. Test Ejector with Hypermixed Alternating Slot Nozzle Installed

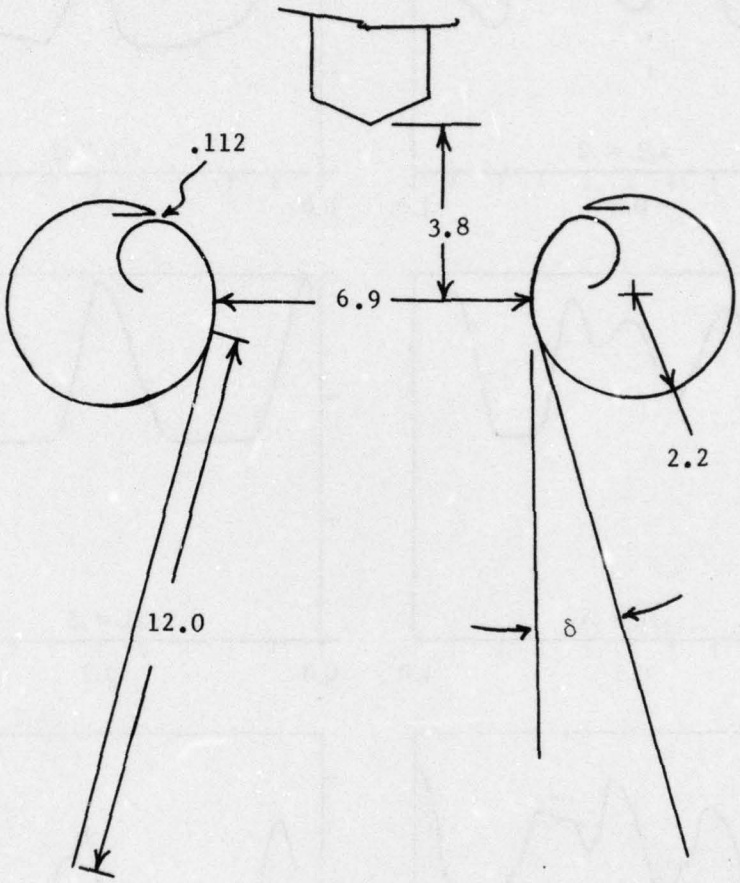

Flow Split: Coanda - .20 Center Nozzle - .55 Coanda - .20 BLC .05

(All dimensions in centimeters)

Figure 40. Sectional View of Final Test Ejector

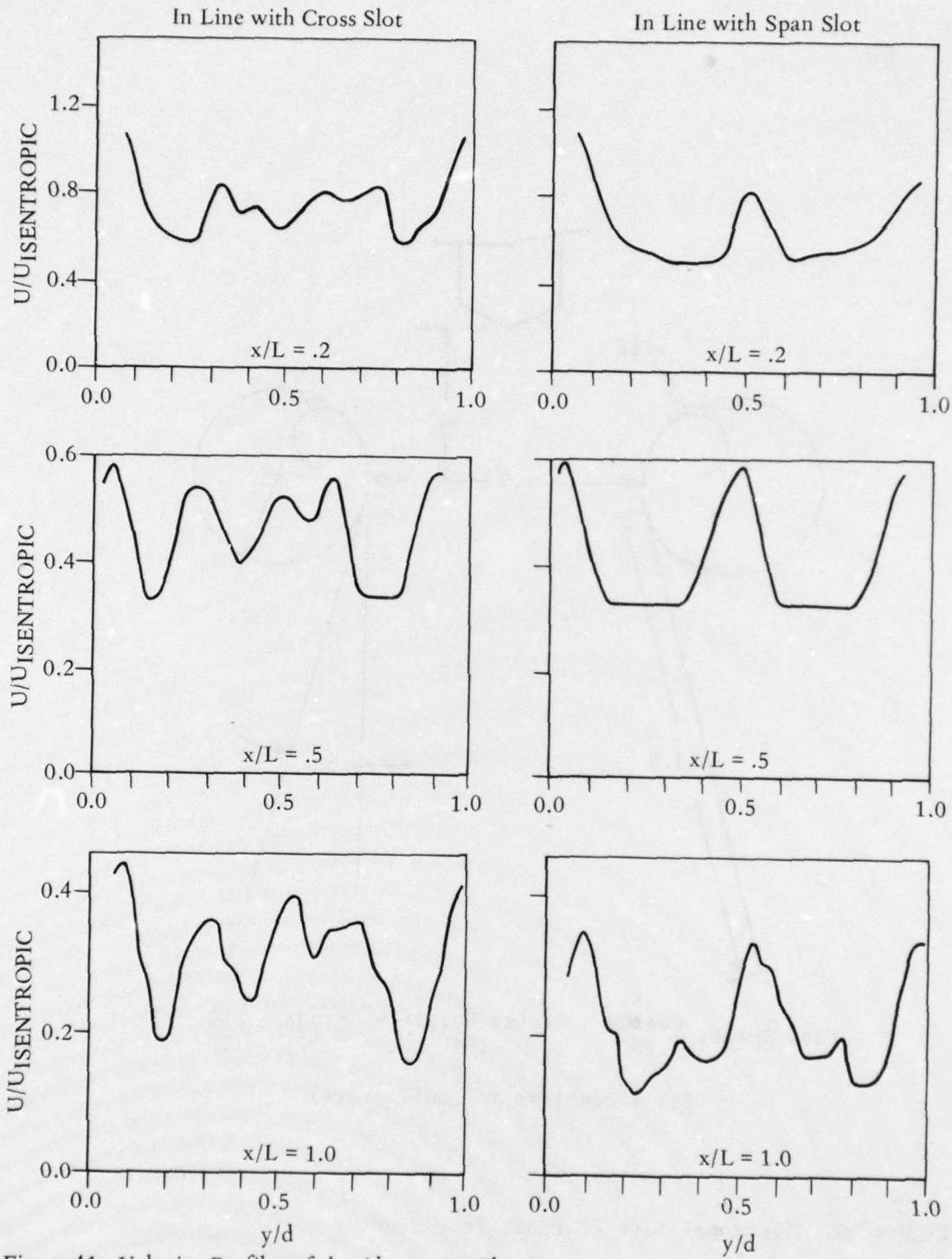

Figure 41. Velocity Profiles of the Alternating Slot Jet

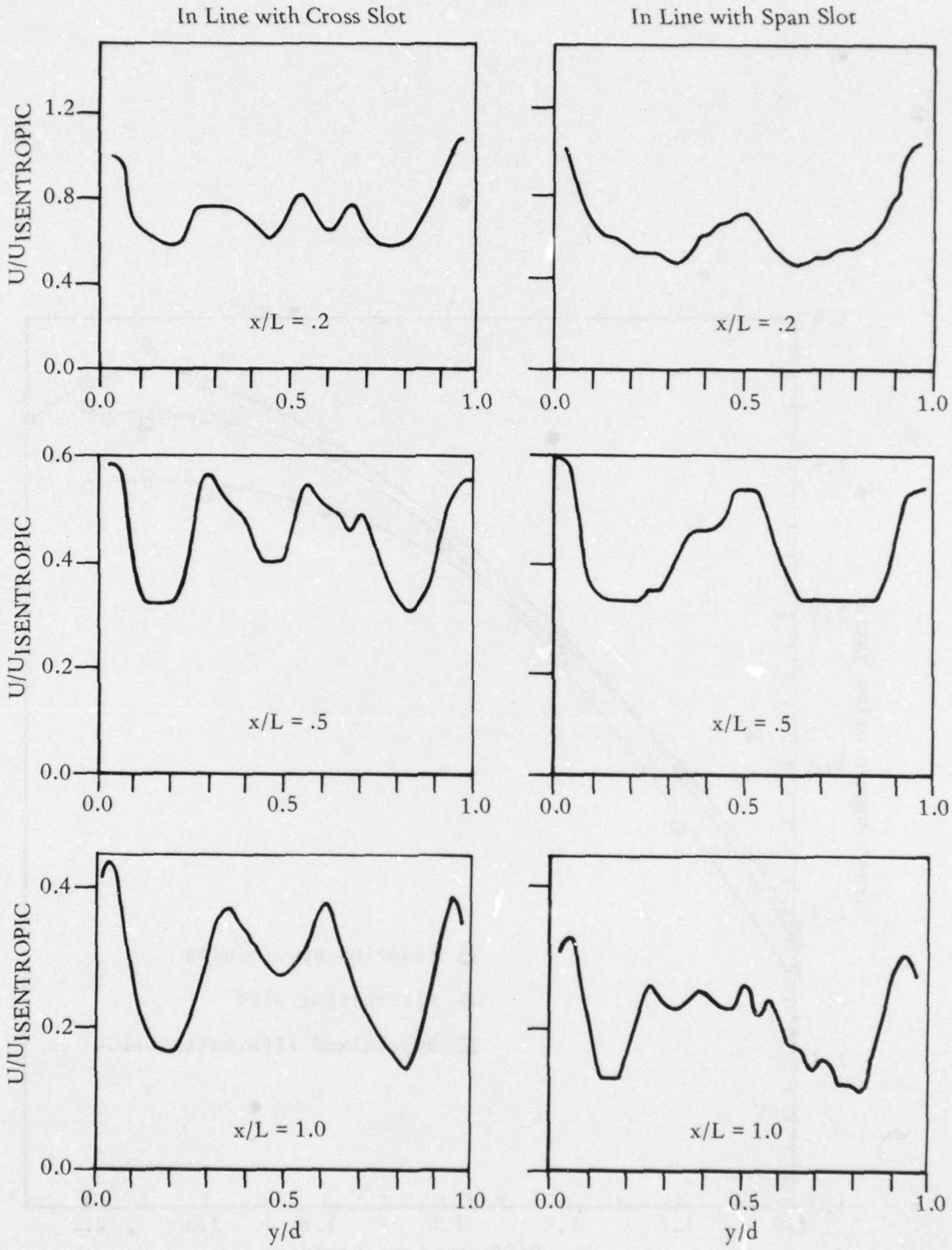

Figure 42. Velocity Profiles of the Hypermixed Alternating Slot Jet

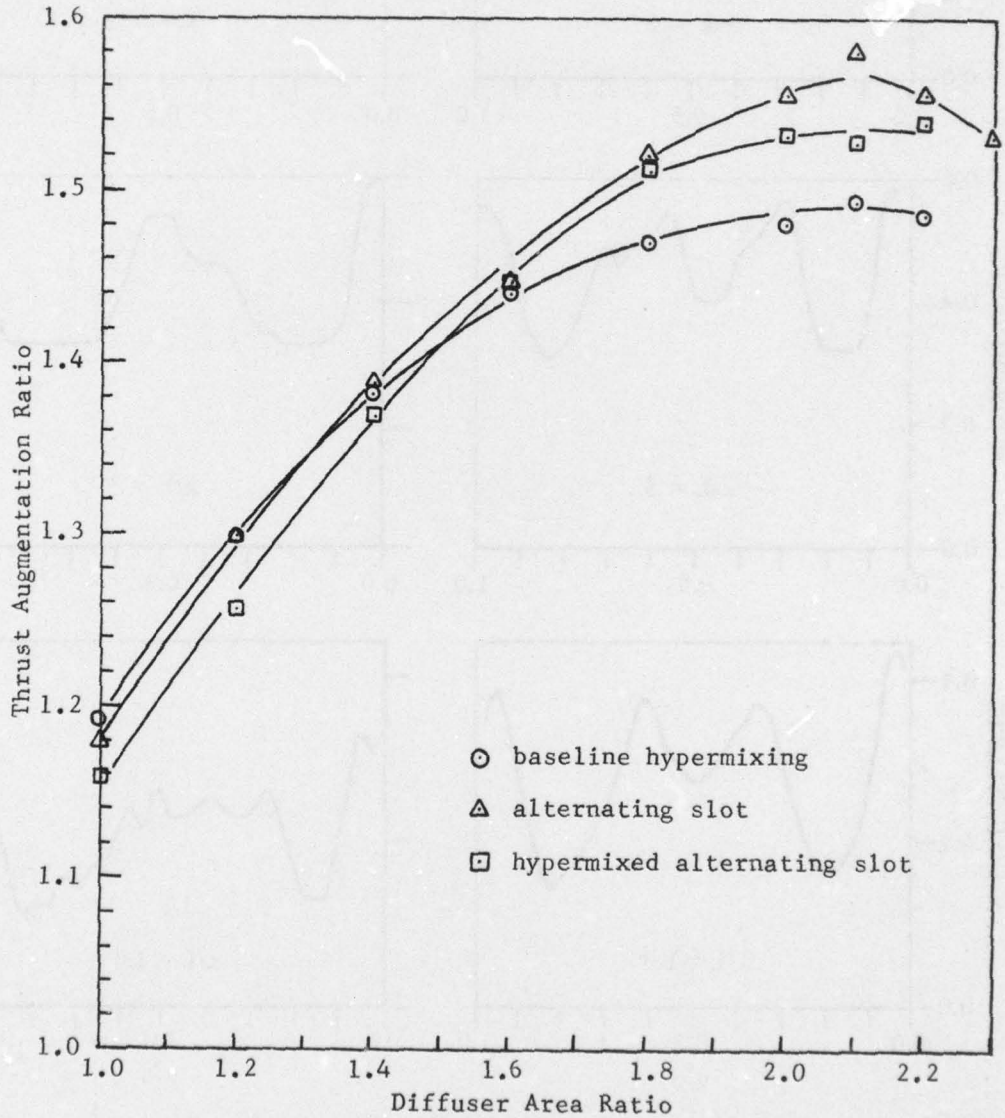

Figure 43. Comparison of Thrust Augmentation for Three Test Nozzles at P_R = 2.1

The smaller increment in augmentation achieved with the hypermixed alternating slot nozzle suggests that there may be some interference between the hypermixing and cross slot mechanisms. Examination of the midspan pitot static surveys indicates that although mixing was increased slightly in the regions of flow directly below the hypermixed span slots, the chordwise spreading of the cross slots was reduced by the hypermixing action. The vortices created by hypermixing seem to draw the cross slot jets toward them.

In Figure 44 a comparison of these nozzles at a pressure ratio of 2.5 is shown. The same performance trends are seen as at the lower pressure ratio. Both the alternating slot and the hypermixed alternating slot configurations gave better performance than the reference hypermixing nozzle, even though the maximum augmentation occurred at a lower diffuser area ratio, $A_3/A_2 = 1.8$. At increased diffuser area ratios, the augmentation declined more rapidly than at $P_R = 2.1$.

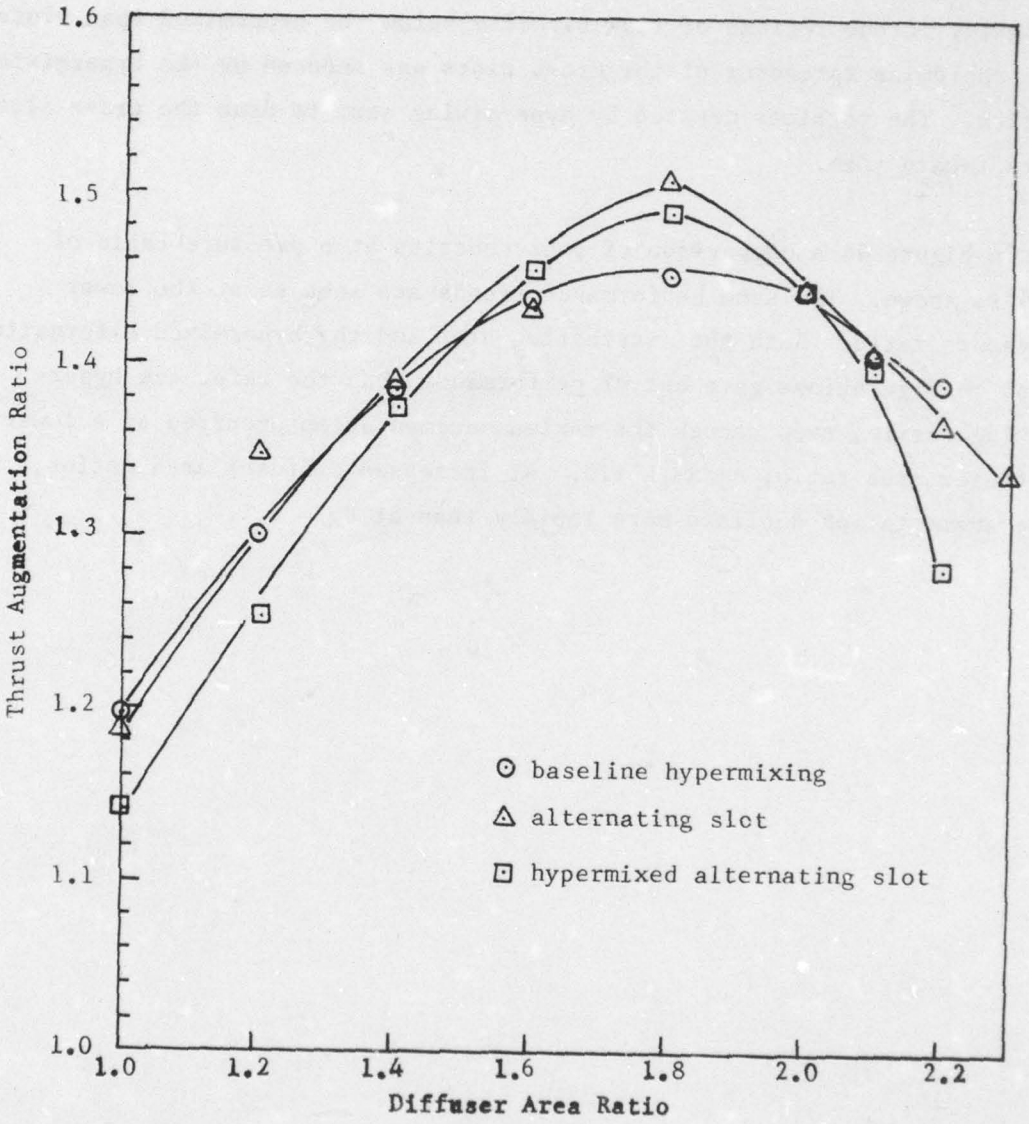

Figure 44. Comparison of Thrust Augmentation for Three Test Nozzles at $P_R = 2.5$

CONCLUSION

The analytical predictions which were tested have therefore been verified. The hypermixing and cross slot mechanisms are not readily combined: the entrainment of a narrow cross slot nozzle is reduced by the addition of a hypermixing vortex. This is because the effect of the vortex is to deflect adjacent sections of the jet into each other and thus inhibit their spreading. The augmentation ratio is reduced approximately $\Delta\phi \sim 0.10$ in this case. Both with and without a hypermixing vortex, the alternating slot nozzle was predicted to increase the augmentation about $\Delta\phi \sim .05$ over the baseline levels. This was also verified by testing.

Increasing the length of the cross slot segment resulted in the largest predicted gain in thrust augmentation. However, these nozzles were not tested because considerable development has already been carried out on this type of nozzle. In addition, it is difficult to incorporate these nozzles in a thin wing or low area ratio ejector, because of losses imposed by volume constraints. Nevertheless, the significant gains predicted provide an incentive for continued study.

In addition to these conclusions, there have been other benefits of this study. For example, even though no increment in thrust augmentation was predicted for the staggered cross slot nozzle, this is an easier nozzle to fold into some wings than the ordinary cross slot nozzle. It is encouraging to know that there is no penalty in those cases. Further, it is helpful to know the limits on augmentation associated with the size of the lobes, because this makes it possible to balance the increased weight or complexity of larger lobes against the gain in augmentation. Lastly, some previously unexplained anomalies and "strange" lobes observed in measured velocity profiles are now understood in terms of the overall development of the jet.

REFERENCES

1. Bevilaqua, P. M., "Lifting Surface Theory for Thrust-Augmenting Ejectors," AIAA Journal, Vol. 16, No. 5, May 1978, pp. 475-481.

2. Quinn, B. P., "Compact Ejector Thrust Augmentation," Journal of Aircraft, Vol. 10, No. 8, August 1973, pp. 481-486.

3. Bevilaqua, P. M., "Evaluation of Hypermixing for Thrust Augmenting Ejectors," Journal of Aircraft, Vol. 11, No. 6, June 1974, pp. 348-354.

4. Fearn, R., and Weston, R. P., "Vorticity Associated with a Jet in a Cross Flow," AIAA Journal, Vol. 12, No. 12, December 1974, pp. 1666-1671.

5. DeJoode, A. D. and Patankar, S. V., "Prediction of Three Dimensional Turbulent Mixing in an Ejector," AIAA Journal, Vol. 16, No. 2, February 1978, pp. 145-150.

6. Patankar, S. V. and Spalding, D. B., "A Calculation Procedure for Heat, Mass and Momentum Transfer in Three Dimensional Parabolic Flows," International Journal of Heat and Mass Transfer, Vol. 15, October 1972, pp. 1487-1806.

7. Launder, B. E. and Spalding, D. B., "The Numerical Computation of Turbulent Flows," Computer Methods in Applied Mechanics and Engineering, Vol. 3, No. 2, March 1974, pp. 269-289.

8. Throndson, L. W., "Compound Ejector Thrust Augmenter Development," ASME Paper No. 73-GT-67.

9. Morel, J. P. and Lissaman, B. S., "The Jet Flap Diffuser, a New Thrust Augmenting Device," AIAA Paper No. 69-777.

10. Tennekes, H. and Lumley, J. L., "A First Course in Turbulence," MIT Press; Cambridge, Mass, 1972.

11. Viets, H., "Thrust Augmenting Ejectors," ARL, TR 75-0224, June 1975.

DISTRIBUTION LIST

Office of Naval Research
Code 473
Attn: Mr. Patton
800 North Quincy Street
Arlington, VA 22217 2

Commander
Naval Air Systems Command
Washington, D.C. 20361
Attn: AIR-330 1

Commander
Naval Air Systems Command
Washington, D.C. 20361
Attn: AIR-330B 1

Commander
Naval Air Systems Command
Washington, D.C. 20361
Attn: AIR-330C 1

Commander
Naval Air Systems Command
Washington, D.C. 20361
Attn: AIR-03PA1 1

Commander
Naval Air Systems Command
Washington, D.C. 20361
Attn: AIR-03PA3 1

Commander
Naval Air Systems Command
Washington, D.C. 20361
Attn: AIR-530 1

Commander
Naval Air Systems Command
Washington, D.C. 20361
Attn: AIR-5360 1

Commander
Naval Air Systems Command
Washington, D.C. 20361
Attn: AIR-5361 1

Commanding Officer
Naval Air Propulsion Test Center
Trenton, New Jersey 16828 1

Commanding Officer
Naval Air Development Center
Warminster, PA 19112
Attn: AVTD 1

Melvin J. Hartman
Chief, Compressor Design Section
NASA Lewis Research Center
Cleveland, OH 44135 1

Prof. M. F. Platzer
Chairman Department of Aeronautics
Naval Post Graduate School
Monterey, CA 93940 14

Dr. David Hickey
Large Scale Aerodynamics
NASA Ames Research Center
Moffett Field, CA 94035 1

Mr. Dave Koenig
Large Scale Aerodynamics
NASA Ames Research Center
Moffett Field, CA 94035 1

Dr. Brian Quinn
Director of Aerospace Sciences,
MS8220
Air Force Office of Scientific
Research
Bolling Air Force Base
Washington, D.C. 20332 1

Dr. Herman Viets
Dept. of Engineering
Wright State University
Dayton, OH 45431 1